



Doctoral Thesis

Multiomics Characterization of the Responses to Diurnal and Seasonal Cycles in the Marine Picoeukaryote *Ostreococcus tauri*

Dissertation presented by Ana Belén Romero Losada to obtain the PhD Degree by Universidad de Sevilla.

Supervisors:

Prof. Francisco José Romero Campero

Prof. Mercedes García González

This work was supported by the research projects MINOTAUR (BIO2017-84066-R) and BLOOM (RTC-2017-6080-5) from the Spanish Ministry of Science and Innovation.



Dedicatoria . . .

word cloud

Contents

Index

Abstract.....	14
Introduction.....	18
Chronobiology.....	20
Circadian research.....	24
Ostreococcus tauri.....	27
Systems Biology.....	35
Materials and Methods.....	40
Organism and culture growth conditions.....	42
Organism and growth medium.....	42
Continuous culture conditions in photochemostats.....	42
Experimental design.....	44
Transcriptomic analysis.....	45
Sample Collection.....	45
Cell disruption.....	45
RNA extraction.....	46
RNA purification.....	46
RNA sequencing and processing.....	46
Proteomic analysis.....	47
Sample collection.....	47
Cell disruption.....	47
Proteins extraction.....	47
Proteins digestion.....	47
SWATH acquisition.....	48
Equipment and data acquisition method.....	48
Library construction.....	48
SWATH runs.....	49
Data processing.....	49
Cell cycle analysis.....	49
Sample collection and cell fixation method.....	49
Cell staining method.....	50
Data acquisition and processing.....	50
Analysis of photosynthetic activity.....	50
Sample collection.....	50
Data acquisition.....	50
Analytical determinations.....	51
Sample collection.....	51
Starch Content.....	51
Cell disruption.....	51
Starch solubilization and digestion.....	51
Spectrophotometric quantification.....	52
Carotenoid Content.....	53
Cell disruption.....	53
Carotenoids extraction.....	53
Carotenoids determination and quantification.....	53
Rhythmic patterns analysis.....	54
Rhythmic patterns detection.....	54

Rhythmic patterns comparison.....	54
Hypothesis and Objetives.....	56
Results.....	58
Chapter 1. ALGAEFUN with MARACAS: user-friendly tool for analysing and integrating omic data generated from microalgae.....	61
Implementation.....	62
Integration of different microalgae databases.....	62
Development of functional annotation and genomic packages.....	65
MARACAS implementation: high-throughput sequencing data processing.....	66
ALGAEFUN implementation: functional annotation analysis.....	72
Case of study 1: from RNA-seq raw sequencing data to biological processes and pathways..	77
Case of study 2: From ChIP-seq raw sequencing data to marked genes.....	79
Contribution of ALGAEFUN with MARACAS to the field.....	81
Chapter 2: Transcriptomic analysis of diurnal and seasonal cycles in <i>Ostreococcus tauri</i>	84
Transcriptomic characterization of diurnal rhythmic expression profiles.....	86
Most genes in <i>Ostreococcus tauri</i> present diurnal rhythmic expression profiles under both photoperiods.....	86
Constant light and constant darkness as free-running conditions have different effects over the transcriptome of <i>Ostreococcus</i>	88
Under free running conditions rhythmicity is maintained in different proportions depending on the photoperiod of entrainment.....	93
Transcriptomic characterization of seasonal effects over gene expression profiles.....	97
Seasonal changes induce changes in amplitude and phase over gene expression profiles..	97
Seasonal changes promote the emergence of 12 h period cycles.....	99
Seasonal cycles induced distinct temporal transcriptional programs organizing biological processes during diurnal cycles.....	102
Chapter 3: Proteomic analysis of diurnal and seasonal cycles in <i>Ostreococcus tauri</i>	105
Proteomic characterization of diurnal rhythmic abundance profiles.....	107
Phase offsets and a decrease in rhythmicity are observed when proteomic and transcriptomic data are compared.....	107
Proteomic characterization of seasonal effects over the protein abundance profiles.....	109
The effects of seasons over the wave parameters in the transcriptome are also found in the proteome of <i>Ostreococcus tauri</i>	109
Phase offsets between genes and proteins involved in the same biological process are adjusted by seasons.....	111
Chapter 4: Diurnal and seasonal multi-omic integration with physiological data.....	114
Cell Division Cycle (CDC) of <i>Ostreococcus tauri</i> under diurnal and seasonal cycles.....	114
Temporal program of cell division cycle under summer and winter photoperiod.....	115
Integration of cell division cycle program with transcriptomic and proteomic data.....	118
Diurnal and seasonal rhythm of photosynthesis in <i>Ostreococcus tauri</i>	121
Rhythmic oscillations of photosynthetic efficiency under summer and winter photoperiod	122
Integration of photosynthesis efficiency rhythmic profile with multi-omic data.....	123
Integration of starch content diel oscillations with multi-omic data.....	126
More metabolic pathways of <i>Ostreococcus tauri</i> showing periodic oscillations under diurnal and seasonal cycles.....	128
Carotenoids biosynthesis in <i>Ostreococcus tauri</i> under diurnal and seasonal cycles.....	128

Integration of multi-omics data with oscillations described by carotenoids content in <i>Ostreococcus tauri</i> under diurnal and seasonal cycles.....	129
Nitrate assimilation under diurnal and seasonal cycles in <i>Ostreococcus tauri</i>	132
Integration of key enzyme activities from nitrate assimilation pathway with multi-omic data.....	133
Bibliography.....	137

Abstract

Abstract text

Abstract text

Introduction

Chronobiology

Simply by looking around, it is easy to identify many cyclic processes. We are so used to them that we usually do not perceive how they influence our lives and bodies. There are four environmental cycles known: tides (which repeat every 12 and half hours), lunar cycles (lasting 28.5 days), days (every 24 hours) and years (every 365.25 days). These cycles are also called circatidal, circalunar, circadian, or circannual (Numata et al., 2015).

These four rhythmic processes that arise from gravitational forces are extremely predictable. It is possible, for example, to know the exact time of a high tide months in advance. We constantly see how full moons are always followed by new moons, and everybody goes to bed sure that the sun will rise the next morning. The exact date for the next equinox is known and written in calendars over the world, so the change of season is never a surprise.

Since these four cycles affect earth with an overwhelming precision, earth living organisms have learnt how to anticipate them. That is what chronobiology is about: it is a young science that studies how rhythmic environmental changes affect organisms and how they anticipate to them (Edmunds, 1983; Kuhlman et al., 2018).

Living beings perceive those changes and they are able to react in advance thanks to an endogenous machinery that acts as a clock (Fig. 1). The clock is a central oscillator that is entrained by external cyclic inputs (rhythmic environmental changes) and produce rhythmic outputs of biological processes. Chronobiologists have found biological rhythms regulated by the clock in a wide range of scales. It goes from a molecular level (transcription, translation, protein degradation, metabolites biosynthesis, etc), to a cellular and tissue level (cell division, synaptic connections, apoptosis, etc.) or even complete organisms or populations (Edmunds, 1983; Merrow et al., 2005; Sharma et al., 2022).

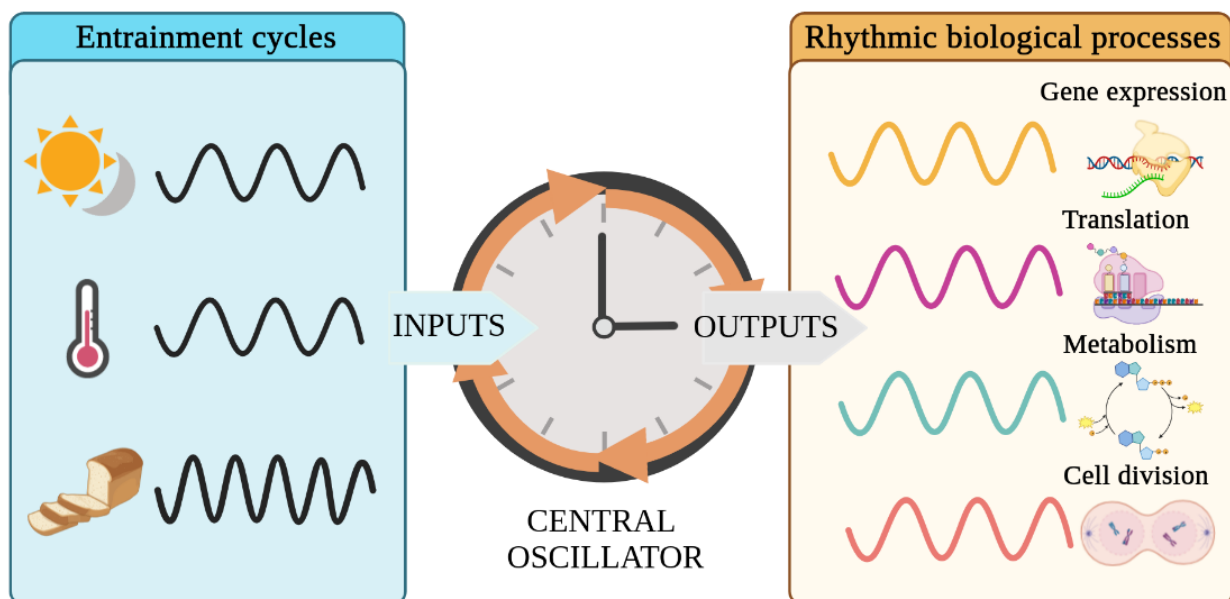


Figure 1: Diagram of the central oscillator known as clock. The clock acts as a central oscillator that is entrained by external cyclic inputs (as light/dark cycles or photoperiod, temperature changes and nutrients availability) generated by diurnal, seasonal, lunar or tidal cycles. As a response, the clock produce rhythmic outputs of biological processes that allow organisms to anticipate those environmental changes. Figure created using Biorender.

A distinctive characteristic of clock-regulated biological rhythms is that they are self-sustained (Pittendrigh, 1960; Roenneberg & Merrow, 2005). For example, when the response of an organism to rhythmic environmental changes (light/dark cycles, food availability, temperature changes, etc.) is studied (Fig. 2-A), it's common to find several biological functions showing a rhythmic profile as well (Fig. 2-B,C). However, some of them would not maintain their rhythmicity under constant conditions because the rhythmic profile observed was a direct acute response to changes in the environment. Therefore, if the environment is constant, the profile will also be constant (Fig. 2-B). Rhythmicity will be maintained un-

der constant environmental conditions only when the studied biological function is regulated by that machinery called clock and, thus, its rhythmicity is self-sustained (Fig. 2-C).

For that reason, every chronobiology experiment is designed as follows: several consecutive days where the organism is exposed to the rhythmic environmental condition (called *zeitgeber*, which is used as synchronizer) are followed by several consecutive days where the organism is exposed to constant conditions (called *free-running* conditions) (Kuhlman et al., 2018). In both scenarios, data are collected every few hours, minutes or seconds depending on the complexity of the experiment. For example, in the case of a circadian experiment, as the one executed in this work, the *zeitgeber* would be a light-dark cycle and the *free-running* conditions would be constant light or constant darkness. Under that experimental design, circadian processes can be identified and discerned from light or dark responding processes.

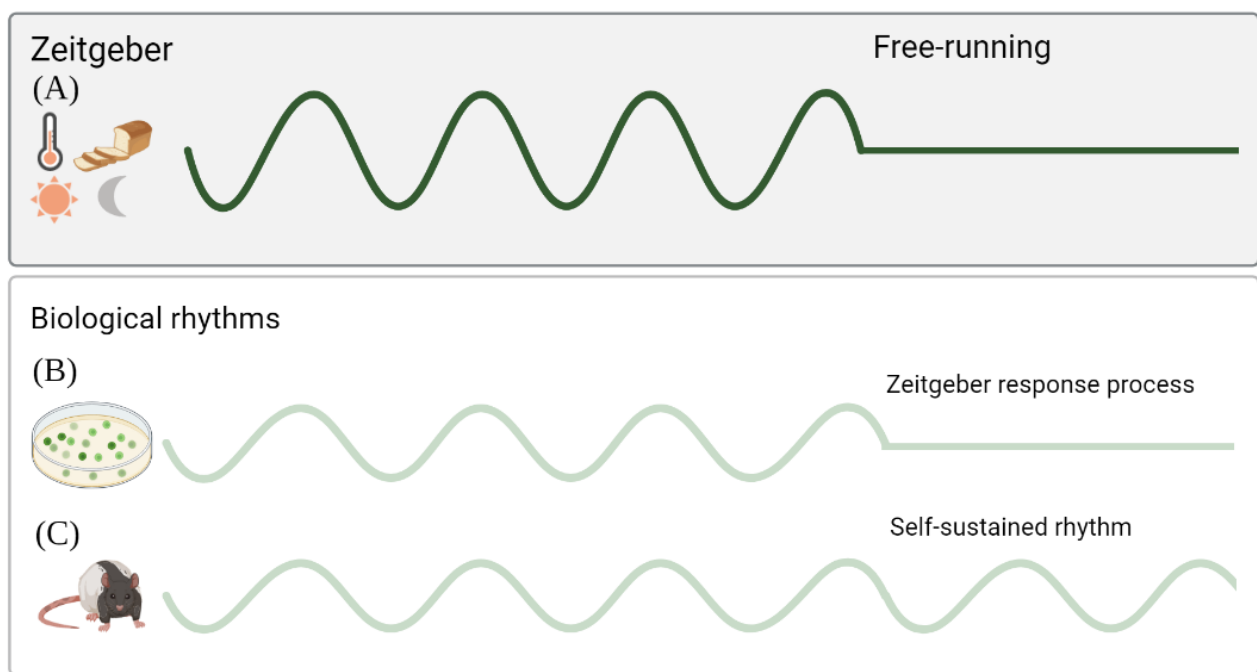


Figure 2: Different patterns of response to rhythmic environmental changes. (A) Environmental input; (B) Biological process that is only responding to the given environmental input; (C) Self-sustained biological process and thus regulated by an endogenous clock. Figure created using Biorender.

Following that experimental design, chronobiologists have described self-sustained biological rhythms reacting to the four different environmental cycles mentioned above. Therefore, some marine organisms show self-sustained circatidal rhythms when they are kept in laboratory tanks without its *zeitgeber*, in this case, the tidal changes (Rock et al., 2022). As

an example, the marine diatom *Hantzschia amphioxys* descends to the sand at high tides and rises to the surface at low tides (Fauré-Fremiet, 1951). In contrast, the self-sustained circalunar processes are yet more unknown (Andreatta & Tessmar-Raible, 2020). One of the most famous ones is the larvae of the insect called Ant Lion, which build small holes in the sand as traps for insects. The size of the traps changes showing a circalunar profile that is maintained under constant conditions (Youthed & Moran, 1969).

The studies about circadian or circannual rhythms are much more numerous, and they have been described in a wide range of organisms (Merrow et al., 2005; Pfeuty et al., 2012; Roenneberg & Merrow, 2005). In animals, circadian rhythms are involved in activity-rest cycles (Roenneberg et al., 2022; Zee & Abbott, 2020), but hundreds of other parameters from ethology to gene expression also show circadian profiles. For example, the olfactory discrimination in mice is higher at night time, even under free-running conditions (Granados-Fuentes et al., 2006). Fungus show circadian rhythmic phenomena, for example, *Neurospora crassa* generates asexual spores every 24 h even under constant darkness (Correa & Bell-Pedersen, 2002). Circadian rhythmic profiles in plants are found in leaf movement, growth rate, stomatal opening, as well as the expression of a wide range of genes (Merrow et al., 2005). All the organisms of the green lineage react in many different ways to circadian cycles (Noordally & Millar, 2015), one of the most known ones is the 24 h cyclic movement in the water column adjusted to their metabolism requirements (Lebert et al., 1999).

Day length or photoperiod is a crucial signal for the circannual timing system. Seasonal changes of photoperiod have been strongly connected to reproduction. In fact, all animal reproductive systems are related to seasons, from gene expression profiles to anatomical structures. Hamsters kept in short day condition have 10-fold smaller testes than the ones kept in long day condition (Klante & Steinlechner, 1994; Nishiwaki-Ohkawa & Yoshimura, 2016). But also in plants, flowering and seed production are photoperiod-regulated (Brandoli et al., 2020; Serrano-Bueno et al., 2017).

Since photosynthetic organisms depend on light to ensure its success, they are highly synchronized with cyclic environmental changes involving light such as circadian rhythms and photoperiods. The chronobiology of microalgae is yet barely studied compared with other photosynthetic organisms despite representing one of the largest polyphyletic groups in the eukaryotic domain (Fig. 3). The genetics and molecular techniques used to identify

clock components in other taxa have not been widely applied to microalgae yet (Noordally & Millar, 2015). This work aims to contribute to the chronobiology community by describing, for the first time, the circadian and photoperiodic changes in one of the older sisters of microalgae, *Ostreococcus tauri*.

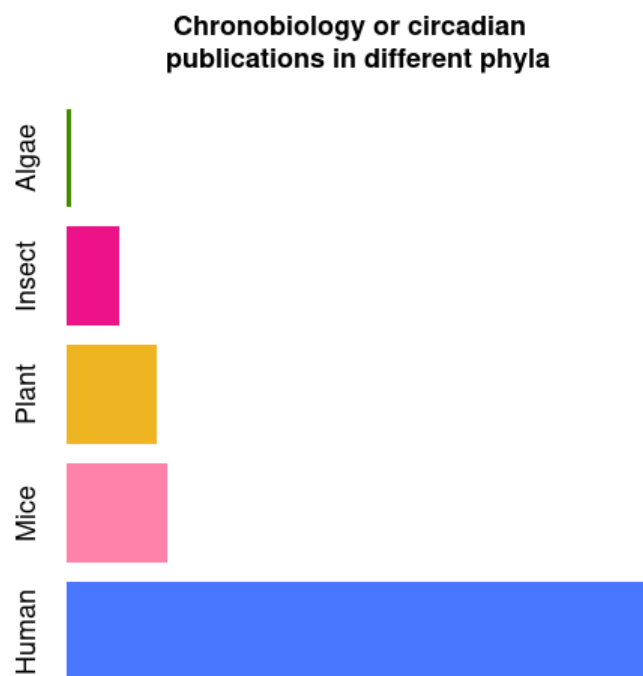


Figure 3: Number of publications found in PubMed using "chronobiology" or "circadian" keywords in their abstracts in July of 2022. For the algae group (using the generic term "algae", "microalgae" and "*Ostreococcus tauri*", "*Chlamydomonas reinhardtii*" and "*Polyedra*" as main model organisms of this group), only 493 publications were found. For the insect group (including the generic term "insect" and "*Drosophila melanogaster*" as main model organism), 5717 publications were found. For plants (including the generic term "plant" and "*Arabidopsis thaliana*" as main model organism), 9734 publications were found. For mice and human, 10771 and 62305 publications were found, respectively.

Circadian research

Our society is worldwide structured in a 24 h / 7 days system. People from different countries and cultures are experiencing jet-lags, shift work, exposure to artificial light and lack of outdoor activities. Circadian clock research is gaining relevance since this phenomena has a crucial impact on human health, behavior and quality of life (Mermet et al., 2017; Roenneberg et al., 2019, 2022; Roenneberg & Merrow, 2016). Understanding the physiol-

ogy, genetics and epigenetics (Ripperger & Merrow, 2011) at a laboratory scale using different model organisms besides mice (as plants, fungus and microalgae ones) will also help in the comprehension of the circadian clock in humans and its variation among individuals.

The synchrony that exists between the sunrise/twilight and organisms have been so obvious for scientists that the underlying molecular mechanisms remained ignored and unexplored for centuries. The first observation indicating that daily rhythms were programmed took place in the 18th century. Jean Jacques d'Ortous De Mairan, a French astronomer, described in less than 350 words (nowadays, less than two tweets) how a mimosa plant inside a closet maintained its daily leaf movement (De Mairan, 1729). For some scientists, it was a clear proof that leaf movement was not controlled by light and darkness. Although De Mairan invited botanists to investigate his discovery to confirm that leaf movement was also maintained when temperature changes are avoid (which inside its closet was difficult to ensure). Nevertheless, it took 30 years to confirm what De Mairan observed, taking attention to temperature for the first time (Kuhlman et al., 2018; Roenneberg & Merrow, 2005).

The history of the circadian research have a lot of gaps between one discovery and another: the physiology of the endogenous nature of the clock in plants wasn't studied until 1832, despite De Mairan observations; similar observations in animals took another century, and 50 years more for humans (Kuhlman et al., 2018; McClung, 2006; Roenneberg & Merrow, 2005). Though circadian research and chronobiology were born in the 18th century, they took relevance and coherence in the 20th century. One of the breaking points in circadian research history was the international conference in Cold Spring Harbor, where 157 pioneers (Colin Pittendrigh, Patricia Decourse, Franz Halberg, etc) of this field met together for the fist time (Evans, 1961). From all the data shared, Pittendrigh summarized the qualities of circadian clocks in 16 generic empirical characteristics that he predicted to be true in all organisms (Pittendrigh, 1960). Nowadays, 62 years later, these empirical characteristics are still being useful though circadian research has suffered a huge development. The new technology approaches have enabled a more controlled experimental design and analysis of the data. The circadian community has already find circadian rhythms in almost all kind of organisms, even non-photosynthetic prokaryotes (Eelderink-Chen et al., 2021). Also the physiology and genetics behind the circadian clock have been

broadly studied in a wide range of phyla, since the first gene of the clock was described in 1971 by Seymour Benzer and Ronald Konopka using mutant screening in *Drosophila melanogaster* (Konopka & Benzer, 1971; Takahashi, 2021) (Fig. 4).

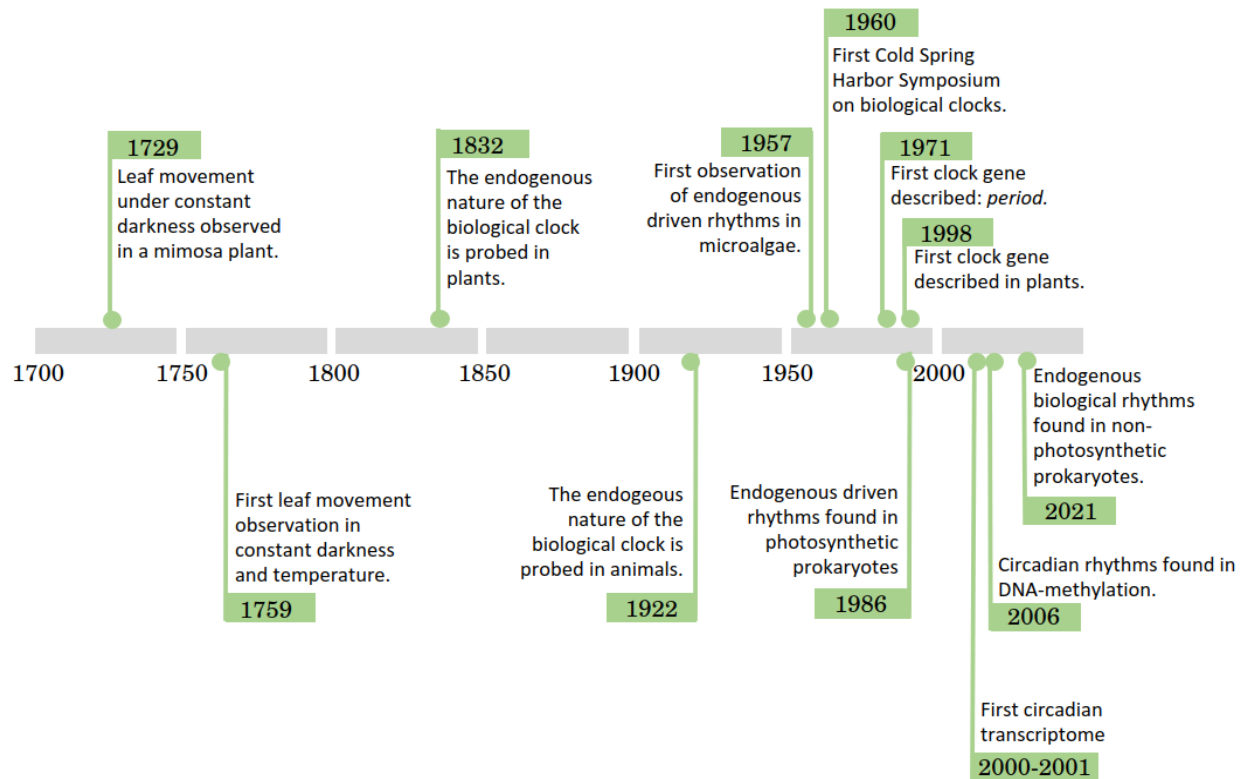


Figure 3: Timeline of circadian research. The main circadian discoveries have been listed in chronological order. (Akhtar et al., 2002; De Candolle, 1832; De Mairan, 1729; Duhamel du Monceau, 1759; Eelderink-Chen et al., 2021; Eissenberg & Elgin, 2006; Evans, 1961; HASTINGS & SWEENEY, 1957; Konopka & Benzer, 1971; Kuhlman et al., 2018; Mitsui et al., 1986; Richter, 1922; Roenneberg & Merrow, 2005; Somers et al., 1998)

As it can be observed in the timeline, circadian rhythms discoveries are very diverse. Chronobiologists usually have strong roots in other fields such as anatomy, physiology, molecular biology, genetics, ecology or mathematics. The knowledge obtained from each field have been shared in order to obtain a better picture of circadian rhythms (Klante & Steinlechner, 1994; Merrow et al., 2005; Nishiwaki-Ohkawa & Yoshimura, 2016). In particular, the contribution of mathematics has been of special relevance in considering biological rhythms as waves. A wave's shape repeat itself periodically, maintaining several characteristics that define the wave as it is. Those characteristics are called wave parameters and are used to quantitative compare different waves. In circadian research, some of the

most used ones are: period (the time between two maximum points), amplitude (how much high the wave reach) or phase (time point where the wave reaches its maximum high).

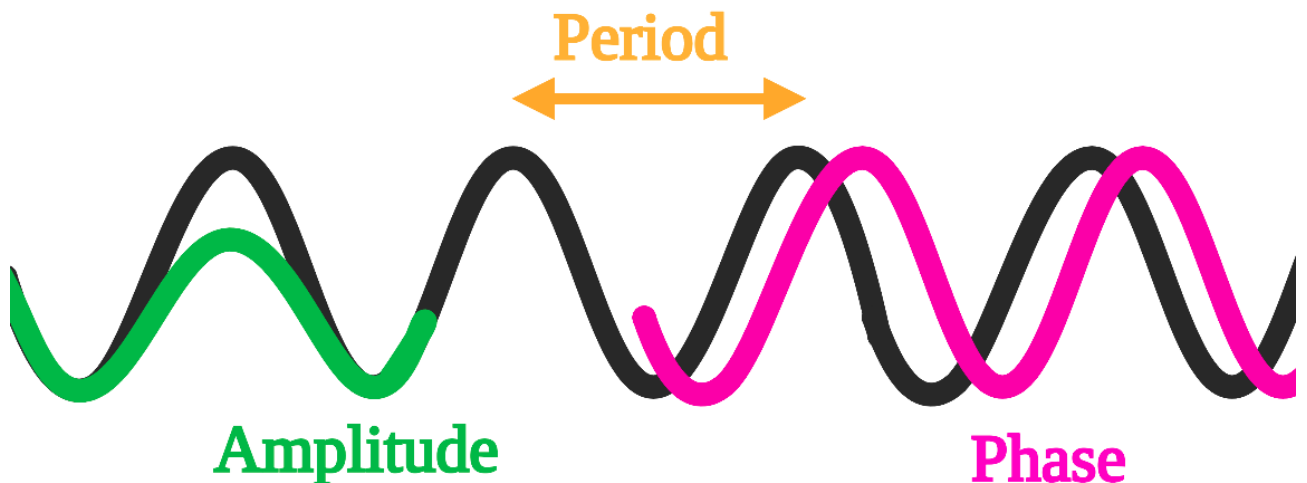


Figure 4: **Graphical representation of classic waves parameters.** Period is represented in yellow, amplitude is represented in green and phase is represented in pink. Figure created using Biorender.

The parameterization of waves using these four parameters enables to mathematically compare different groups of rhythmic data (McClung, 2006; Parsons et al., 2020). In this thesis, a deep study of circadian waves in *Ostreococcus tauri* was achieved using these parameters to find and statistically validate differences between rhythms found in three biological levels (mRNAs, proteins and physiology) under two different photoperiods of entrainment.

Ostreococcus tauri

The green lineage (Viridiplantae), comprehends two of the most important groups of oxygen photosynthetic eukaryotes: green microalgae and their descendants, terrestrial plants.

Microalgae are a very diverse group of photosynthetic single-cell microorganisms of special interest due to their plastic physiology and their biotechnological applications. They can be found in different habitats including water-based ones, from freshwater to oceans. Microalgae grow under a broad range of temperature, salinity, pH and light intensity val-

ues. More than 5000 species of microalgae have been identified in the oceans accounting for the production of 50% of the oxygen necessary to sustain life on Earth (El Gamal, 2010). Microalgae play a central ecological role as primary producers of biomass establishing the base of aquatic trophic chains. They have also been of great interest for the scientific community due to the large and yet increasing number of their biotechnological applications. Specifically, microalgae have been described as a high yield source of carbon compounds and good candidates to mitigate CO₂ emissions. The fixation of CO₂ is coupled with growth and biosynthesis of compounds of biotechnological interests such as polysaccharides, lipids, vitamins and antioxidants. They are currently large-scale cultured (to produce biostimulants in agriculture, health supplements, pharmaceuticals and cosmetics), as well as, successfully applied in wastewater treatment coupled with the fixation of atmospheric CO₂ (Abinandan et al., 2018; Borowitzka, 2013; H. Chen et al., 2019; García-Cubero et al., 2018).

Nowadays, the development of high-throughput sequencing is clarifying some aspects of the evolution of the green lineage (Bachy et al., 2022; Becker & Marin, 2009; Benites et al., 2021; Leliaert et al., 2012; Merchant et al., 2007). An early divergence of two discrete clades from an ancestral green microalga is hypothesized. These two main clades are: the Streptophyta, including land plants and charophyte (green algae that are their closest ancestors/older sisters); and the Chlorophyta, comprising the core chlorophytes and their closest ancestors/older sisters the prasinophytes (Bachy et al., 2022; Leliaert et al., 2012; Tragin & Vaulot, 2019) (Fig. 5).

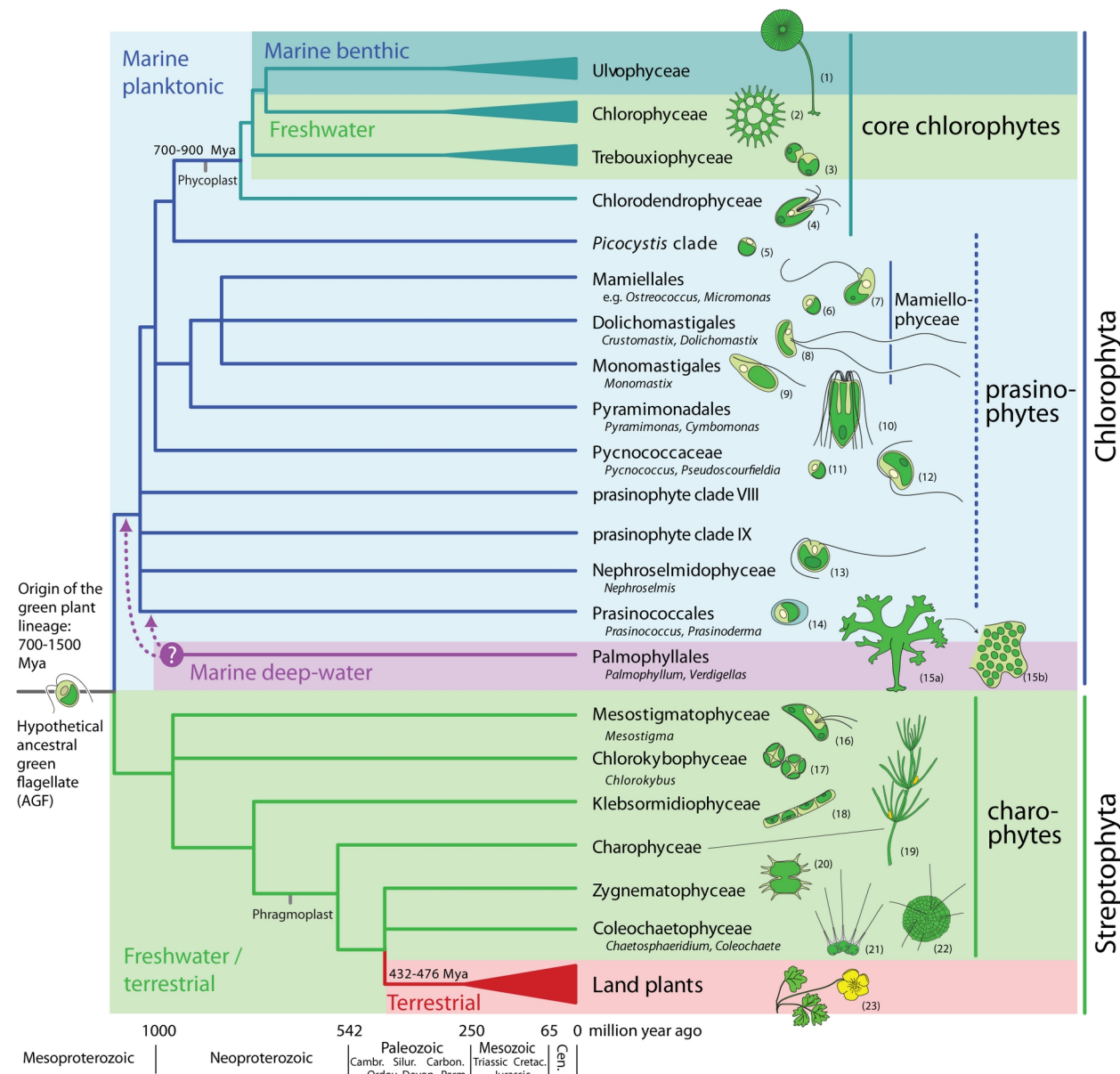


Figure 5: Phylogenetic relationships among the main lineages of green plants. Figure obtained from (Leliaert et al., 2011). The tree topology is a composite on accepted relationships based on molecular phylogenetic evidence. Uncertain phylogenetic relationships are indicated by polytomies. The divergence times are rough approximations based on the fossil record and molecular clock estimates. Drawings illustrate representatives of each lineage: (1) Acetabularia, (2) Pediastrum, (3) Chlorella, (4) Tetraselmis, (5) Picocystis, (6) Ostreococcus, (7) Micromonas, (8) Crustomastix, (9) Monomastix, (10) Pyramimonas, (11) Pycnococcus, (12) Pseudoscourfieldia, (13) Nephroelmid, (14) Prasinococcus, (15) Verdigellas (a: general habit, b: individual cells in a gelatinous matrix), (16) Mesostigma, (17) Chlorokybus, (18) Klebsormidium, (19) Chara, (20) Xanthidium, (21) Coleochaete, (22) Chaetosphaeridium, (23) Ranunculus.

Previous hypotheses posited the domination of the marine waters by the so-called red lineage conformed by diatoms and dinoflagellates, while the green lineage was thought to have less importance in marine water than in terrestrial environments (Worden et al., 2004). These two lineages established their differences a long time ago when the endosymbiotic events took place, giving rise to the green lineage (one single endosymbiotic event) and the red lineage (two or even more endosymbiotic events) (Leliaert et al., 2012). However, in the last decade, metabarcoding studies have completed the previous hypotheses based in microscopic and traditional molecular techniques. These studies have confirmed the importance of the green lineage in marine waters. Also, the cosmopolitan distribution of prasinophytes has been described, especially the older sisters from the order Mamiellales (Collado-Fabbri et al., 2011; Demir-Hilton et al., 2011; Leconte et al., 2020; Tragin & Vaulot, 2019; Worden et al., 2004).

In that taxonomic context is placed *Ostreococcus tauri*, which is considered a green mamiellale microalgae (Fig 5-6). Its contribution to the marine phytoplankton is crucial in a wide range of oceans and seas all over the world (Benites et al., 2021; Collado-Fabbri et al., 2011; Demir-Hilton et al., 2011). As an example, different *Ostreococcus* strains have caused blooms in the Atlantic and Pacific Oceans (O'Kelly et al., 2003; Worden et al., 2004). Furthermore, a certain *Ostreococcus* strain was found to be the most prevalent Mamiellales in the Mediterranean Sea (Tragin & Vaulot, 2019). In spite of its ecologically important role (Chapman, 2013; Worden et al., 2004) and presence in natural environments, *Ostreococcus tauri* is the world's smallest free-living eukaryote known to date (around 1 µm). Due to its small size, *Ostreococcus tauri* have been "invisible" to field researchers for a long time. It was first described in a bloom that took place on the french Thau Lagoon, using flow cytometry. Nowadays, it is known that *Ostreococcus tauri* cells contain a nucleus, only one chloroplast and one mitochondrion, a starch granule and a very reduced or almost non-existent cytoplasmic compartment (Moreau, H, Grimsley, N. Derelle, E, Ferraz, C, Escande, ML, Eychenié, S , Cooke, R, Piganeau, G, Desdevises, Y, Bellec, 1995). ([CITA MAL](#))

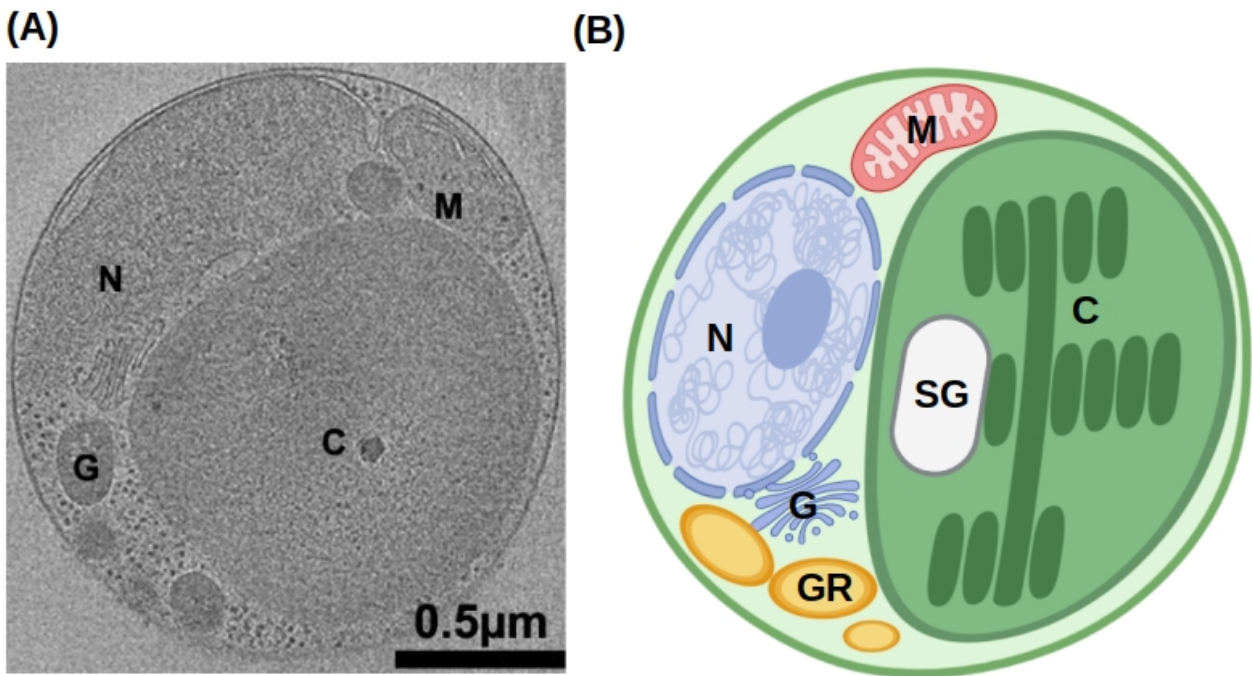


Figure 6: *Ostreococcus tauri*. (A) Tomographic 2D section from an *O. tauri* cell from (Henderson et al., 2012). (B) An illustrated diagram of a *O. tauri* cell based on 3-D segmentation from the same study. Labels: nucleus N, chloroplast C, Golgi body G, mitochondrion M, starch granule SG and granules GR.

Meanwhile, genome sequencing approaches to understand marine phytoplankton were focus on the prokaryote component of it (Berube et al., 2018; Palenik et al., 2003). It wasn't until 2006 when the genome of *Ostreococcus tauri* was sequenced by the first time (Derelle et al., 2006). From that point, an increasing number of picoeukaryotes genomes were sequenced, including a second version of the genome of *Ostreococcus tauri* (Blanc-Mathieu et al., 2014). These contributions allowed the identification of unique aspects of its genome, showing that its simplicity goes among its plain cell structure.

A genome size of 12.56 Mb distributed in 20 chromosomes. Nothing remarkable at first sight since *Saccharomyces* has similar numbers. The fascinating fact comes when the number of genes of these two organisms are compared. With a similar genome size, *Saccharomyces cerevisiae* has around 6275 protein coding genes, while *Ostreococcus tauri* has 8166 (Blanc-Mathieu et al., 2014; Derelle et al., 2006; Engel et al., 2014). This makes *Ostreococcus tauri* the most gene dense free-living eukaryote known to date.

In addition to its short intergenic regions, *Ostreococcus tauri* has reduced the size of gene families keeping only one copy of each gene or even merged different genes in one.

These features contribute to its genome compaction, with the only exception of a long internal duplication on chromosome 19 hypothesized to be of recent origin due to its lack of divergence. Other special features of chromosome 19, as well as chromosome 2, are that they contain 77% of the transposable elements of the genome, they have lower G+C content and even a different codon usage in low G+C content loci of chromosome 2 (Blanc-Mathieu et al., 2014; Derelle et al., 2006). The first hypotheses about these chromosomes were that they had a different origin than the rest of the genome. Currently, only the chromosome 19 is considered an “alien” chromosome since the most of its protein coding genes are not related to the green lineage. However, chromosome 2 protein coding genes are essential housekeeping genes not duplicated and related to the green lineage, so from that point it started to be considered a sex-related or mating-type chromosome (Benites et al., 2021; Blanc-Mathieu et al., 2014) .

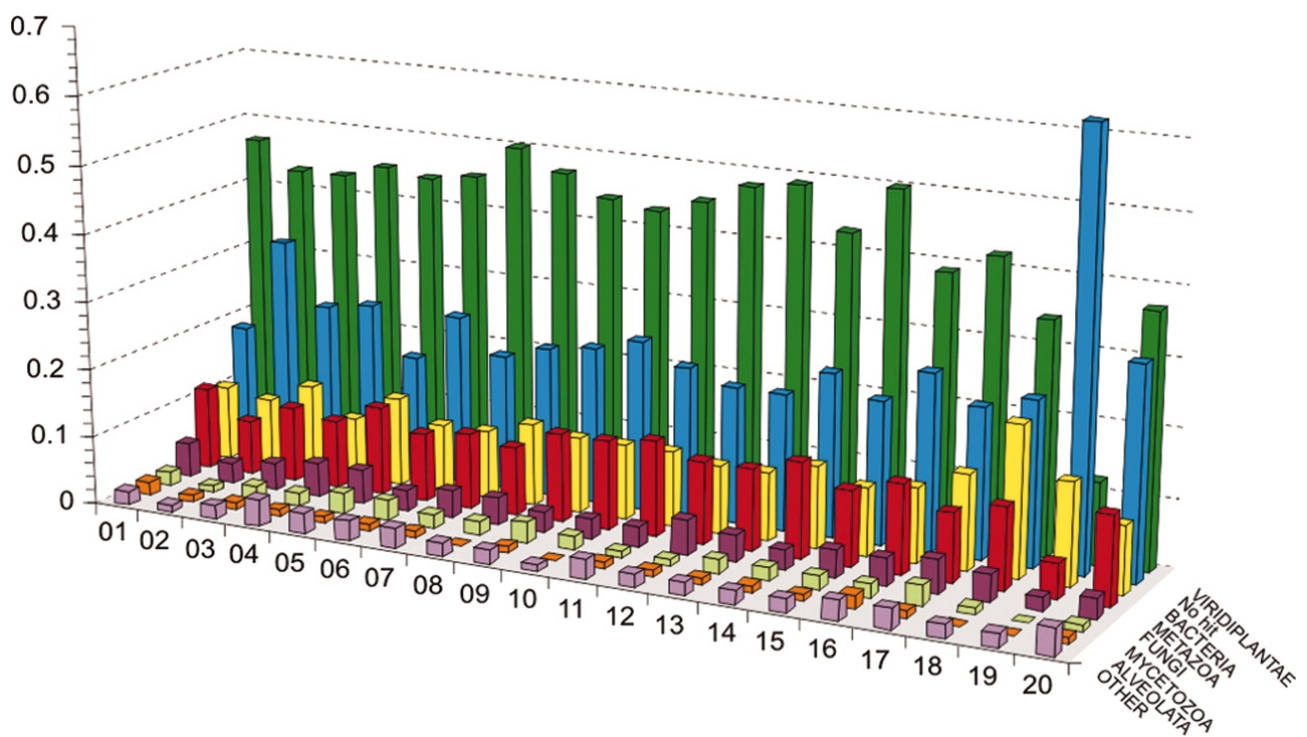


Figure 7: Taxon distribution of best hits for genes from each of the *O. tauri* chromosomes. Figure from (Derelle et al., 2006). The number corresponding to each chromosome is represented in the x axis, the percentage of best hits is represented in y axis. Each color stands for: viridiplantae, green; no hit, blue; bacteria, yellow; metazoa, red; fungi, purple; mycetozoa, light yellow; alveolates, orange; others, light purple.

Although sex is now accepted as a ubiquitous and ancestral feature of eukaryotes (Sekimoto, 2017; Swanson et al., 2011), direct observation of sex is still lacking in most unicel-

lular eukaryotic lineages. These type of genomic regions so-called mating-type has been characterized in other Chlorophyta (Sekimoto, 2017) and, recently, in *Ostreococcus tauri*, which appears to encode two highly divergent haplotypes. These Mamiellales mating-types regions candidates are likely to be the oldest mating-type loci described to date (Benites et al., 2021; Leconte et al., 2020).

Overall, *Ostreococcus tauri* is proposed as a novel model organism due to its structural and genomic features. In addition, inside the green lineage there is a lot of diversity and actually it is difficult to find a model organism that can represent the hole lineage (Cock & Coelho, 2011). However, its taxonomy classification makes *Ostreococcus tauri* a potential green lineage ancestor (Derelle et al., 2006; Leliaert et al., 2012) and the knowledge gained using it can be easily extrapolated to a wide range of photosynthetic organisms.

In Systems Molecular Biology research massive data are generated to study complete biological systems. Working with complex organisms can be a problem since the system of study would be maximize (De Keersmaecker et al., 2006; Jamers et al., 2009; Joyce & Palsson, 2006; Weckwerth, 2011). When *Ostreococcus tauri* is compared with other microalgae that are already sequenced and had been used as model organisms, it turns clear the simplification that it brings to Systems Molecular Biology studies (de los Reyes, Romero-Campero, Ruiz, et al., 2017; Derelle et al., 2006; Krumholz et al., 2012; Le Bihan et al., 2011; Lelandais et al., 2016).

Table 1: Genomic features of different green lineage model organisms. Their genome size and protein coding genes (Blaby et al., 2014; Blanc-Mathieu et al., 2014; Craig et al., 2021; Derelle et al., 2006; Hori et al., 2014; Lamesch et al., 2012; Swarbreck et al., 2008; M. Yang et al., 2018) are compared with their number of predicted transcription factors. (Rayko et al., 2010; Zheng et al., 2016)

	Genome size (Mb)	Number of protein coding genes.	Number of transcription factors.
<i>Arabidopsis thaliana</i>	135	27474	1779
<i>Klebsormidium nitens</i>	104	17055	286
<i>Chalmydononas reinhardtii</i>	110	14000	279
<i>Phaeodactylum tricornutum</i>	27.4	10567	212
<i>Ostreococcus tauri</i>	12.56	6275	102

Ostreococcus tauri allowed us to generate, analyze and interpret massive data from the complete system with less computational and experimental costs, so a holistic understanding of the chronobiology in this mammelleale was finally achieved.

Systems Biology

In the last 50 years, sequencing methods have been exponentially improved. First-generation DNA sequencing methods were developed about 45 years ago. In addition, one of the most biggest international projects, the Human Genome Project, started 20 years ago (Ideker et al., 2001; Veenstra, 2021). In this project an extremely ambitious idea was pursued: to sequence the hole human genome. However, its impact in science transcends beyond that goal. Different groups cooperated all over the world, not only to sequence the complete human genome, but to develop new sequencing methods in order to make the process easier and cheaper (Abascal et al., 2020).

During the Human Genome Project, 13 years were needed to sequence a single complete human genome and the overall costs were 2.7 billion dollars. Currently, with the emergence of next-generation sequencing methods, around 100000 human genomes have been sequenced in the last 6 years. The Illumina HiSeq System generates around 500 gigabase sequences per second, dropping the cost of sequencing a complete human genome to \$1500 in only 10 years of difference (Prendergast et al., 2020; Veenstra, 2021). Ultimately, it changed how science was approached.

All these new approaches led to a mass development of methods to sequence and identify the complete transcriptome (total mRNAs transcripts). Sequencing of complete transcriptomes offered a massive amount of information never seen before. However, genes and their products (proteins) are highly related since they interact and regulate each other forming positive and negative feedback loops, so still a lot of information was missing. Researchers began to understand organisms and processes as systems with important modules (mRNA, proteins, metabolites, etc) that interact with each other forming parts of large networks (Joyce & Palsson, 2006; Veenstra, 2021; Weckwerth, 2011).

While this holistic view of biological systems were gaining strength, traditional reductionist methods (focusing in only one gene, protein or metabolite) were the most popular and affordable ones. Scientific research was limited by the time and effort needed to integrate all events that take place simultaneously within a biological system from a set of individual results (Karahalil, 2016; Mazzocchi, 2012; Veenstra, 2021). There is an ancient Indian fable that illustrate how a holistic view and ontological reasoning contributes to knowledge, it is

called "Blind men and an elephant". A poem of John Godfrey Saxe is one of the most famous written versions of it:

" It was six men of Indostan
To learning much inclined,
Who went to see the Elephant
(Though all of them were blind),
That each by observation
Might satisfy his mind.

The First approached the Elephant,
And happening to fall
Against his broad and sturdy side,
At once began to bawl:
"God bless me! but the Elephant
Is very like a wall!"

The Second, feeling of the tusk,
Cried, "Ho! what have we here
So very round and smooth and sharp?
To me 'tis mighty clear
This wonder of an Elephant
Is very like a spear!"

The Third approached the animal,
And happening to take
The squirming trunk within his hands,
Thus boldly up and spake:
"I see," quoth he, "the Elephant
Is very like a snake!"

The Fourth reached out an eager hand,
And felt about the knee.
"What most this wondrous beast is like
Is mighty plain," quoth he;
"This clear enough the Elephant
Is very like a tree!"

The Fifth, who chanced to touch the ear,
Said: "E'en the blindest man
Can tell what this resembles most;
Deny the fact who can
This marvel of an Elephant
Is very like a fan!"

The Sixth no sooner had begun
About the beast to grope,
Than, seizing on the swinging tailgeneraliza-
tions
That fell within his scope,
"I see," quoth he, "the Elephant
Is very like a rope!"

And so these men of Indostan
Disputed loud and long,
Each in his own opinion
Exceeding stiff and strong,
Though each was partly in the right,
And all were in the wrong! (...)"

After touching different parts of the animal, one of them concluded that the elephant was like a snake (he was touching only the elephant's trunk), another one concluded that it was like a fan (since he was only touching the animal's ear), and so on. Each of them were sure about their findings, but reaching an agreement was impossible since they did not treat their collected data as parts of a complex system, instead of independent truths.

During a long time in scientific research, systems biology studies that would bring that holistic view of living systems have been impossible to achieve due to a lack of technologies available. The development of systems biology is related to technology advances (Fig. 8) such as computational science, artificial intelligence and, the already mentioned, next-generation sequencing methods (Ideker et al., 2001; Karahalil, 2016; Veenstra, 2021; Weckwerth, 2011).

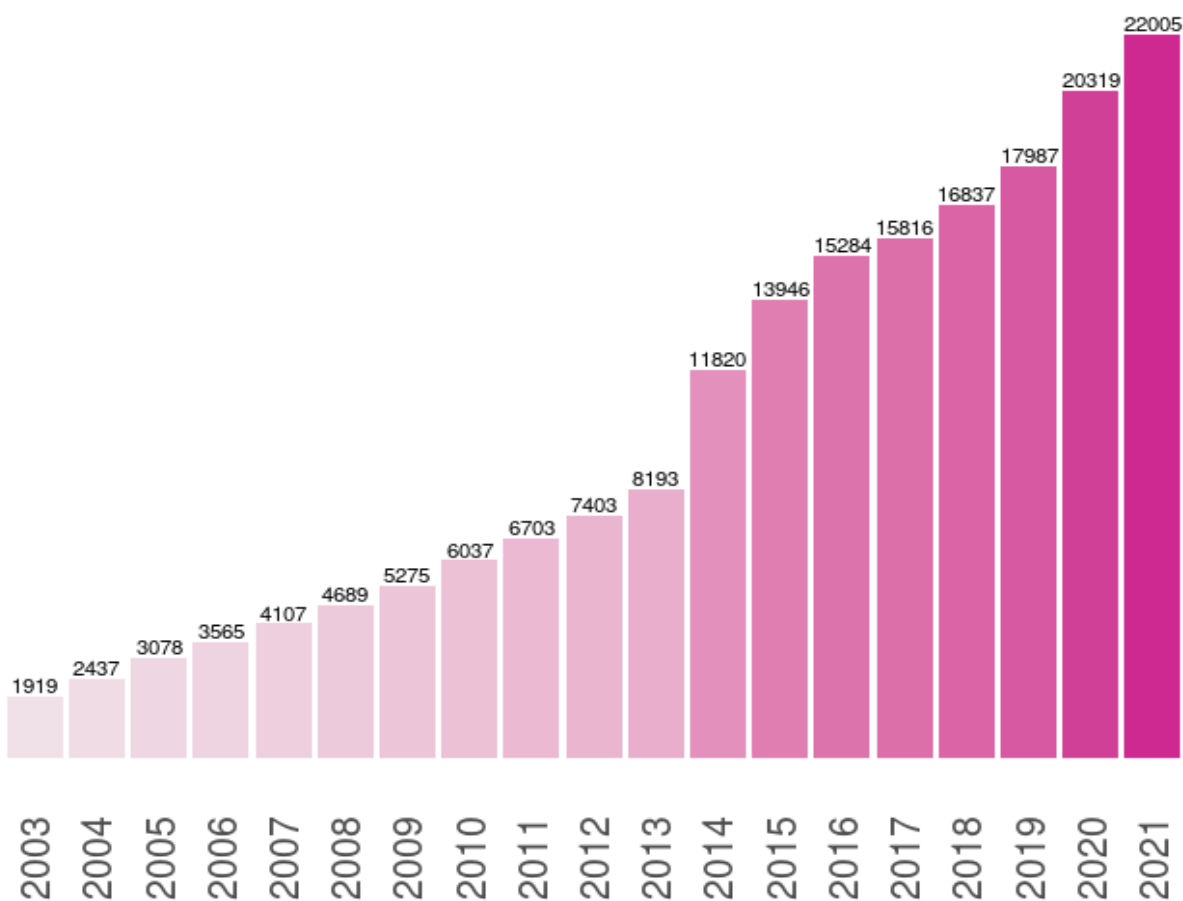


Figure 8: Publications on systems biology. Exponential increase in the number of publication using the term "systems biology" in PubMed since the year when the Genome Human Project was completed (2003). The number on the top of each bar corresponds to the exact number of publications of that year.

Nowadays, the so-called omics methods made it possible to massively measure all those important modules or biological levels that form part of the studied systems: transcriptomics, proteomics, metabolomics, etc. Systems biology aims to improve our understanding of living systems through the integration of our knowledge on how different biological components work simultaneously. The typical methodology of a systems biology study starts by obtaining omic data and its subsequent integration. Then, the results are computationally and statistically analyzed and the phenomenons observed are experimentally probed. Consequently, predictive models can be developed in order to simulate how a biological system would behave when perturbed (Jamers et al., 2009; Veenstra, 2021; Weckwerth, 2011; Zurbriggen et al., 2012).

During the progression of this work, the generation and analysis of massive data from two different omics techniques (transcriptomics and proteomics) is achieved. The main purpose is studying *Ostreococcus tauri* as a biological system by integrating the omics results with traditional physiological measurements as a biological validation of the effects observed in the computational analysis.

Specifically, the transcriptomic method used was RNA-seq, which is the main contemporary method used for this omic. The development of next-generation sequencing methods has contributed to RNA-Seq analyses enabling working with a wide variety of different classes of RNAs, not requiring transcript-specific probes (unlike microarrays, the almost obsolete previous method used in transcriptomic analyses), and not only to identify but also to quantify abundance of transcripts (Ditz et al., 2021; Veenstra, 2021; Wang et al., 2009).

Meanwhile, the field of proteomics have been directly connected with the development of mass spectrometry (MS) technology. During the first part of the century, there were two lines of development working separately for what would be known as proteomics today: identification (2-D electrophoresis gel) and quantification (using isotope tags) of proteins. Nowadays, technology has enable the development of proteins identification and quantification methods so the number of proteins that can be quantified/identified today is around several thousands (Shen et al., 2022; Veenstra, 2021). In this thesis, a large scale proteomic analysis is achieved by SWATH using liquid chromatography MS / MS. SWATH

proteomics enables protein identification and characterization, as well as label free relative quantification (M. X. Chen et al., 2021; Ludwig et al., 2018).

Currently, the era of systems biology is increasing the amount of data generated per study and, consequently, the computational and mathematical knowledge required to analyze and integrate these results increases too. Unfortunately, most laboratories are not historically designed to incorporate these requirements yet due to a lack of qualified researchers gathering solid knowledge from the different disciplines needed: computational sciences, mathematics/statistics and molecular biology. The last new generations of young researchers are working to develop software applications, efficient data analysis algorithms and user-friendly app-tools to enable the progress of systems biology studies making it more accessible for the hole scientific community (Coleto-Alcudia & Vega-Rodríguez, 2020; Romero-Campero et al., 2016; Romero-Losada et al., 2022).

Systems biology studies in microalgae have been recently started and there is a lack of tools for microalgae to analyze and interpret omics data. One of the objectives of this doctoral dissertation is to contribute to the progression of systems biology studies in the microalgae research community developing the web-app ALGAEFUN with MARACAS. In that way, any researcher can analyze and functional annotate RNA-seq and ChIP-seq data without previous knowledge in computational or mathematical analysis (Romero-Losada et al., 2022).

In summary, this doctoral thesis aims to contribute to the microalgae research community with two major items: the development of free and open source tools that facilitates systems biology studies in microalgae and the understanding of the diurnal and seasonal rhythmic changes in *Ostreococcus tauri* as a complete system knowing the expressed genes, the proteins present and how the main functions are being executed.

Materials and Methods

Organism and culture growth conditions.

Organism and growth medium.

The sequenced strain of *Ostreococcus tauri*, RCC4221, was used in this study. Sterilized artificial sea water (ASW) (Kester et al., 1967) supplemented nitrogen source, potassium source and vitamins were used as growing medium. A complete list of media components and concentrations needed to grow *Ostreococcus tauri* are described in Table 2.

Table 2: List of media components used in this study as growing medium for *Ostreococcus tauri* cultures.

	Concentration in solution	Concentration in medium
Solución I	400 g/L NaNO ₃	222.22 mg/L NaNO ₃
Solución II	2.8 g/L Na ₂ HPO ₄ 10 g/L K ₂ HPO ₄	1.56 mg/L Na ₂ HPO ₄ 5.56 mg/L K ₂ HPO ₄
Solución III	5.36 g/L NH ₄ Cl 10.4 g/L Fe-EDTA 74.4 g/L Na ₂ -EDTA 4.6·10 ⁻² g/L ZnSO ₄ 2.8·10 ⁻² g/L CoSO ₄ 1.6·10 ⁻² g/L Na ₂ MoO ₄ · 2H ₂ O 5.0·10 ⁻³ g/L CuSO ₄ 3.4·10 ⁻² g/L H ₂ SeO ₃ 3.6·10 ⁻² g/L MnCl ₂ · 4H ₂ O	2.98 mg/L NH ₄ Cl 5.78 mg/L Fe-EDTA 41.33 mg/L Na ₂ -EDTA 2.56·10 ⁻² mg/L ZnSO ₄ 1.56·10 ⁻² mg/L CoSO ₄ 8.89·10 ⁻² mg/L Na ₂ MoO ₄ · 2H ₂ O 2.78·10 ⁻³ mg/L CuSO ₄ 1.89·10 ⁻² mg/L H ₂ SeO ₃ 2.0·10 ⁻² mg/L MnCl ₂ · 4H ₂ O
Solución IV	0,2 g/L Thiamin-HCl 1.50·10 ⁻³ g/L Biotin 1.50·10 ⁻³ g/L Cyanocobalamin	0.22 mg/L Thiamin-HCl 1.67·10 ⁻³ mg/L Biotin 1.67·10 ⁻³ mg/L Vitamin B12

Continuous culture conditions in photochemostats.

Photochemostats or photobioreactors consisting in bubble column with a volume of 1.8 L of capacity (7 cm diameter, 47 cm height) were used for continuous regime cultivation in the laboratory. A detailed description of their design is represented in Figure 9. Each photochemostat is inoculated with the same cell concentration and are kept at batch regime during several days to ensure its adaptation before starting a continuous regime.

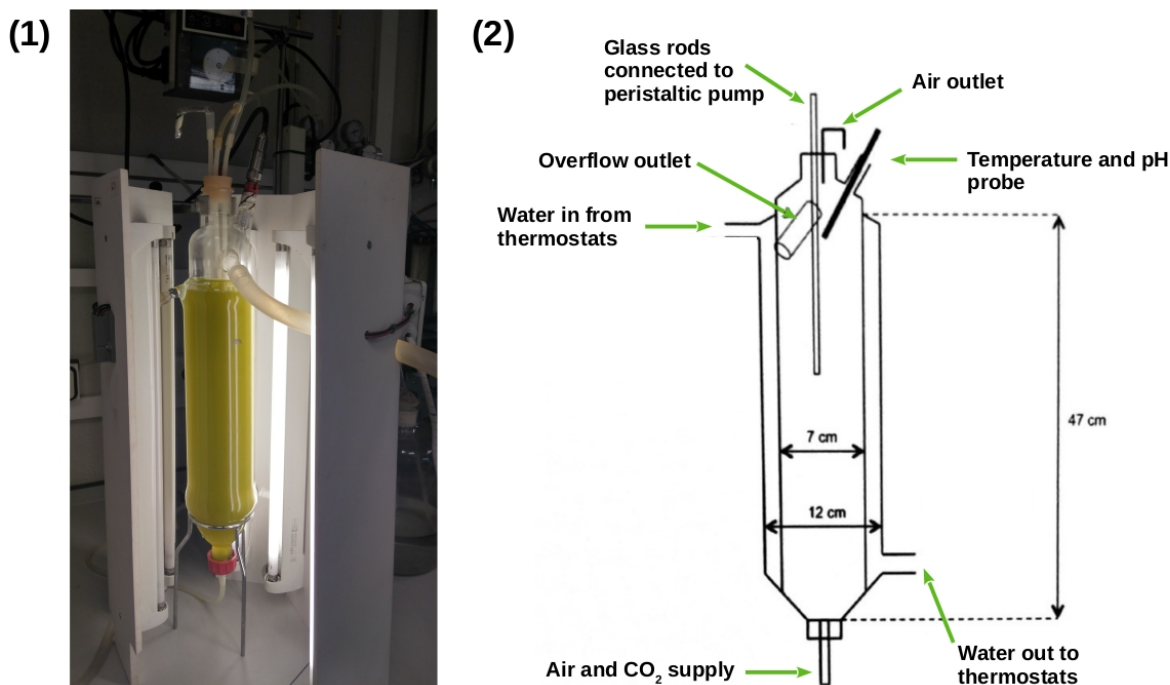


Figure 9: Growth system used for continuous cultures. (1) Picture of one of the photochemostats used. (2) Schematic detailed design of photochemostats.

Photochemostats were provided with a double wall forming a water jacket circulating from a bath that kept the culture temperature constant at 20°C. Air and CO₂ supply through the base of the chemostat ensured an optimal neumatic agitation. The air flow rate was regulated by a rotameter, adding 1 L air L culture 'min⁻¹ (no entiendo este dato).

Culture conditions were constantly measured and computationally controlled by a Lab-Jack: pH, dilution rate and illumination regime. For pH control, the reactor was equipped with a combined pH electrode (Crison, model 3100/225), connected to a pH controller (Crison, model pH 217/220-R1). The controller opened a electrovalve when the pH exceeded the threshold value stablished, allowing pure CO₂ to pass through along with the air stream. Once the pH value was recovered, the electrovalve was closed, leaving the culture medium in neumatic agitation exclusively by the described air supply.

To operate in continuous mode, the upper part was closed with a silicone cover fitted with glass rods of 4 mm internal diameter that reached the middle part of the reactor, allowing the supply of fresh medium. The dilution rate were maintained constant at 0.3 d⁻¹ (overflow is discarded to avoid volume increase) by a peristaltic pump (P-3, Pharmacia) in order to

keep photobioreactors in steady state. Cultures at steady state with 45 µg/mL chlorophyll content were used in our experiments. When a photobioreactor reaches the steady state it means that the culture is growing at exponential phase but a constant concentration of cells is reached. This allows to take samples during long periods of time without changing the culture conditions.

In addition, instead of a sudden transition from dark to light and from light to dark, our Lab-Jack controlled system gradually increased light until an irradiance of $1500 \mu\text{E m}^{-2} \text{ s}^{-1}$ is reached simulating the natural photoperiod (Fig. 10). Each photochemostat is illuminated using six Phillips PL-32 W/840/4p white-light fluorescent lamps. Furthermore, they are surrounded by a wooden box and a completely opaque fabric to avoid any external light input.

Experimental design.

The study focused on the two extreme photoperiods: summer long day conditions (LD, 16h light : 8h dark) and winter short day conditions (SD, 8h light : 16h dark). The experimental design (Fig. 10) consisted of three days under long day or short day conditions followed by three days under free running conditions (constant light or constant dark). Cells were harvested at specific times in the daily cycle, expressed in zeitgeber time (ZT), where ZT0 corresponds to dawn, ZT4 to 4h after dawn and so on. In this study, samples were taken every 4h (from ZT0 to ZT20) during the three days of alternating light/dark cycles, so there is a total of 6 samples for each day of sampling. No samples were collected during the first day of free running condition to allow culture acclimation. Then samples were collected once again every four hours starting at subjective dawn during two days.

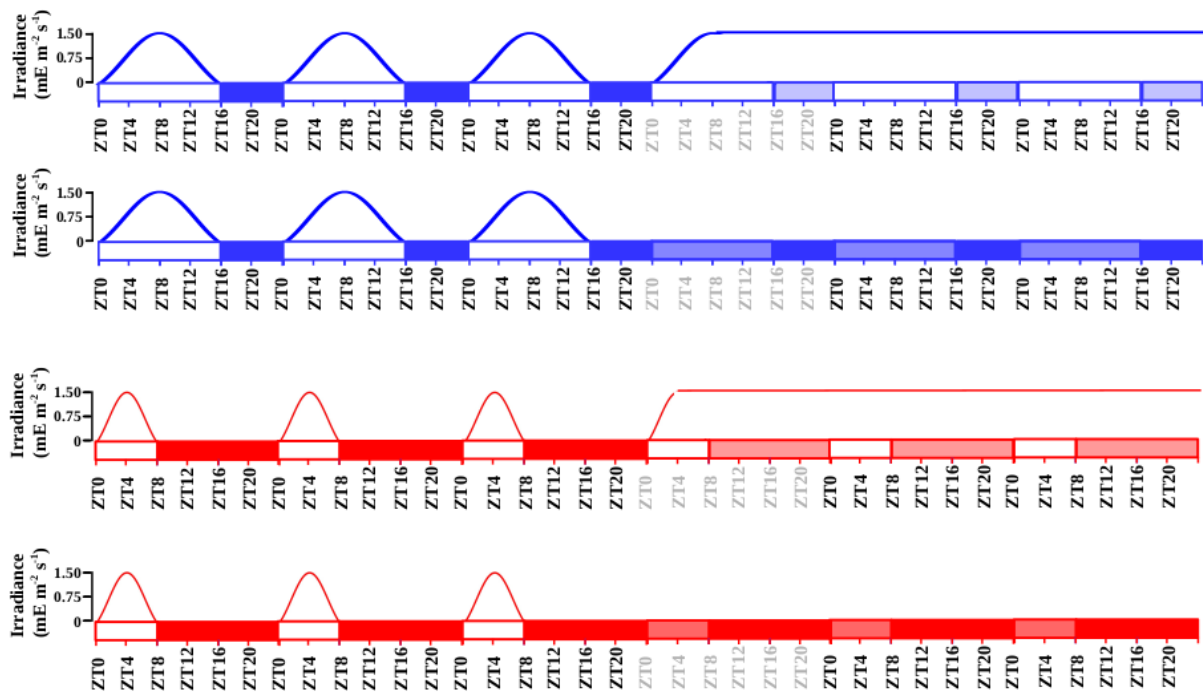


Figure 10: Schematic description of the experimental design. Gradually increased and decreased irradiance is represented during each light phase. Long day conditions are represented in blue and short day conditions in red. Photoperiods (light periods) correspond to white rectangles and skotoperiods (dark periods) to blue/red filled rectangles. Light blue and red filled rectangles are used to represent subjective photoperiods and skotoperiods under free running conditions.

Transcriptomic analysis

Sample Collection

From each chemostat, a volume of 50mL of cell suspension were harvested (4 min centrifugation at 5000 x g and 4°C) for each time point. Pellets were washed using Phosphate-buffered saline solution (PBS) and flash frozen with liquid Nitrogen before stored at -80°C.

Cell disruption

Frozen pellets were resuspended in 400 µL of disruption buffer (García-Domínguez & Florencio, 1997) and directly added to a 1,5 mL Eppendorf tube (RNase free and phenol-proof) containing 400 µL of phenol:chloroform 1:1 and 100 µL of acid washed glass beads

(0.25–0.3 mm diameter; Braun, Melsungen, Germany). Mechanical disruption was performed by 30 min of repeated cycles of 60 s of vortexing and 60 s of incubating on ice.

RNA extraction

The tubes containing cellular extracts, disruption buffer, phenol:chloroform and acid washed glass beads were centrifuged (4 °C) for 15 min at 13000 x g. Three different phases appear after the centrifugation: an upper aqueous phase containing RNA, a white interphase containing DNA and a lower organic phase containing proteins, lipids and glass beads. The upper aqueous phase is collected and added to a new tube containing 400 µL of phenol:chloroform 1:1. This process was repeated three times more with centrifugations of 5 min, followed by a step using only chloroform to avoid phenol contamination of the samples. Finally the supernatant is incubated overnight at -20 °C in a solution of 80 µL 10 M LiCl and 550 µL of 100% EtOH for RNA precipitation.

After incubation, samples were centrifuged 10 min at 13000 x g and 4°C. Pellets were dried to avoid EtOH contamination.

RNA purification

RNA purification was performed using the Isolate II RNA Plant Kit (Bioline). Washing, DNase treatment and elution were carried out following the manufacturer instructions. The final RNA concentration and integrity were measured using a bioanalyzer 2100 (Agilent RNA 6000 Nano Kit).

RNA sequencing and processing

Library was prepared in accordance with the manufacturer's instructions and the sequencing was carried out on the Illumina NextSeq500 sequencer. Approximately, 10 million 75nt long single end reads were generated for each sample. The *Ostreococcus tauri* genome sequence and annotation v3.0 were used as reference genome (Blanc-Mathieu et al., 2014). Futher computational analysis were carried out using MARACAS from ALGAEFUN with MARACAS (Romero-Losada et al., 2022).

Proteomic analysis

Sample collection

From each chemostat, a volume of 50mL of cell suspension were harvested (4 min centrifugation at 5000 x g and 4°C) for each time point. Pellets were washed using Phosphate-buffered saline solution (PBS) and flash frozen with liquid Nitrogen before stored at -80°C.

Cell disruption

Directly onto frozen pellets, 1 mL of Trizol, 100µL of acid washed glass beads (0.25–0.3 mm diameter; Braun, Melsungen, Germany) and 40µL of Protein Inhibitor Cocktail PIC (25x) were applied. Followed by 3 disruption cycles (60s agitation-60s incubation on ice) using a Mini-Beadbeater (BioSpec Products).

Proteins extraction

Proteins were extracted using TRI Reagent (Sigma-Aldrich), according to the manufacturer's instructions. The resulting proteins pellets were washed with 2mL of 0.3 M guanidine solution in 95% EtOH. They were resuspended by 10min of sonication (**falta modelo**) cycles (30 s sonication - 30 s of incubating at 4 °C) and then centrifugated at 4 °C during 5 min at 8000 x g. This washing process was repeated twice, followed by two additional washing using 90% EtOH instead of the guanidine solution. The final pellets were resuspended in ammonium bicarbonate 50 mM/0.2% Rapidgel (Waters) and total proteins were quantified using Qubit system.

Proteins digestion.

Of each samples, 50 µg of proteins were incubated with DTT (final concentration 4.5 mM) for 30 min at 60 °C. Then, iodoacetamide to a final concentration of 10 mM were added to continue the incubation for 30 min more, under total darkness at room temperature. The treatment with trypsin was done overnight at 37 °C in a 1:40 trypsin:protein. After that, formic acid (**concentración?**) was added and incubated at 37°C for 1h. Finally, 2% acetonitrile (v/v) were added to reach a concentration of the digested sample around 0.5 µg of protein/µl of solution.

SWATH acquisition

Equipment and data acquisition method.

The analysis were performed on a time-of-flight TOF triple quadrupole hybrid mass spectrometer MS (5600 plus, Sciex) equipped with a nano electrospray source coupled to an nanoHPLC Eksigent model 425. The Sciex software Analyst TF 1.7 was used for equipment control and data acquisition. Peptides were first loaded onto a trap column (Acclaim PepMap 100 C18, 5 µm, 100 Å, 100 µm id × 20 mm, Thermo Fisher Scientific) under iso-cratical order in 0.1 % formic acid/2% acetonitrile (v/v) at a flow rate of 3 µL/min for 10 min. Subsequently, they were eluted on a reversed-phase analytical column, with the built-in emitter (New Objective PicoFrit column, 75 µm id × 250 mm, packed with ReproSil-PUR 3 µm). In the case of the samples corresponding to the short day conditions, the analytical column was Acclaim PepMap 100 C18, 3 µm, 100 Å, 75 µm id × 250 mm, Thermo Fisher Scientific, coupled to a PicoTip emitter (F360-20-10-N-20_C12 from New Objective). Peptides were eluted with a linear gradient of 5-35 % (v/v) of solvent B in 120 min at a flow rate of 300 nL/min. Formic acid 0.1 % (v/v) was used as solvent A and acetonitrile with formic acid 0.1 % (v/v) were used as solvent B. The source voltage was selected at 2600 V and the temperature was maintained at 100 °C. Gas 1 was selected at 20 PSI, gas 2 at zero, and curtain gas at 25 PSI.

For proteins identification, Data Dependent Acquisition DDA method were used. It consisted of a TOF-MS with a scan window of 400-1250 m/z (accumulation time of 250 ms) followed by 50 MS/MS with a scan window of 230-1500 m/z (accumulation time of 65 ms) and with a cycle time of 2574 s.

Library construction

The spectral library was constructed by making 1 run with a mixture of the biological replicates corresponding to each time point (ZTO, ZT4, ZT8, ZT12, ZT16, ZT20) with the DDA method described. ProteinPilot v5.0.1 software (Sciex) was used to identify the proteins in the library. A pooled search of all runs was performed. The parameters of the Paragon method were: trypsin as enzyme and iodoacetamide as cysteine alkylating agent.

The Ostreococcus tauri annotated proteome file from ORCAE (Sterck et al., 2012) linked to a Sciex Contaminants database were used in library construction. A false positive analysis (FDR) was performed and those with FDR < or equal to 1 were considered.

SWATH runs

For each sample, the equivalent of 1 µg of digested protein was injected into each run. Before that, a standard (MS synthetic peptide calibration kit from Sciex) was injected to self-calibrate the equipment, control the sensitivity and chromatographic conditions. The described DDA method was used for SWATH runs with 60 ms of accumulation time and 3.7 s of cycle time. (preguntar a rocio si cambia el metodo o no)

Data processing

The library generated by DDA (1 % FDR) was used in the analysis performed using the Sciex software PeakView 2.2 with the microapp SWATH 2.0, together with the data obtained from the SWATH runs. Using this program, the chromatographic traces of the ions were extracted and dumped into the Marker view 1.2.1.1 program where the list of identified proteins with their corresponding areas was generated. The parameters for extraction of ions and obtaining the areas were: 10 peptides per protein, 7 transitions of each peptide, threshold of confidence of the peptides set at 90 and FDR 1%. The parameters for extraction of the ions and obtaining the areas were: 10 peptides per protein, 7 transitions of each peptide, threshold of confidence of the peptides set at 90 and FDR 1%.

The software NormalizerDE 1.6.0 (Willforss et al., 2019) was used to test several normalization methods in order to probe which one achieved the minimum replicate variation relative to Log2. Quantile normalization was selected as normalization method based on this comparison. Data were imputed with mean (mean imputation method), which means that the missing value on a certain variable is replaced by the mean of the available cases.

Cell cycle analysis

Sample collection and cell fixation method

A volume of 1.5mL of cell suspension were harvested for each time point. These samples were diluted 1:10 in PBS to be sure the cell concentration is suitable to the assay. Two mL of these dilutions were centrifugated (**condiciones??preguntar a Meriyou**) and cells in the pellets were fixed with 10 mL of 100% EtOH before stored at -20°C for at least 24h.

Cell staining method

After fixation, cell suspensions were centrifuged for 5 min at 3500 x g (room temperature) and resuspended in 1 mL of PBS. They were washed once with PBS and sonicated for 3 minutes in a Ultrasonic Cleaner (JSP, US21, ultrasonic power 50W), in order to eliminate cell clumps and aggregates before staining.

In the staining process, 2 μ L of the Vibrant DyeCycle Green (V35004, ThermoFisher) were added to each sample and incubated 30 min (37°C) for DNA labeling. Final stain concentration was 10 μ M. Treatment with RNase was not necessary as Vibrant DyeCycle Green is a DNA-selective stain. After incubation, cells were washed ([con qué???](#) preguntar a meriyou) and transferred to flow cytometry tubes for cell cycle analysis.

Data acquisition and processing

Flow Cytometry acquisition were performed with a BD FACS Canto II (BD Biosciences) where stained DNA were excited by a 488nm laser and emission was collected in a 530/30 nm PMT. Flow rate was low and linear amplification were established for the acquisition.

Data were analyzed using FlowJo v.10.6.1 (Becton Dickinson & Company BD). Analysis was performed using one of the univariate cell cycle platform that FlowJo provides, specifically the Watson pragmatic algorithm (Watson et al., 1987) to adjust the data to the model.

Analysis of photosynthetic activity

Sample collection

Fresh culture was harvested at the different specific times of the day. The samples were diluted 1:1 with growing medium and incubated at 20 °C in total darkness during 10 min.

Data acquisition

In order to analyze photosynthetic parameters, Pulse-Amplitude-Modulation PAM fluorometry measurements were performed using a Waltz DUAL-PAM-100. After the darkness incubation, the non-actinic modulated light (450nm, 2.8 μ E μ E m⁻² s⁻¹) was turned on in order to measure F_o (fluorescence basal level). Then, to determine F_M (the maximum fluorescence level), a saturating red light pulse of 655nm and 5000 μ E m⁻² s⁻¹ is applied to the

sample during 400ms. The F_v/F_M , that corresponds to the maximum potential quantum efficiency of Photosystem II when all reaction centers were open, was calculated as:

$$\frac{F_v}{F_M} = \frac{(F_M - F_o)}{F_M}$$

Analytical determinations

Sample collection

At each time point, 50 mL of fresh culture was harvested and centrifuged at 7000 x g **during 10 min**. Then pellets were washed with 1% ammonium formate (p/v) to eliminate salts from the growing medium and lyophilized.

Starch Content

Cell disruption

Approximately 2-3 mg of lyophilized biomass of each sample was added to hermetic tubes containing 1 mL of glass beads (0.25–0.3 mm diameter; Brau n, Melsungen, Germany) and 2 mL of chloroform:methanol (2:1). Three disrupting cycles (60s agitation-60s incubation on ice) were applied to the samples using Mini-Beadbeater (BioSpec Products). Then cellular extracts were separated from the beads and saved in new tubes. Cellular extracts were centrifuged for 4 min at 13000 x g and the supernatant was discarded. The addition of chloroform:methanol (2:1) and centrifugation steps were repeated until the pellets were white in order to ensure the elimination of pigments and lipids that could disturb the determination process. Finally, pigment free pellets were dried.

Starch solubilization and digestion

Proposed protocol for plants in (Rufty & Huber, 1983) was adapted to *Ostreococcus tauri*.

Starch granules in dry pellets were alkaline solubilized with 1mL of 0.2 M KOH and heated at 100 °C. After 30 min, samples were gradually cooled and pH was adjusted to 5.0 by adding 300 µL of 1 M acetic acid.

Starch digestion involves the breakdown by 7.4 U of α-amylase to small linear and branched oligosaccharides during a 30 min incubation at 37°C; and the release of glucose

residues by 5 U of amyloglucosidase during 1-2 h incubation at 55 °C. Both diluted in 0.1 M of sodium acetate pH 4.5 were added to 200 µL of each sample. Finally, in order to stop enzymatic reactions, the samples were incubated at 100 °C for 2 min and centrifuged at 13000 x g for 10 min to discard any pellet.

Spectrophotometric quantification

The quantification of released glucose residues from starch was achieved following (Rufy & Huber, 1983) protocol. They propose the combination of two different enzymatic activities: hexoquinase that phosphorylates glucose residues; and glucose-6-phosphate dehydrogenase (G6PDH) that reduce NAD⁺ using the phosphorylated glucose generated by the hexoquinase. NADH absorbance can be measured at 340nm and its concentration is related to glucose residues concentration 1:1 (Fig. 11).

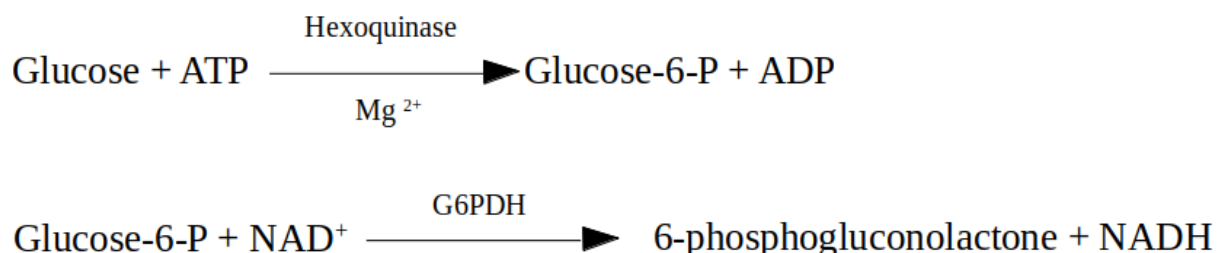


Figure 11: Enzymatic activities that link NADH production to glucose residues released from starch.

To achieve that measurement, quartz spectrophotometer cuvettes were filled with :

- 100 µL of the sample
- 500 µL of hexoquinase buffer (100mM HEPES pH 7.7, 10 mM MgCl₂, 0.04% BSA p/v, 1mM DTT)
- 100 µL of ATP mix (containing 10mM ATP diluted in Hepes 100 mM ph 7.7)
- 100 µL of NAD⁺ mix (containing 4 mM NAD⁺ diluted in Hepes 100 mM ph 7.7)
- 2 µL of 2.5 U µL⁻¹ glucose-6-phosphate dehydrogenase
- 200 µL of destile water.

The absorbance of that mixture was measured at 340 nm twice. The first measure is followed by the addition of 5 μ L of 1 U μ L $^{-1}$ hexokinase enzyme and the incubation at 27 °C for 20 min to ensure the efficiency of the reaction. The second measure was used to calculate the amount of NADH produced during the reaction. Using calibration curve based on processed samples that contained known concentrations of starch, NADH absorbance is related to the amount of glucose residues and consequently to the initial amount of starch in each the sample.

Carotenoid Content

Cell disruption

Four milligrams of lyophilized biomass was added to an hermetic tube containing 1 mL of glass beads (0.25–0.3 mm diameter; Braun, Melsungen, Germany) and 1 mL of pure acetone. Three disrupting cycles (60s agitation-60s incubation on ice) were applied to the samples using Mini-Beadbeater (BioSpec Products).

Carotenoids extraction

Carotenoids extraction was achieved following (Del Campo et al., 2004) proposed method. Darkness was maintain during the entire process to avoid pigments degradation.

Cellular extracts were collected and saved in new tubes after a 4 min centrifugation of the samples at 13000 x g. This process was repeated six times or until the supernatant turns colorless. Supernatans of each sample were joined in the same tube (one per each sample) and acetone were evaporated using a stream of nitrogen gas. Finally, 350 μ L of acetone were added to each tube, and if was distributed in HPLC tubes following manufacturer's instructions.

Carotenoids determination and quantification

A Hitachi HPLC (Elite LaChrom), equipped with a photodiode-array detector (Hitachi L-2455) was used. Separation was performed on a Waters NovaPak C-18 (3.9×150 mm, 4 μ m particle size, 60 Å pore size) column. Following **CITA** proposed method, the eluents used to create a gradient through the mobile phase were: eluent A (ammonium acetate 0.1 M and H₂O-methanol 15:85 v/v) and eluent B (methanol-acetonitrile-acetone 44:43:13 v/v).

Temperature was maintained constant (20 °C) during the whole process and eluents flow at 800 µL min⁻¹.

Different carotenoids were identified following retention times and absorption profiles of previous known carotenoids analyzed. Quantification was calculated as a percentage of the total peak area.

Rhythmic patterns analysis

Rhythmic patterns detection

The R package RAIN (Thaben & Westermark, 2014) from Bioconductor was used to statistically identify rhythmic patterns in the different data collected.

Three complete diurnal cycles from both photoperiods were used to detect rhythmic patterns in the different data of this study: expression levels of genes, abundance of proteins, maximum potential quantum efficiency of Photosystem II, amount of cells in the different cell cycle phases and amount of different carotenoids and starch.

Rhythmic patterns with a single maximum point over a complete diurnal cycle were detected by setting the period parameter from RAIN to 24 hours. A similar process was used to detect more complex rhythmic patterns (the ones with two or even three maximum points per day), but changing the period parameter from RAIN to 12 and 8 hours respectively. A 0.05 p-value threshold was used in all scenarios.

In addition, the last two diurnal cycles and two consecutive days of continuous light or darkness were considered for the RAIN analysis described above. In that way, RAIN can statistically test if a similar pattern is maintained after changing the cycling light regime to a continuous light or darkness input and it prevents a bias towards any of the two conditions.

Rhythmic patterns comparison

Once that rhythmic patterns in our data were detected by RAIN, waves were characterized to enable comparison between them. This was carried out using the R package Circacompare that performs a fitting to the data as co-sinusoidal curve with a particular parametrization that is used to test for statistical significant differences between the two circadian pat-

terns under comparison. (Parsons et al., 2020). Specifically, a p-value threshold of 0.05 was used.

The significance of the global differences in the different rhythmic parameters was performed using the Mann-Whitney-Wilcoxon non parametric test implemented in the R function *wilcox.test*.

Hypothesis and Objectives

(texto de hipotesis)

Results

Chapter 1. ALGAEFUN with MARACAS: user-friendly tool for analysing and integrating omic data generated from microalgae.

In order to characterize the molecular systems regulating microalgae physiology, high throughput sequencing technologies have been recently applied obtaining the genome sequences of a wide range of microalgae (Blanc et al., 2012; Bowler et al., 2008; Cheng et al., 2019; Corteggiani Carpinelli et al., 2014; Hori et al., 2014; Merchant et al., 2007; Moreau et al., 2012; Morimoto et al., 2020; Ottesen et al., 2013; Palenik et al., 2007; Polle et al., 2017; Roth et al., 2017; Worden et al., 2009). This has promoted the emergence of molecular systems biology studies and the use of different omics like transcriptomics, based on RNA-seq data (Hoys et al., 2021; Serrano-Pérez et al., 2022), and cistromics, based on ChIP-seq data (Ngan et al., 2015; X. Zhao et al., 2021) in microalgae. Nonetheless, the progress of this type of studies on microalgae is limited by the lack of freely available and easy-to-use online tools to analyze and integrate omics data. Processing of the massive amount of high-throughput sequencing data and analysis of the resulting sets of genes and genomic loci obtained from molecular systems biology studies requires computational power, time, effort and expertise that some research groups on microalgae may lack. In addition, researchers must explore different data-bases separately, which makes the integration of the results and the generation of biological meaningful information more difficult. Therefore, it is imperative the development of frameworks integrating microalgae genome sequences and annotations with tools for high-throughput sequencing data analysis and functional enrichment of gene and genomic loci sets.

In order to cover microalgae research community needs and to promote studies in molecular systems biology we have developed the web portal ALGAEFUN with MARACAS using the R package Shiny ([cita? No la encuentro](#)) and other Bioconductor packages.

Our web portal consists of two different tools. First, MARACAS (MicroAlgae RnA-seq and Chip-seq AnalysiS) implements a fully automatic computational pipeline receiving as input RNA-seq or ChIP-seq raw data from microalgae studies and produces set of differentially expressed genes or lists of genomic loci, respectively. These results can be further ana-

lyzed using our second tool, ALGAEFUN (microAlgae FUNctional enrichment tool). When receiving the results from an RNA-seq analysis, sets of genes are functionally annotated by performing Gene Ontology (GO) (Ashburner et al., 2000; Carbon et al., 2019) and metabolic pathways enrichment analysis (Kanehisa et al., 2016; Moriya et al., 2007; Ogata et al., 1999). When genomic loci from a ChIP-seq analysis are inputted, a set of potential target genes is generated together with the analysis of the distribution of the loci over gene features, as well as metagene plots representing the average mapping signal. This set of potential target genes can be further studied using the features for functional enrichment analysis in ALGAEFUN, as described above. The code for ALGAEFUN with MARACAS is publicly available at their respective GitHub repositories from the following links: <https://github.com/fran-romero-campero/ALGAEFUN> and <https://github.com/fran-romero-campero/MARACAS>.

Implementation

Integration of different microalgae databases.

ALGAEFUN with MARACAS supports 14 different microalgae species that cover an ample spectrum of their phylogeny (Fig.12): *Chlamydomonas reinhardtii* (Blaby et al., 2014; Merchant et al., 2007), *Volvox carteri* (Prochnik et al., 2010), *Chromochloris zofingiensis* (Roth et al., 2017), *Dunaliella salina* (Polle et al., 2017), *Haematococcus lacustris* (Morimoto et al., 2020) (Chlorophyceae), *Coccomyxa subellipsoidea* (Blanc et al., 2012) (Trebouxiophyceae), *Ostreococcus tauri* (Blanc-Mathieu et al., 2014; Palenik et al., 2007), *Bathycoccus prasinos* (Moreau et al., 2012), *Micromonas pusilla* CCMP1545 (Worden et al., 2009) (Mamiellophyceae), *Phaeodactylum tricornutum* (Bowler et al., 2008; M. Yang et al., 2018), *Nannochloropsis gaditana* (Corteggiani Carpinelli et al., 2014; Radakovits et al., 2012) (Stramenopiles), *Klebsormidium nitens* (Hori et al., 2014), *Mesotaenium endlicherianum* (Cheng et al., 2019) and *Spirogloea muscicola* (Cheng et al., 2019) (Charophyceae). Supported species include microalgae used in basic scientific research, as well as those used in biotechnology industry like *H. lacustris* (Hoys et al., 2021), *N. gaditana* (Ajjawi et al., 2017) or *P. tricornutum* (Cui et al., 2019; Pereira et al., 2021). (PENSAR SI PONERLO COMO UNA TABLA)

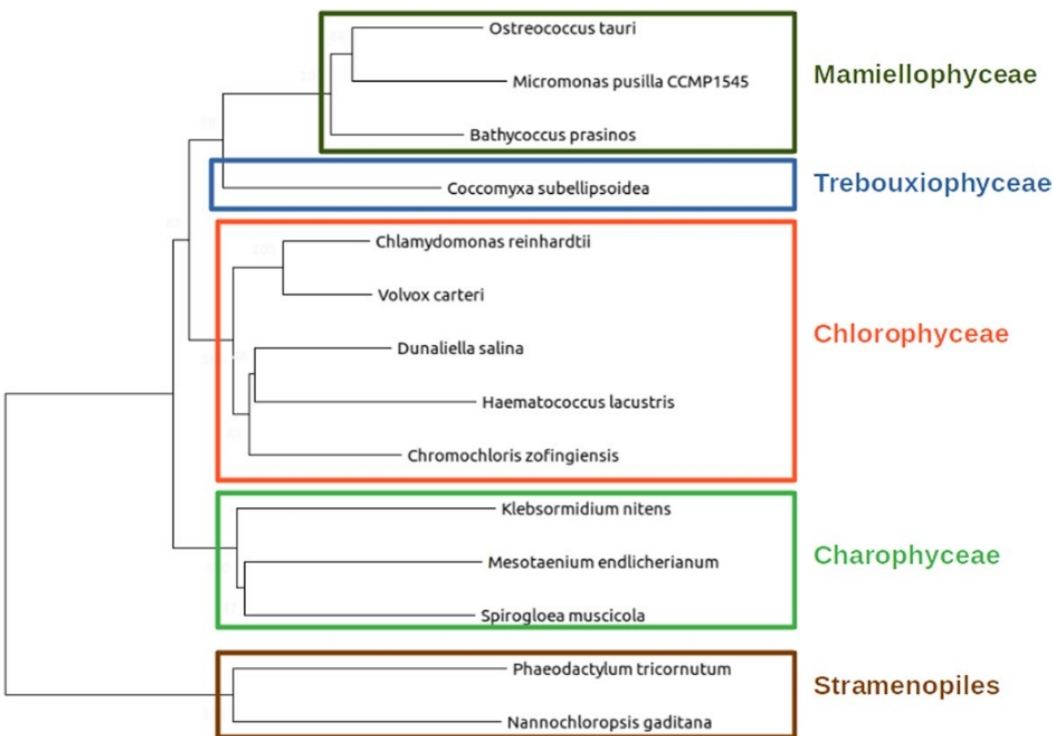


Figure 12: Phylogenetic relationship between the different microalgae species supported in AL-GAEFUN with MARACAS.

One of the goals of our tool is to integrate available genome sequences, functional annotations and genomic feature annotation files (Gene transfer file *GTF*) for the already sequenced microalgae species in order to generate easily accessible resources. These data have been systematically collected from different freely available data bases, depending on the microalgae, and summarized in Table 3. Specifically, for *N. gaditana* and *P. tricornutum*, we accessed Ensembl protist (Howe et al., 2021), a web based unicellular species genome browser storing gene annotation; *B. prasinos* is included in Orcae (Sterck et al., 2012) an online genome annotation resource built on the wiki philosophy; for *C. reinhardtii*, *V. carteri*, *C. zofingiensis*, *D. salina* and *C. subellipsoidea* the JointGenome Institute (JGI) / Phytozome (Goodstein et al., 2012), a web portal integrating omics for photosynthetic organisms was queried; for *M. endlicherianum* and *S. muscicola* a figshare associated to publication was accessed; *M. pusilla*, *O. tauri*, *B. prasinos* and *K. nitens* genome sequence and annotation was downloaded from the JGI / PhycoCosm (Grigoriev et al., 2021), a comparative algal genomic resource; and the genome of *H. lacustris* was available at NCBI genome database ([cita web?](#)).

Table 3: Resources used to collect genome sequences, functional and gene feature annotations for each supported microalgae.

Ensembl protists	PhycoCosm	Phytozome	Genomes NCBI datasets	Figshare associated to publication
<i>N. gaditana</i>	<i>B. prasinos</i>	<i>C. reinhardtii</i>	<i>H. lacustris</i>	<i>M. endlicherianum</i>
<i>P. tricornutum</i>	<i>K. nitens</i>	<i>V. carteri</i>		<i>S. muscicola</i>
	<i>M. pusilla</i>	<i>C. zofingiensis</i>		
	<i>O. tauri</i>	<i>D. salinas</i>		
		<i>C. subellipsoidea</i>		

(VALORAR SI LA TABLA ES NECESARIA)

Genome sequence and gene feature annotation files were downloaded in fasta format and GTF, respectively. When necessary, different chromosome and/or scaffold files were colligated programmatically to produce a single genome file. The GTF format in the gene feature annotation files consists of a data frame with nine columns. Each line corresponds to a specific gene feature. The first eight columns must contain information related to the type of feature (3' UTR, 5' UTR, gene, CDS or mRNA), chromosome start and end positions, the strand where it is positioned, and some other attributes in a well-defined format. The ninth column is not restricted to a specific format and can contain any type of information. Nonetheless, the mappers used in MARACAS assume that this last column follows the format taken by GTF files in the data-base Ensembl. In order to be able to use GTF files from other databases besides Ensembl, we developed an R script to translate any GTF file into the format followed by Ensembl and required by HISAT2 (Kim et al., 2015).

Systematic functional annotation files consisting of Gene Ontology (GO) and KEGG (Kyoto Encyclopedia of Genes and Genome) Orthology (KO) terms were also downloaded for each microalgae from the previously mentioned databases. Gene Ontology terms seek the development of a human-readable and machine-readable hierarchical vocabulary to relate genes with their molecular functions, biological processes in which they are involved and the cellular components where they perform their function (Ashburner et al., 2000; Carbon et al., 2019). Complementary, KEGG Orthology terms associate genes to metabolic pathways and modules based on their orthologous relationships in sequenced

genomes (Kanehisa et al., 2016; Moriya et al., 2007; Ogata et al., 1999). However, for microalgae species lacking these annotation systems, HMMER (biological sequence analysis using profile hidden Markov models) (Potter et al., 2018) was used to identify protein domains according to the PFAM (Protein Family) nomenclature (Mistry et al., 2021). PFAM terms were subsequently converted into GO terms using pfam2go ([necesaria la cita? No encuentro na](#)). KO terms were associated to genes applying KAAS (KEGG Automatic Annotation Server) (Moriya et al., 2007). Whenever possible, other systematic functional annotation format were also included: Protein Analysis Through Evolutionary Relationships (PANTHER) terms (Mi et al., 2021), that classifies, based of evolutionary families and sub-families, gene products into classes capturing molecular function, biological process and metabolic pathways; Enzyme Commission numbers (EC numbers), that consists of a numerical classification identifier for enzymes, related to the biochemical reactions they perform; and Eukaryotic Orthologous Groups (KOG) terms, used to identify orthologue and paralogue groups of proteins (Galperin et al., 2021).

Development of functional annotation and genomic packages.

In order to use all these annotation systems in ALGAEFUN two different types of R annotation packages were developed and were made freely available on our Github repository ([cito web?](#)).

The systematic sources of functional annotation mentioned previously were gather together using the function makeOrgPackage from the Bioconductor R package AnnotationForge (Carlson & Pagès, 2019) which generated annotation packages for each microalgae. These packages are instrumental when performing functional enrichment analysis over gene sets obtained from RNA-seq data analysis.

Gene featuring annotation of each microalgae from the previously downloaded and processed GTF files is stored in different packages applying the function makeTxDbFromGFF from the Bioconductor R package GenomicFeatures (Lawrence et al., 2013). These packages are central to carry out analysis over genomic loci obtained in ChIP-seq analysis.

Both functional annotation and gene featuring packages of each microalgae are freely available on our Github repository, in order to enable the research community in microal-

gae to use them and perform omics analysis independently from the tools available from ALGAEFUN with MARACAS.

MARACAS implementation: high-throughput sequencing data processing.

The computational core of this tool consists of a parallel fully automatic computational pipeline or workflow synchronized through blackboards. This workflow is managed by the job scheduling system SLURM (Simple Linux Utility for Resource Management) and bash scripting. The inputs to our pipeline comprise the pre-computed index of the corresponding microalgae reference genome, the previously processed gene feature annotation file in GTF format (both already included in MARACAS) and the raw sequencing data in fastq format from RNA-seq and ChIP-seq microalgae studies provided by the user. In turn, this workflow produces, as outputs, two lists of differentially expressed genes or DEGs (activated and repressed genes) when the fastq files correspond to a RNA-seq study; or a list of genomic loci or regions significantly occupied by the transcription factor or histone modification of interest in the case of a ChIP-seq study.

MARACAS requires the user to input specifications such as the microalgae of interest, the names for control and experimental conditions, number of replicates and location of raw high-throughput sequencing files. In case of analyzing already published omic data, its accession number can be loaded instead. Additionally, the user can set the statistical parameters to perform the corresponding analysis. Specifically, the fold-change and significance level cutoff thresholds for the identification of differentially expressed genes can be selected. In addition, user can choose as read mapper software either the short read mapper HISAT2 (Hierarchical Indexing for Spliced Alignment of Transcripts 2) or the pseudoalignment method implemented in kallisto. Whereas HISAT2 is an exact method requiring several hours for processing a typical sample (Kim et al., 2015; Pertea et al., 2016), kallisto produces near-optimal gene expression quantification in only a few minutes (Bray et al., 2016). Meanwhile, in the MARACAS ChIP-seq data analysis, pipeline is used the ultra-fast and memory-efficient short read mapper bowtie2 (Langmead & Salzberg, 2012). All this information is collected into a parameters file (Table 4 and Table 5), which is the main input received by the pipeline.

Table 4: Description of parameters file used as input in MARACAS for RNA-seq analyses.

Parameters file for RNA-seq analyses	
data_source	This parameter indicates the source of the data to be analyzed. It can take the value <i>FILES</i> when the fastq files are already located in a folder in the computer where MARACAS is installed or the value <i>DB</i> when the data has been already deposited in the GEO database.
cluster	Parameter specifying the execution mode. <i>SERVER</i> mode executes MARACAS with a sequential analysis of the different samples. Whereas <i>SLURM</i> mode executes MARACAS in a parallel manner, processing samples simultaneously in different computational nodes. In this last case, SLURM needs to be installed in user's computer cluster.
number_processors	Number of processors that can be used by MARACAS.
paired_end	It can take the values <i>FALSE</i> , when your data is single end, and <i>TRUE</i> , when your data is paired end.
working_directory	It indicates the location where the analysis folder will be generated.
microalgae	Name of the microalgae of interest.
read_mapper	This parameter specifies the software tool to perform read mapping. Two different options are provided: <i>HISAT2</i> and <i>Kallisto</i> .
main_folder	Name of the folder that will be created at the working directory to contain the outputs from the analysis.
number_of_samples	Total number of samples to be analyzed.
control_condition_name	Name of control condition.
experimental_condition_name	Name of experimental condition.
loc_sampleN	When <i>paired_end</i> : <i>FALSE</i> and <i>data_source</i> : <i>FILES</i> , this parameter indicates the path and file name of sampleN. N will take values from 1 to <i>number_of_samples</i> .
acc_sampleN	When <i>data_source</i> : <i>DB</i> , this parameter specifies accession number of fastq files in GEO.
loc_sample_leftN loc_sample_rightN	When <i>paired_end</i> : <i>TRUE</i> and <i>data_source</i> : <i>FILES</i> , this parameters indicates the path and file name of the fastq samples containing the left and right reads, respectively.
condition_sampleN	This parameters specifies which condition name of the ones chosen in <i>control_condition_name</i> or <i>experimental_condition_name</i> correspond to each sample.
fold_change q_value	These parameters specify the fold-change and q-value used to determine differential expressed genes in the experimental condition when compared to the control condition.

Table 5: Description of parameters file used as input in MARACAS for ChIP-seq analyses.

Parameters file for ChIP-seq analyses	
data_source	<i>FILES</i> or <i>DB</i> as it is explained in Table 4.
cluster	<i>SERVER</i> or <i>SLURM</i> as it is explained in Table 4.
number_processors	Number of processors that can be used by MARACAS.
paired_end	<i>FALSE</i> or <i>TRUE</i> as it is explained in Table 4.
working_directory	It indicates the location where the analysis folder will be generated.
microalgae	Name of the microalgae of interest.
main_folder	Name of the folder that will be created at the working directory to contain the outputs from the analysis.
number_of_replicates	Total number of samples to be analyzed.
included_control	It can receive <i>yes</i> if your experimental design includes a control condition such as input, mock or similar. Use <i>no</i> in negative cases.
mode	Use the values <i>transcription_factor</i> or <i>histone_modification</i> to specify if your ChIP-seq data was generated for a transcription factor or a histone modification study.
transcription_factor	When <i>mode: transcription_factor</i> this parameter specifies the name of the chosen transcription factor.
histone_modification	When <i>mode: histone_modification</i> this parameter specifies the name of the chosen histone modification.
loc_chip_replicate_N loc_control_replicate_N	When <i>paired_end: FALSE</i> and <i>data_source: FILES</i> , this parameter indicates the path and file name of ChIP sample and, in case of <i>included_control: yes</i> , the control sample. N will take values from 1 to <i>number_of_replicates</i> .
chip_replicate_N control_replicate_N	When <i>data_source: DB</i> , this parameter specifies accession number of ChIP sample in GEO. In case of <i>included_control: yes</i> , <i>control_replicate_N</i> will specify the one for control sample in GEO.
loc_chip_replicate_left_N loc_chip_replicate_right_N loc_control_replicate_left_N loc_control_replicate_right_N	When <i>paired_end: TRUE</i> and <i>data_source: FILES</i> , this parameter indicates the path and file name of the ChIP samples containing the left and right reads, respectively. If <i>included_control: yes</i> , they also indicate this information for control samples.

The first step in our workflow loads the parameters file and generates the working directory including one folder where the samples are downloaded or copied, another one where the results are generated and a third one, called “logs”. In this last folder, several text files are generated containing messages written by the different processes in the pipeline that are useful to keep track of the important events. More interestingly, a different type of text file, called blackboard, is created and the computational processes in our workflow are given read and write permissions for it. Files functioning as blackboards are used for indirect communication between the computational processes in the parallel pipeline in order to synchronize them. In the next step, the pipeline forks into two different modes to process either RNA-seq or ChIP-seq data.

The fork of our pipeline dedicated to RNA-seq analysis is represented in Fig. 13. Depending on the raw data source, the first step consists of either downloading and extracting the corresponding fastq files from a database or copying them to the specified working directory. Next, a quality control of these raw data is performed and short reads are mapped to the reference genome using HISAT2 or kallisto. When HISAT2 is used, this step generates BAM (Binary Alignment Maps) files that contain the mapped reads. The following steps take this mapping as input and perform transcripts assembly and expression quantification using STRINGTIE (Pertea et al., 2015, 2016). In this step, GTF files with the assembled transcripts and CTAB files (chemical table files) with the expression quantification values are generated for all samples. However, when kallisto is used, transcripts are mapped and quantified in the same step, so a TSV (tabular separated values) file containing the result of the quantification is generated (Bray et al., 2016). These processing steps are carried out in parallel, simultaneously for each sample, being synchronized using a blackboard file. These parallel processes write on the blackboard when a goal is reached (for example, BAM files are generated) in order to keep track of their progress. When all parallel processes reach the goals, the following sequential steps of the pipeline are executed. They consist of a differential expression analysis carried out using the Bioconductor R packages Ballgown (Frazee et al., 2015; Pertea et al., 2016) and Limma (Ritchie et al., 2015). Specifically, DEGs are selected using the statistics based on a moderated t-student. Finally, a differentially expression gene report is generated, containing text files with activated and repressed genes, principal component analysis visualization, and several informative graphs, such as scatter plots, volcano plots, box-plots and bar-plots.

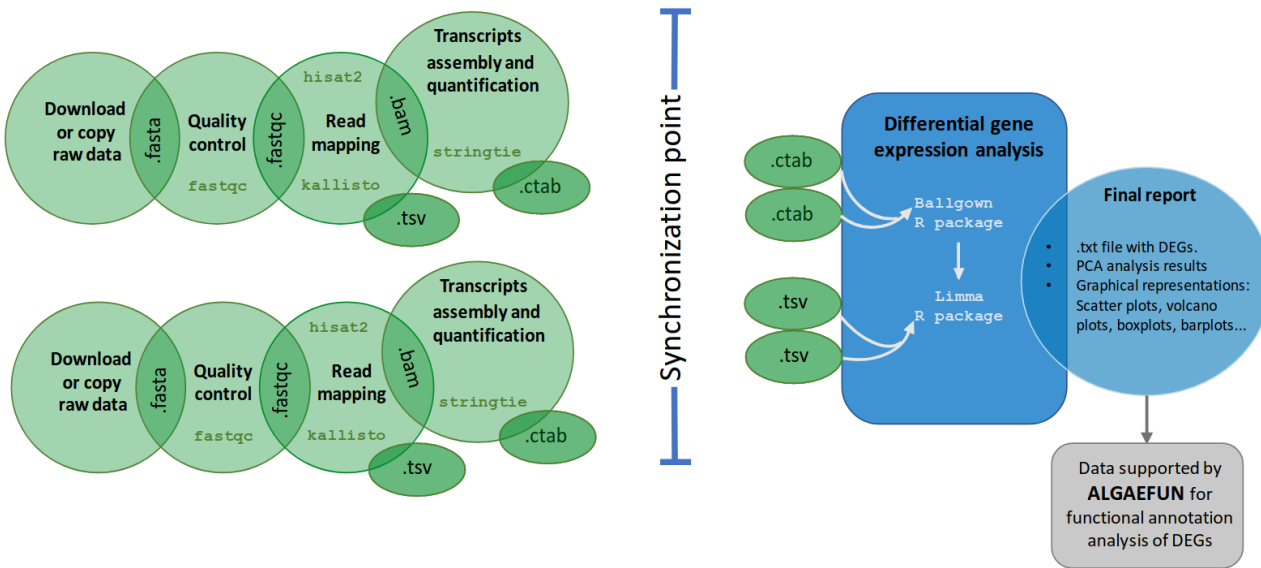


Figure 13: Workflow of the automatic pipeline for the analysis of RNA-seq data in MARACAS. The maracas-rna-seq pipeline receives as input a parameter file as described in Table 4 and Table 5. After data acquisition in fastq format, sequence quality analysis is performed using `fastqc`. Read mapping and gene expression quantification is then performed using `HISAT2` and `stringtie` or `kallisto` depending on the user choice. A synchronization point ensuring the completion of all samples processing to quantify gene expression is necessary before identifying DEGs using the R packages `ballgown` and `limma`. Gene expression estimates measured as raw count, FPKM (Fragments per Kilobase of exon and Million of mapped reads) or TPM (Transcripts per Million) are stored in TSV files. Reports in html and pdf format are generated with details on sequence quality analysis, mapping process and normalization. Graphics for exploratory analysis such as principal components, box-plots, scatter-plots, volcano-plots and bar-plots of individual genes are also included. These reports include links to download gene expression estimates as well as lists of activated and repressed DEGs. The outputs of this pipeline are compatible with the input formats for ALGAEFUN in order to facilitate further functional enrichment analysis and visualization.

The second fork of our pipeline dedicated to ChIP-seq analysis (Fig. 14) shares with the above RNA-seq fork the first steps consisting of downloading or copying the fastq raw files for the ChIP samples (data corresponding to the chromatin immunoprecipitation condition) and control samples into the generated working directory and performing a quality control. Specifically, in this part of the workflow, short read mapping to the reference genome is executed using `bowtie2` (Langmead & Salzberg, 2012) and the synchronization point requires that BAM files for every ChIP and control sample is generated. This synchronization point is also achieved using a blackboard. After synchronization, the last step takes as input all mappings in BAM format and performs peak calling using the software tool `macs2`

(Gaspar, 2018). This final step consists of the identification of genomic loci or regions significantly enriched with mapped reads, indicating the genomic occupation of the transcription factor or histone modification of interest. The output files of this pipeline consists of a BED (Browser Extensible Data) file, collecting the genomic loci or regions identified during the analysis, and a BW (BigWIG) file, containing the number of mapped reads or signal in each position of the genome.

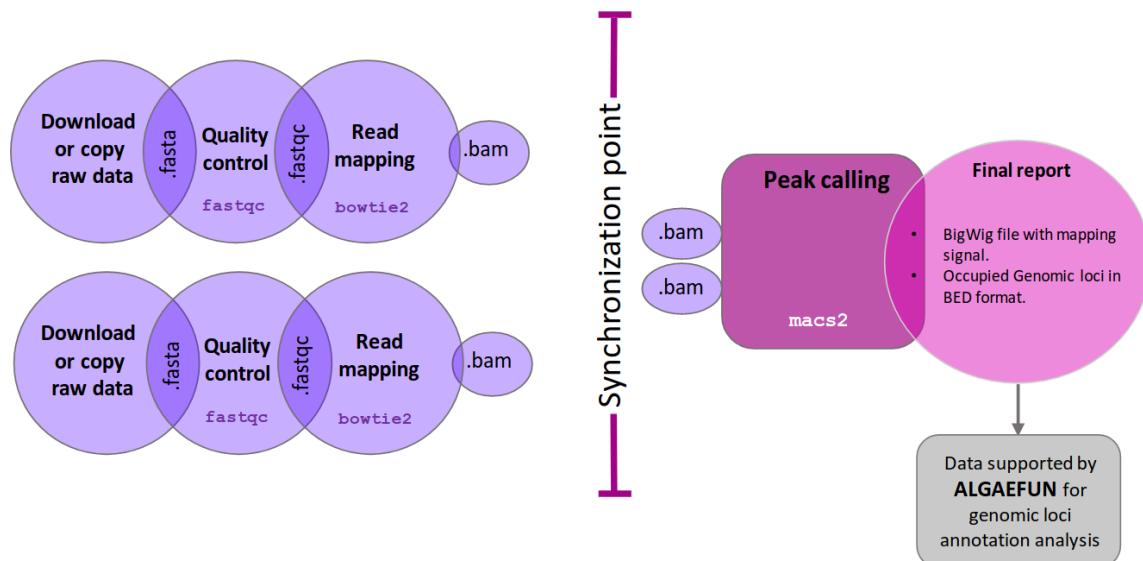


Figure 14: Workflow of the automatic pipeline for the analysis of ChIP-seq data in MARACAS. The maracas-chip-seq pipeline receives as input a parameter file as described in Table 4 and Table 5. After data acquisition in fastq format, sequence quality analysis is performed using fastqc. Read mapping to the reference genome is performed using bowtie2 and is stored in BAM format. A synchronization point ensuring the end of all replicates processing is necessary before carrying out peak calling with macs2. Reports in html and pdf format are generated with details on sequence quality analysis and mapping process. These reports include links to download the identified peaks in BED format and the genome wide mapping signal in bigwig format. These outputs are compatible with the input formats for ALGAEFUN in order to facilitate further annotation and visualization of the identified genomic loci significantly bound or occupied by the transcription factor or histone modification of interest.

ALGAEFUN implementation: functional annotation analysis.

The generated output from MARACAS, either sets of genes or genomic loci, can be functionally annotated using the next software tool in the portal, ALGAEFUN. Although this tool can also be used to functionally annotate genes sets or genomic loci generated independently from other tools.

The user interface of ALGAEFUN is shown in Fig. 15 and Fig. 16. Two different modes of operation, depending on the kind of input data to be analyzed, are implemented in ALGAEFUN.

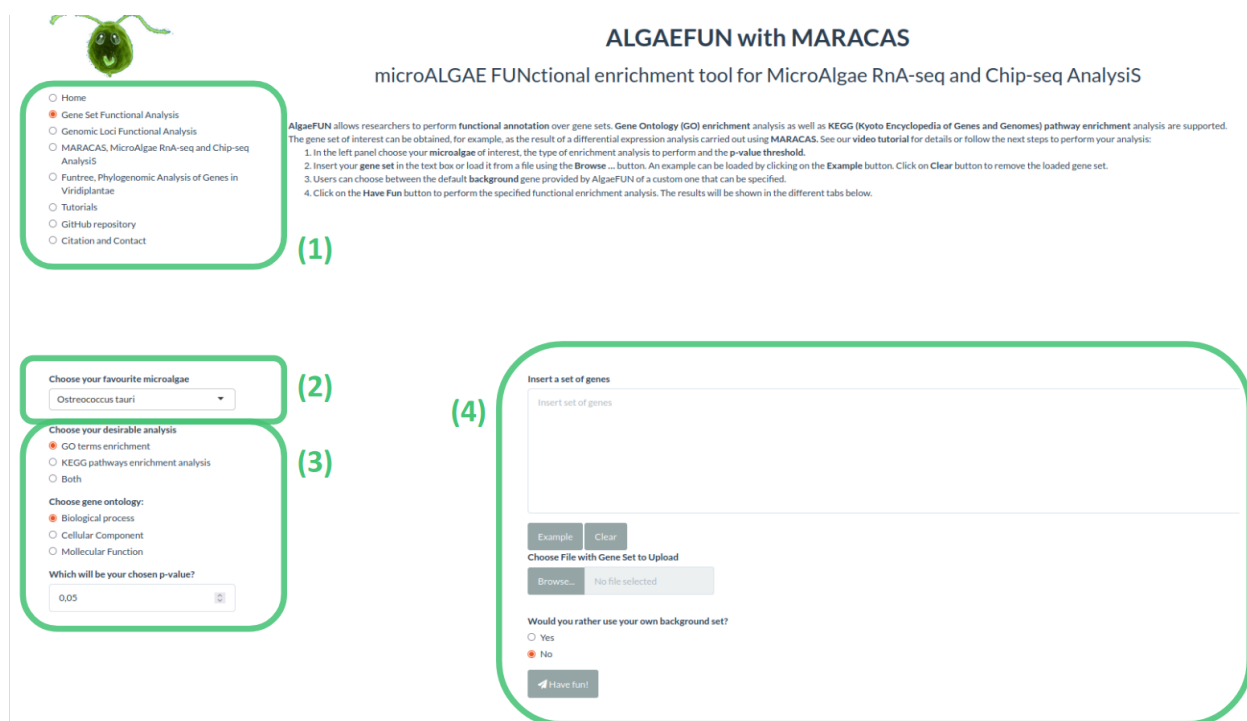


Figure 15: Microalgae Functional Annotation tool (ALGAEFUN) user interface for gene sets functional annotation. (1) Navigation bar for selecting the tool to use between the ones included in our web app; (2) Drop-down menu to select the microalgae of interest; (3) Sidebar panel to select parameters for GO and/or KEGG pathway enrichment; (4) Main panel to input set of genes to analyze and select gene background.

In one of the modes, input data consists of sets of genes obtained, for instance, from an RNA-seq study. Here after selecting this analysis mode (Fig. 15-1), the user chooses the microalgae of interest (Fig. 15-2) and the analysis to carry out, a GO term and/or KEGG pathway enrichment analysis at the selected significance level (Fig. 15-3). The set of genes to study can be inputted through a text box or uploading a file. Users can also choose whether using their own background gene set or the entire microalgae genome

(Fig. 15-4). In order to allow users to explore the functionalities of ALGAEFUN and to check the required gene id format, an example gene set for each microalgae are included. This example can be accessed and inputted in the corresponding text box by clicking on the example button (Fig. 15–4). These examples were generated during the testing of MARACAS using previously published RNA-seq data sets and analysis (**los tengo q citar todos? No se ya ni cuales son algunos**) and have in turn been used in the testing and validation of ALGAEFUN. The GO term and KEGG pathway enrichment analysis are carried out using the Bioconductor R package ClusterProfiler (Wu et al., 2021). This package implements statistical analysis and visualization of functional profiles for gene clusters or sets using the annotation packages developed for each microalgae, integrating the systematic sources of functional annotation previously discussed. The outputs for the GO term and KEGG pathway enrichment analysis are presented in two different tabs. The first output in the GO enrichment tab consists of a table that summarizes the results from the GO enrichment analysis carried out over the input gene set. The user can find one row for each GO term and six columns that represent some relevant information about the enrichment. The first column shows the GO term identifier, followed by the second column where the user can find a description of it. Users can access more information about the GO term represented in a specific row by clicking on its identifier to be redirected to the web portal AmiGO (Carbon et al., 2009) where GO terms are described in detail. The third and fourth column represents the p-value and q-value, and the fifth one shows the enrichment value: $E = (m/n) / (M/N)$. The value “m” is the number of genes from the inputted gene set annotated with the corresponding GO term whereas “M” is the number of genes from the background annotated with the mentioned GO term. In a similar way, “n” is the number of genes with annotation from the gene set whereas “N” is the number of genes with annotation from the gene background. Finally, the last column shows the genes from the input set of genes annotated with each GO term. The user can click them to get more information from the gene entry on the corresponding database from which annotation was retrieved for the specific microalgae under study. Furthermore, ALGAEFUN also generates several graphs that represent the GO term enrichment. Five visualization methods are used to illustrate the results:

- Acyclic graph: Each node stands for a GO term and the color of them indicates the level of significance (from grey, non-significant, to intense red, highly significant). An

arrow is drawn from GO term A to GO term B when A is a more general GO term than B.

- Bar-plot: Each bar represents an enriched GO term whose length corresponds to the number of genes in the gene set annotated with the given GO term. Once again, the bar color shows the level of significance (from blue, less significant, to red, more significant).
- Dot-plot: Each dot represents an enriched GO term. The x-position of the dot corresponds to the ratio between the number of genes annotated with the corresponding GO term and the total number of annotated genes in the gene set. The dot color captures the level of significance (from blue, less significant, to red, more significant).
- Enrichment Map (emap-plot): Each node represents an enriched GO term and the size of each node is proportional to the number of genes annotated with the corresponding GO term in the inputted gene set. The node colors represent the level of significance (from less significant in blue to more significant in red). These nodes are connected by edges when the corresponding GO terms are semantically related.
- Gene-concept network (cnet-plot): The beige nodes represents GO terms and the grey nodes genes. An edge is drawn from a gene to a GO term when the gene is annotated with the corresponding GO term. The size of nodes representing GO terms is proportional to the number of genes annotated with the corresponding GO term.

The outputs shown on the KEGG pathway enrichment tab consist of:

- Table summarizing the result of the KEGG pathway enrichment analysis: Each row represents a pathway significantly enriched in the inputted gene set with respect to the selected gene background. The first column represents the KEGG pathway identifier and the user can click on it to read more information about the pathway. The second column contains a description of it. The third and fourth column present the p-value and q-value, and the fifth column displays the corresponding enrichment value E (m/n; M/N) as previously described. Finally, the last column shows the list of

genes from the inputted gene set assigned to the corresponding enriched pathway. KEGG pathways can be more informative than GO term since they are not general but specific to the corresponding organism of interest.

- KEGG pathway map: Users can choose a specific enriched pathway using a drop-down menu to generate the corresponding KEGG pathway map where genes from the inputted gene set are highlighted in red.
- Table summarizing the result of the KEGG module enrichment analysis: Each row represents a module significantly enriched in the gene set with respect to the selected gene universe. The columns in this table are organized in the same manner as the previously described. KEGG modules are distinct recurrent components of KEGG pathways in this respect they are more specific and can be more informative.

In the other mode, input data consists of genomic loci or regions obtained, for instance, from a Chip-seq study.

This analysis mode is selected from the side bar panel in Fig. 16-1. Their microalgae interest can be selected using the drop-down menu from Fig. 16-2. Next, the distance around the transcriptional start site (TSS) that will be considered defining gene promoters must be specified. Gene features that will be considered when assigning gene targets to genomic loci or regions also need to be selected (Fig. 16-3). Genomic loci or regions to analyze can be inputted through a text box or uploading a file. Additionally, a BW file containing the number of mapped reads or signal in each position of the genome can be uploaded (Fig. 16-4). Similar to the previous mode, it is possible to explore the functionalities of this tool and check the required genomic loci or regions format, using an example included for each microalgae by clicking on the example button (Fig. 16-4). These examples have been generated during the testing of MARACAS, using previously published ChIP-seq data sets and analysis, and have in turn been used in the testing and validation of ALGAEFUN. The functional annotation of the inputted genomic loci or regions is performed using the Bioconductor R packages ChIPseeker (Yu et al., 2015) and ChIPpeakAnno (L. J. Zhu, 2013). These package implements statistical analysis and visualization of genomic loci and regions using the gene feature annotation packages generated for our tool. The outputs generated in this type of analysis consist of:

- A pie chart representing the distribution of the genomic loci or regions over the different type of gene features selected by the user such as the promoter, 3' UTR, 5'UTR, intron or exon.
- A table enumerating the target genes associated one generated when the data comes from a RNA-seq study. It represents each gene located in the enriched genomic loci and its different annotation terms. This set of genes can be downloaded and subsequently annotated functionally using ALGAEFUN.
- A visualization of the average level of signal around TSS and transcriptional end site (TES). For each individual gene, it generates a visualization of the signal and identification of DNA motifs recognized by transcription factors and regulators in microalgae.

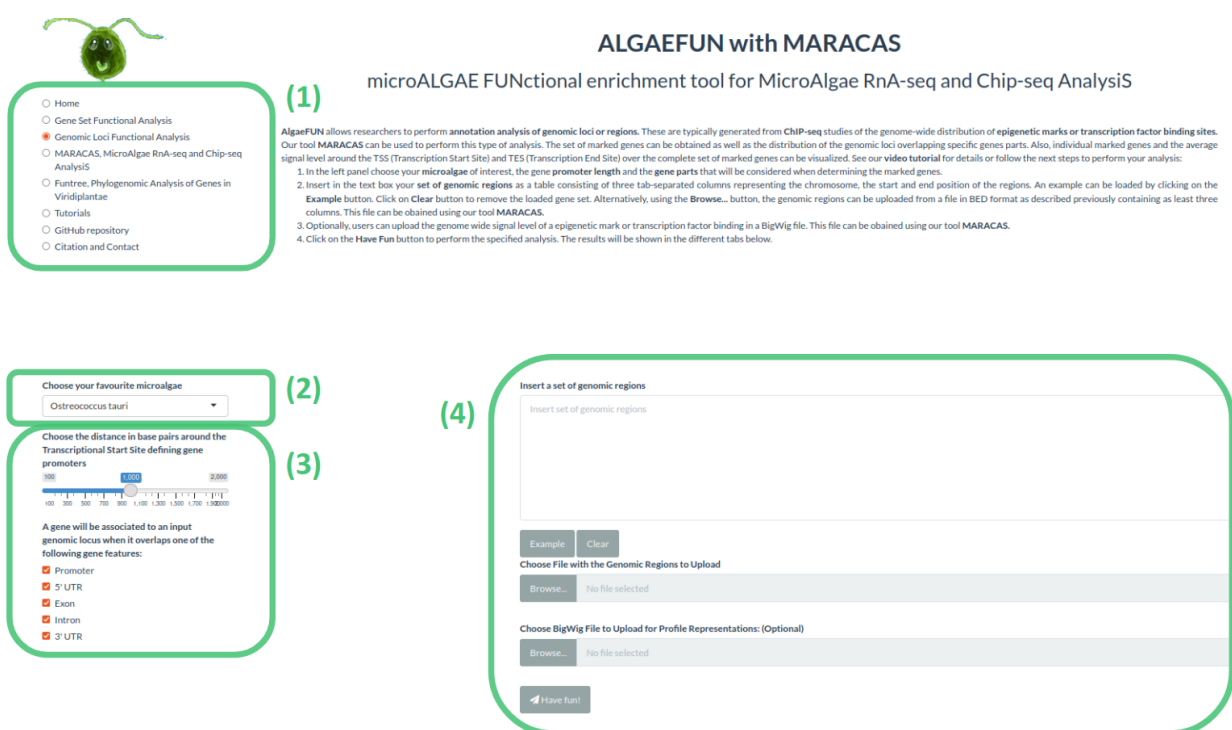


Figure 16: Microalgae Functional Annotation tool (ALGAEFUN) user interface for genomic loci annotation. (1) Navigation bar for selecting the tool to use; (2) Drop-down menu to select the microalgae of interest; (3) Sidebar panel to select parameters for the identification of the promoter regions and the gene features or parts that will be considered to assign genes to genomic loci; (4) Main panel to input set of genomic loci and signal in bigWig format obtained from a ChIP-seq analysis.

Case of study 1: from RNA-seq raw sequencing data to biological processes and pathways.

This case of study is based on RNA-seq data generated by us and illustrate the generation of relevant information suitable for publication. It consists in a RNA-seq study carried out using *Haematococcus* which has a key role in the bio-production of astaxanthin (Hoys et al., 2021; Serrano-Pérez et al., 2022). The analysis has been performed for vegetative *Haematococcus pluvialis* cells, grown both under N sufficiency and under moderate N limitation in order to unveil the transcriptomic program enhancing astaxanthin biosynthesis under N deprivation and it illustrate the type of information that ALGAEFUN with MARACAS is able to reveal from raw sequencing data.

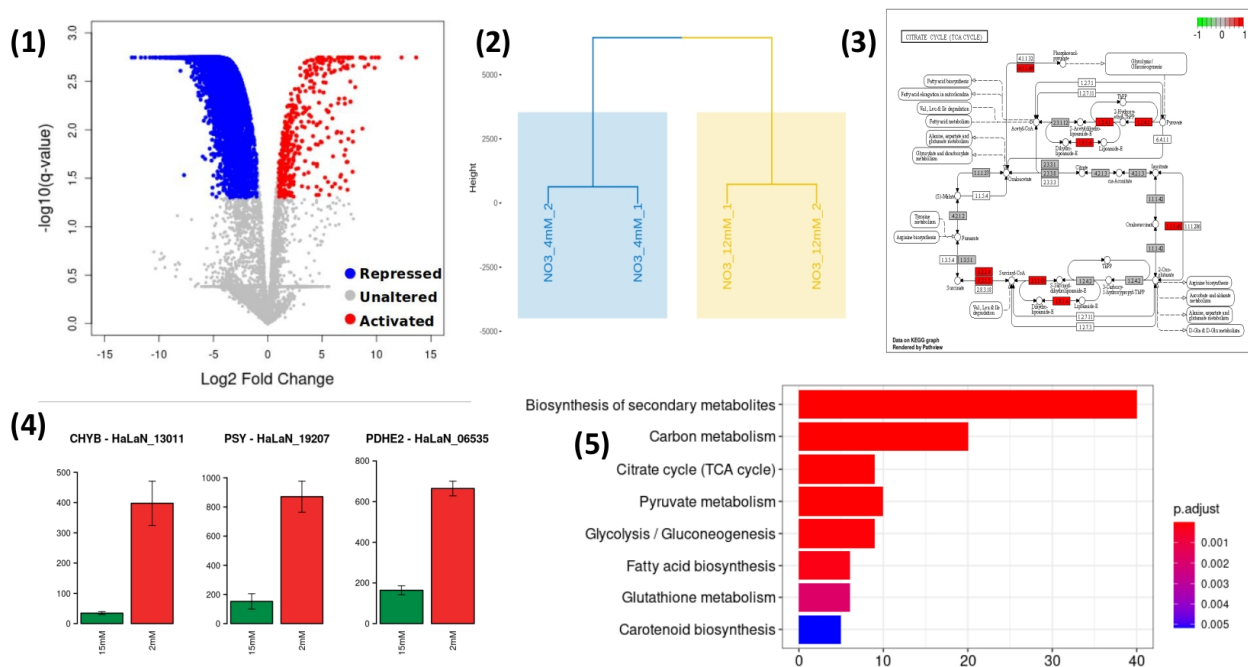


Figure 17: Results obtained from MARACAS final report and from ALGAEFUN analysis. (1) Volcano-plot generated by MARACAS showing the global effect over the transcriptome as well as the activated and repressed genes detected (in red and blue color, respectively); (2) Hierarchical clustering combined with PCA generated by MARACAS; (3) KEGG representation of one of the enriched pathways generated by ALGAEFUN, genes present in the list used as input are colored in red color; (4) Bar-plots representing individual gene expression levels of key enzymes, figure generated by MARACAS. Expression level of the selected gene under N sufficiency is represented in green color. Red color is used to represent moderate N deprivation conditions; (5) Vertical bar-plot representing the enriched biological process in the set of genes used as input, figure generated by ALGAEFUN. Gradient from red to blue color is used to represent p-value.

The high-throughput sequencing raw data in fastq format is processed using MARACAS in order to obtain the set of differentially expressed genes using a criterion solely based on a fold-change value of 1.5. The report produced by MARACAS describe all samples as of high quality and notified no problem during read mapping to reference genome with mapping rates greater than 86%. Scatter plots comparing gene expression between samples are also produced in the MARACAS report. High Pearson correlations greater than 98% are identified between replicates of the same condition. Accordingly, automatically hierarchical clustering combined with Principal Components Analysis (PCA) that leads to the identification of more stable clusters, due to the noise reduction achieved with PCA, is performed by MARACAS (Fig. 17-2). It identifies two clearly separated clusters constituted by the control (N sufficiency) and experimental condition samples (moderate N deprivation). Volcano plots comparing moderate N limitation with N sufficiency transcriptomes are used in the report to represent the repressed genes and activated genes identified with a fold-change threshold of two and a q-value threshold of 0.05. Moderate N limitation has shown a strong repressing effect over the transcriptome with respect to N sufficient conditions, identifying 414 activated and 5348 repressed genes (Fig. 17-1). These lists of genes can be then inputted into ALGAEFUN to determine significantly over-represented biological processes or pathways affected in the studied experimental conditions.

As described previously, ALGAEFUN can perform two different types of functional enrichment analysis when a set of genes from an RNA-seq analysis is used as input: GO terms and KEGG pathways enrichment. The GO terms analysis can identify, for example, specific biological processes enriched in the set of genes. One of the available graphical representations of the GO enrichment results in ALGAEFUN are the bar-plot included in Figure 17-5 that presents the biological processes enriched in the activated set of genes obtained from the *Haematococcus* RNA-seq study under moderate N limitation experiment. Reduced availability of nitrogen activates processes like biosynthesis of secondary metabolites, TCA cycle or pyruvate metabolism at a transcriptomic level. GO term analysis provide a general overview of the functional annotation of gene sets since they constitute universal functional terms not specific to a particular organisms. Complementary, KEGG pathway enrichment is specific to the corresponding organisms and can be more informative in some cases. It allows to identify the transcriptomic activated enzymes in enriched path-

ways (Fig. 17-3). The genes involved in these processes can be further studied individually and their expression level in both conditions can be compared (Fig. 17-4).

ALGAEFUN with MARACAS analysis described differential expression of hundreds of genes affecting key pathways converging into astaxanthin biosynthesis and storage. The affected pathways were further studied at metabolic level and a massive cell reprogramming was verified for the cells growing under moderate N limitation. Furthermore, a major advance has been made in discerning the underlying control mechanisms by finding differentially activated enzymes in astaxanthin biosynthesis pathway. Also, the identification of the prevalent DNA sequences in the promoters of these key enzymes is carried out, so common transcription factors, as bHLH, possibly regulating these key enzymes in astaxanthin biosynthesis pathway are identified for the first time (CITA PAPER haematococcus).

Case of study 2: From ChIP-seq raw sequencing data to marked genes.

As mentioned before, the development of ALGAEFUN with MARACAS has motivated our lab to generate transcriptomic as well as cistromic and epigenomic data. Although we have our own ChIP-seq data obtained during the study of epigenetic marks in *Ostreococcus tauri*, here we show, as an example of how the ALGAEFUN with MARACAS tool works, the re-analysis of raw data from a previously published epigenetic study in *Chlamydomonas reinhardtii*.

Histone modifications play a central role in gene expression control. The genome-wide distribution of the repressive mark H3K27me3 has been determined in *C. reinhardtii* (Ngan et al., 2015). After Chip-seq raw data was re-analyzed using MARACAS, as previously described, the 12,814 genomic loci identified as significantly occupied by H3K4me3 in the *Chlamydomonas* genome under standard growth conditions and the corresponding genome wide mapping signal file in BigWig format are uploaded in ALGAEFUN. The region of two kilobases around the TSS is considered as gene promoter and all the gene features are selected to determine the H3K4me3 marked genes. The outputs are presented in the graphical interface in different tabs. A downloadable table with the marked genes and their available annotation is generated. This gene list can, in turn, be analysed by ALGAEFUN to perform a GO term and/or pathways enrichment analysis. A total of 11,558 H3K4me3 marked genes are identified. Graphs representing the distribution of the genomic loci overlapping different gene features (Fig. 18-a) and the **distribution of up-**

stream and downstream signal around TSS and TES are also represented. In agreement with the previously published results, the 90.75% of the genomic loci occupied by H3K4me3 are located at gene promoters in *Chlamydomonas*.

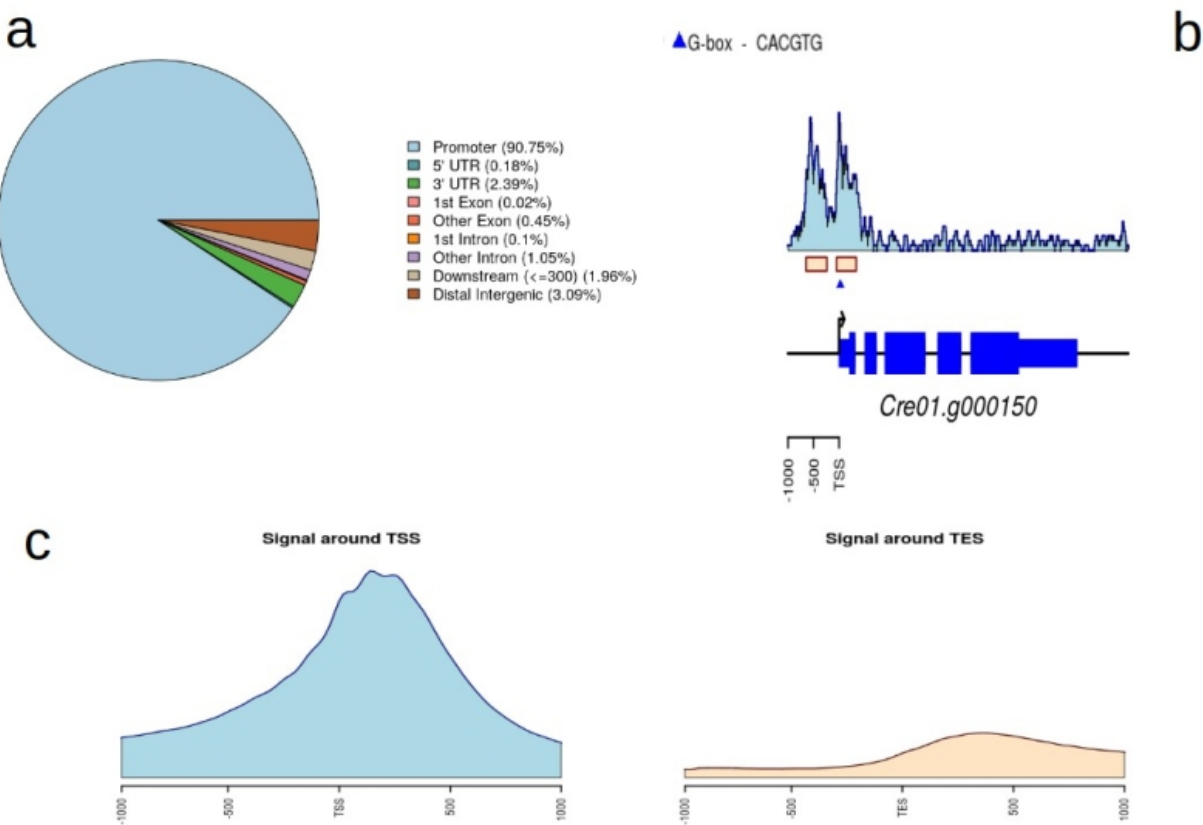


Figure 18: Summary of the outputs generated by ALGAEFUN when a genomic loci list is used as input. a) Pie chart representing the distribution of peaks or genomic loci over the different type of gene features such as the promoter, 3' UTR, 5' UTR, intron or exon; b) Visualization of the signal and identification of DNA motifs recognized by transcription factors and regulators in photosynthetic organisms for an individual gene; c) Visualization of the average level of signal around TSS and TES over the target genes.

As in this case study, when a BigWig file with the genome wide mapping signal is provided, specific marked genes can be selected to visualize the signal profile over their gene bodies and promoters. A gene example presenting two H3K4me3 peaks on its promoter is depicted to illustrate this functionality in Figure 18-b. Moreover, DNA motifs recognized by specific transcription factors and regulators in photosynthetic organisms can be identified in the promoter of the selected gene. Finally, a visualization of the average level of signal around Transcriptional Start Site (TSS) and Transcriptional End Site (TES) across all

marked genes is generated (Fig. 18-c). For the case of H3K4me3 in *Chlamydomonas* further evidence is obtained, showing that this epigenetic mark specifically and exclusively locates at the TSS of marked genes and not at the TES.

Contribution of ALGAEFUN with MARACAS to the field.

ALGAEFUN with MARACAS constitutes one of the first steps that has been taken for the development of tools that would enable the microalgae research community to exploit high throughput next generation sequencing data by applying systems biology techniques. The first difference between ALGAEFUN with MARACAS with respect to already existing tools consists in the wide range of supported microalgae species (Fig. 8). For the model microalgae *Chlamydomonas reinhardtii*, researchers can find several online tools to functionally annotate set of genes, such as Algal Functional Annotation Tool (tilde en López!!) (Lopez et al., 2011) and ChlamyNET (Romero-Campero et al., 2016). Only the online tool AgriGO (Tian et al., 2017) offers the possibility of analysing a restrictive number of different microalgae species beyond *Chlamydomonas*. The second biggest difference between ALGAEFUN and other tools is the annotation systems they use. Most available functional enrichment tools can only perform functional annotation of gene sets based exclusively on GO enrichment analysis. The identification of significantly enriched KEGG pathways in the inputted sets of genes is only supported by ALGAEFUN and Algal Functional Annotation Tool. A fundamental difference between ALGAEFUN and other tools consists of the statistical tests. Whereas AgriGO and ChlamyNET are based on Fisher's exact test, ALGAEFUN and Algal Functional Annotation Tool compute statistical significance according to Hypergeometric tests. It has been shown that, in general, the hypergeometric test has more statistical power than Fisher's exact and χ^2 (Masseroli et al., 2004). Moreover, none of these tools can be used as a complete and integrated tool to process high-throughput sequencing raw data from RNA-seq or ChIP-seq experiments, or functionally annotate genomic loci obtained from a ChIP-seq analysis. In this respect, ALGAEFUN with MARACAS improves and implements several novel functionalities of similar already existing software tools, Table 6.

Table 6: Comparison between ALGAEFUN with MARACAS and other functional enrichment analysis tools

	Algal functional annotation tool	AgriGo	ChlamyNET	ALGAEFUN with MARACAS
Gene sets as input	YES	YES	YES	YES
Genomic loci as input	NO	NO	NO	YES
GO enrichment	YES	YES	YES	YES
KEGG pathways enrichment	YES	NO	NO	YES
Several microalgae	NO	YES	NO	YES
Statistical test	Hypergeometric tests	Fisher's exact test	Fisher's exact test	Hypergeometric tests

ALGAEFUN with MARACAS is a constantly growing tool that will include new microalgae whenever their sequenced genomes are available. Also it has settle the bases to build numerous tools by other members of the laboratory that will for sure be a crucial toolbox for the microalgae research community doing systems biology studies. **Definitely, ALGAEFUN with MARACAS has facilitated the progress of my doctoral work as well as motivated studies of molecular biology of systems in our laboratory with important contributions to the field. Since molecular systems biology has much to contribute to microalgae research, we hope that ALGAEFUN with MARACAS will reach the hands of many research groups and will be as useful to them as it has been to us. (DISCUTIR SI NO PEGA EN ESTO EN UNA TESIS)**

Chapter 2: Transcriptomic analysis of diurnal and seasonal cycles in *Ostreococcus tauri*

High-throughput transcriptome sequencing produced approximately 10 million short reads per sample (ANEXO 1). This allowed us to accurately estimate gene expression levels measured as FPKM (Fragments Per Kilobase of exon per Million reads mapped) in the transcriptomes corresponding to each data point of our time series. Indeed, out of the 7668 genes currently annotated in the *Ostreococcus tauri* genome (Blanc-Mathieu et al., 2014; Palenik et al., 2007), only 3 genes were never expressed and 260 genes never exceeded an expression level of 10 FPKM. This shows that practically the entire *Ostreococcus tauri* genome is expressed under seasonal and diurnal cycles. First, we focus in the 36 transcriptomes corresponding to the time points taken during three days under LD and SD conditions and perform a hierarchical clustering analysis. ([explicar que es?](#)) The transcriptomes corresponding to the same time points during the three different days tend to cluster together (Fig. 19-1). This indicates a high circadian synchronization in our cultures. Moreover, these 36 transcriptomes assemble together into three different groups (Fig. 19-1). The first cluster corresponds to midday. The transcriptomes at time points ZT4 and ZT8 under LD and ZT4 under SD constitute this cluster. These time points correspond to the moments of maximum irradiance under both LD and SD conditions. The second cluster conforms the dusk group. Here the transcriptomes at time points ZT12 and ZT16 under LD and ZT8 under SD are grouped. These time points coincide with the end of the light period in both LD and SD conditions when incident light irradiance is low. The third cluster represents night/dawn and comprises the transcriptomes at time points ZT20, ZT0 under LD and ZT12, ZT16, ZT20 and ZT0 under SD. The transcriptomes at time points in the LD and SD nights or dark periods constitute two distinct groups suggesting noticeable differences in the transcriptomic responses during the night under LD and SD conditions. It is also noteworthy the higher similarity between the dusk, night/dawn transcriptomes when compare to the midday one (Fig. 19-1).

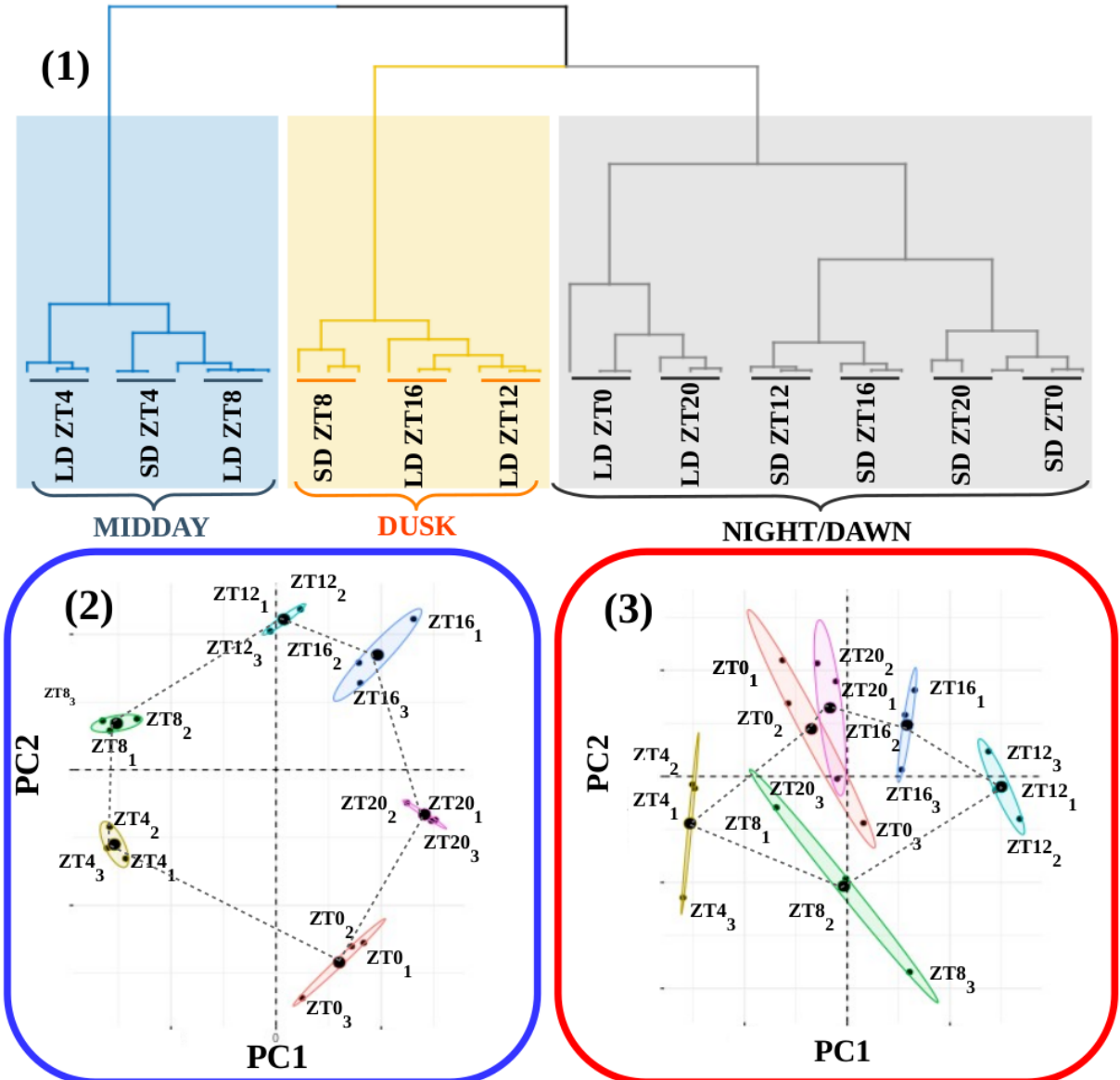


Figure 19: RNA reliability. (A) Hierarchical clustering of the RNA-seq data corresponding to the 36 time points collected under alternating dark/light cycles simulating long and short day conditions. The three global transcriptomes corresponding to the same time points from different days cluster together showing robust rhythmicity in our cultures. Three distinct clusters are observed corresponding to midday (blue rectangle: LD ZT4, SD ZT4 and LD ZT8), dusk (yellow rectangle: SD ZT8, LD ZT16 and LD ZT12) and night/dawn (grey rectangle with two clear subclusters distinguishing between LD and SD: LD ZT0 and LD ZT20 on one hand and SD ZT12, SD ZT16, SD ZT20 and ZT0 on the other hand). (B) Principal Component Analysis of the time point global transcriptomes under long day conditions. Small dots correspond to the 2D projection of each time point global transcriptome. Big dots correspond to the average of the three replicates 2D projections for each time point. Ellipses mark the 95% confidence regions corresponding to each time point global transcriptome. (C) Principal Component Analysis of the time point global transcriptomes under short day conditions. Points and ellipses are used as described before.

In order to obtain a deeper understanding of the underlying structure in our data we performed principal components analysis separately over the LD (Fig. 19-2) and SD (Fig. 19-3) transcriptomes. Under LD conditions, we observed that the transcriptomes corresponding to the same time point in the three different days tightly cluster together globally constituting a circular structure. Nonetheless, under SD conditions more variability is observed and the time point transcriptomes form a structure resembling an ellipse. This could indicate that whereas in LD conditions gene expression is globally cycling precisely with a similar period a more complex behavior is expected under SD conditions. Also, it is remarkable the high similarity between the transcriptomes corresponding to ZT0 and ZT20 under SD conditions that is not present under LD conditions. This suggests that the transcriptomic response at the end of a SD night is already preparing all molecular systems for the incoming light availability at dawn whereas this anticipation is not as clearly observed under LD conditions. In overall, these results support that our experimental design grants a high level of synchronization in our data allowing us to proceed to the identification and comparison of genes exhibiting rhythmic expression patterns under LD and SD conditions.

Transcriptomic characterization of diurnal rhythmic expression profiles

Most genes in Ostreococcus tauri present diurnal rhythmic expression profiles under both photoperiods

We used the bioconductor R package RAIN (Rhythmicity Analysis Incorporating Non-parametric Methods) (Thaben & Westermark, 2014), as described in Materials and methods, to identify genes exhibiting diurnal rhythmic expression patterns under the both seasonal conditions. Specifically, we used time series consisting of three days with rhythmic light / dark periods from our experiment. Independently from the photoperiod, more than 6000 genes comprising approximately 80% of the entire *Ostreococcus* genome present diurnal periodic rhythmic expression patterns. This result is in agreement with previous studies in *Ostreococcus tauri* (Monnier et al., 2010) under different photoperiods and other microalgae such as *Chlamydomonas reinhardtii* (Zones et al., 2015). The specific rhythmic genes under each photoperiod are practically coincident (Fig. 20-A) (Supplemental Table 3—ANEXO?).

In order to further explore the remaining 20% of the genome of *Ostreococcus tauri* that didn't show rhythmic expression patterns under any photoperiod, we compared their highest expression values with the ones reached by rhythmic genes. We found that genes exhibiting rhythmic expression patterns under both LD and SD conditions present a maximal level of expression three times greater than genes detected as non rhythmic. This difference was significant according to a p-value of 1.45×10^{-4} computed using Mann-Whitney-Wilcoxon test (Fig. 20-B). The current methods for detecting rhythmic gene expression are known to perform optimally only for highly expressed genes (Laloum and Robison-Rechavi, 2020). Therefore, the genes identified as non rhythmic in this study could indeed be rhythmic although their low expression level have prevented our methods from detecting them.

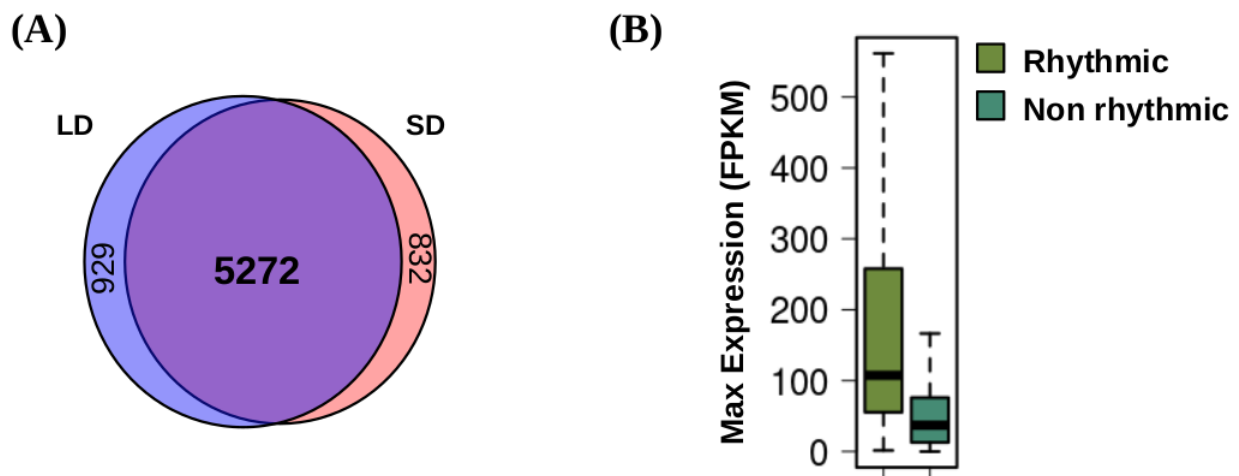


Figure 20: Diurnal rhythmic expression patterns detected in the transcriptome of *Ostreococcus tauri* under both photoperiods: (A) Venn diagram comparing rhythmic genes under LD conditions (light blue circle) and SD conditions (light red circle). Genes with rhythmic expression patterns are almost identical under both photoperiodic entrainments. (B) Boxplot representing the maximum expression level of rhythmic genes (light green) and non-rhythmic genes (dark green). Differences observed are statistically probed (p -value of 1.45×10^{-4}) using Mann-Whitney-Wilcoxon test. Gene expression levels are measured as FPKM (Fragments Per Kilobase of transcript per Million fragments mapped).

Constant light and constant darkness as free-running conditions have different effects over the transcriptome of *Ostreococcus*

In order to explore the effect of the transition to continuous light on rhythmic gene expression patterns we compared three rhythmic characteristics of the expression profiles under LD or SD to the corresponding ones under LL and DD. This was carried out using the R package *circacompare*. As it was mentioned in Materials and methods, *cicacompare* performs a fitting to the data as co-sinusoidal curve with a particular parametrization that is used to test for statistical significant differences between the two circadian patterns under comparison.

When comparing our LD and LL data, a decrease of amplitude in the rhythmic expression profiles is observed. Specifically, most genes (97.68%) that maintain their rhythmicity under LL conditions (with previous LD entrainment) presented a decrease in amplitude when transferred to LL (Fig. 21-A), being significant in more than half of them with a p-value lower than 0.05. Also a positive phase shift (increasing phase) is observed in 76.28% of those genes being significant in 14.98% of them. However, when comparing LD with DD data, the reduction in amplitude is less widespread (Fig. 21-A), being observed in 79.43% of the DD rhythmic genes and being significant in 31.62% of the them with p-value lower than 0.05. Also, in contrast to LL, negative phase shifts (decreasing phase) is observed in rhythmic expression profiles under DD conditions. Specifically, 87.32% of the rhythmic genes under DD (with LD entrainment) presented an anticipation in phase that was significant in 34.16% of them. Most of them present negative phase shifts between 0 and 5 h of difference, whereas most of genes presenting positive phase shifts under LL conditions exhibit between 0 and 5 h of difference (Fig. 21-B).

The global reduction of amplitude in rhythmic gene expression profiles under LL and DD when compared to LD ones (Fig. 21-A) is significant with p-values 4.225738e-140 and 1.087318e-60 respectively. More precisely, the reduction in amplitude is significantly lower under LL than under DD with a p-value of 6.706823e-28.

Next we perform the analysis of the effects of free-running conditions over rhythmic genes with previous SD entrainment. First, comparing their expression profiles under SD and LL, it can be observed that the decrease in amplitude is more drastic than the one observed when LD-LL conditions are compared. Specifically, most genes (87.9%) that maintain their rhythmicity under LL conditions (with SD entrainment) presented a drastic decrease in

amplitude when transferred to LL (Fig. 21-E), being significant in 34.6% of them with a p-value lower than 0.05. In agreement with LD entrainment, a positive phase shift around 5 h of difference (Fig. 21-F,G) is also observed in 68.28% of rhythmic genes under LL with SD entrainment, being significant in 14.98% of them with a p-value lower than 0.05. However, when comparing SD with DD data, the reduction in amplitude is almost non-existent (Fig. 21-E), being observed only in 35.97% of the rhythmic genes (under SD and DD) and being significant in 23.58% of them with p-value lower than 0.05. Negative phase shifts are observed in 47.7% of the genes maintaining DD with SD entrainment, being significant in 28.83% of them. However, most genes have a phase shit around 0 (Fig. 21-F), suggesting that phase shifts are not so drastic in DD after SD entrainment (Fig. 21-G).

The global drastic reduction of amplitude in rhythmic gene expression profiles under LL when compared to SD ones is significant with a p-value 5.951216e-65 (Fig. 21-D). In contrast to what was observed after LD entrainment, a slight but significant increase in amplitude under DD was detected when compared to SD with a p-value of 2.502664e-08 (Fig. 21-D). There are no drastic changes in phase or amplitude when SD rhythmic expression profiles are transferred to constant darkness conditions. This suggests a highly similarity between SD and DD conditions, probably due to long periods of dark entrainment.

Free-running conditions have been widely studied in nocturnal mammals (Bartoszewicz et al., 2010; Hundahl et al., 2012; Imai et al., 2020), plants (Edwards et al., 2010; Ohara et al., 2015) and other organisms(Biebach et al., 1991; Vatakis et al., 2018). The effect over the amplitude of biological rhythms has been previously observed at different biological levels and is commonly associated with a lost of synchrony (Paajanen et al., 2021; Vatakis et al., 2018) (Fig. 22). This suggests that LL conditions promote a larger lost of synchrony than DD conditions at the transcriptomic level in *Ostreococcus* under both photoperiods of entrainment.

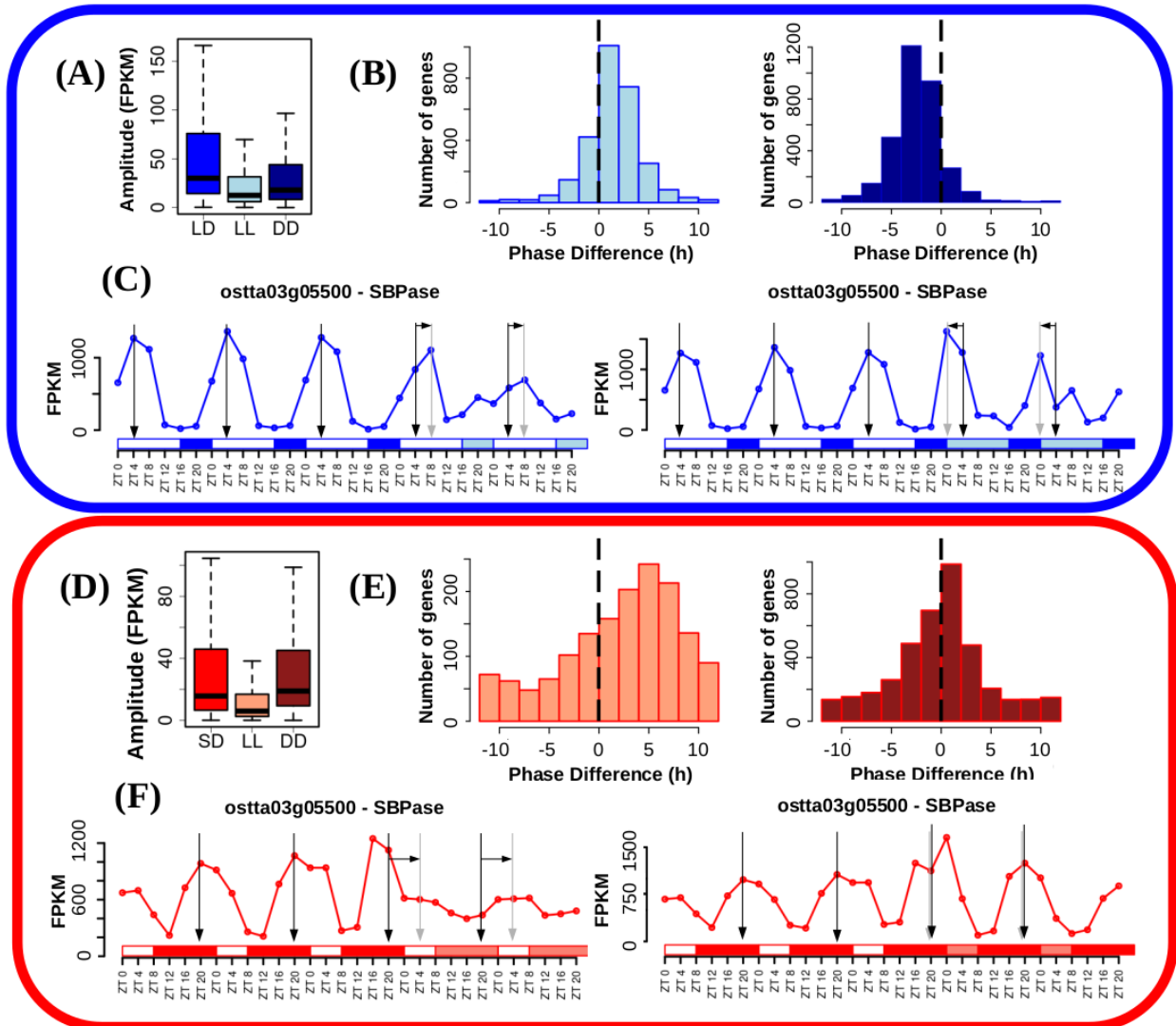


Figure 21: Free running conditions effects over gene expression profiles. (A) Boxplot representing rhythmic genes amplitude reached under long day conditions (blue), when cultures were kept under free running conditions consisting of constant light (light blue) and when cultures were kept under free running conditions consisting of constant dark (dark blue). LL and DD amplitudes are significantly reduced with respect to LD according to p -values of $4.225738e-140$ and $1.087318e-60$. LL amplitudes are also reduced when compared to DD according to a p -value of $6.706823e-28$. P -values were computed using Mann-Whitney-Wilcoxon test. (B) Histograms showing the distribution of the number of genes exhibiting positive and negative phase shifts under LL (light blue, left) and DD (dark blue, right) free running conditions when compared to LD. Vertical dashed lines mark no shift. Positive forward phase shifts are observed when cultures are transferred from LD to LL whereas negative backward phase shifts are apparent when transferred to DD. (C) Gene expression profiles under LD, LL and DD of Sedoheptulose-bisphosphatase (*ostta03g05500*, SBPase). Vertical black arrows mark LD phases, vertical grey arrows mark LL and DD phases and horizontal black arrows represent phase shifts. SBPase illustrates how genes after LD entrainment present reduced amplitudes under LL and DD, forward phase shifts under LL and backward phase shift under DD being these changes more drastic under LL than DD. (D) Boxplot representing rhythmic genes amplitude under short day conditions (red), when cultures were kept under free running conditions consisting of constant light (light red) and when cultures were kept under free running conditions consisting of constant dark (dark red). LL amplitudes are significantly reduced with respect to LD

according to p-values of $5.951216e-65$. A slight but significant increase in amplitude under DD was detected when compared to SD with a p-value of $2.502664e-08$. P-values were computed using Mann-Whitney-Wilcoxon test. (E) Histograms showing the distribution of the number of genes exhibiting positive and negative shifts in phase or maximum expression level time point under LL (light red, left) and DD (dark red, right) free running conditions when compared to SD. Vertical dashed lines mark no shift. (F) Gene expression profiles under LD, LL and DD of Sedoheptulose-bisphosphatase (*ostta03g05500*, SBPase). SBPase illustrates how genes after SD entrainment present reduced amplitudes and forward phase shifts only under LL with no significant change under DD.

The free-running rhythms observed in *Ostreococcus* are possibly found in other photosynthetic organisms as well. There is a huge lack of research of this topic but positive and negative phase shifts under LL and DD, respectively, have been also observed in algal-coral symbiosis content in photosynthetic pigments (Sorek et al., 2013).

However, since plants growth is dependent on photosynthesis and thus in light, the effects of DD conditions over biological rhythms in photosynthetic organisms are yet poorly described. Our results bring new approaches about the effects of free running conditions in the green lineage, showing for the first time the strong desynchronizing effect of LL compared to DD conditions in a photosynthetic organism. Moreover, the effects of LL and DD observed over the transcriptome of *Ostreococcus* in this study (desynchronization, positive phase shifts under LL and negative phase shifts under DD) agree with the ones typically described in nocturnal animals. Also, constant light is commonly used as a circadian disruption model in those organisms (Bartoszewicz et al., 2010; Hundahl et al., 2012; Imai et al., 2020; Vatakis et al., 2018), which agrees with the strongly desynchronizing effect over the transcriptome of *Ostreococcus*. This suggest for the first time a strong dependence on dark periods in *Ostreococcus* and possibly other photosynthetic organisms.

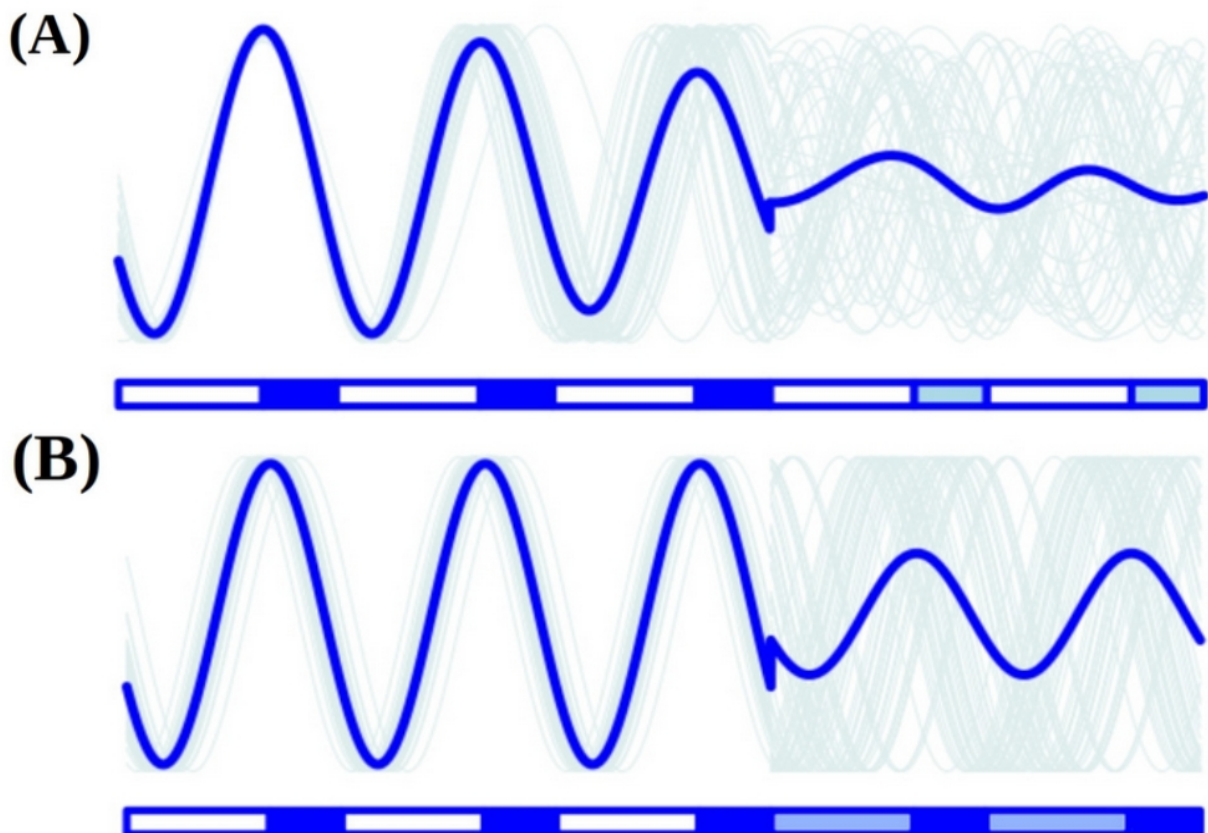


Figure 22: Reductions in amplitude under free running conditions can be explained by a decline in culture synchrony. (A) Culture average gene expression profile under LD and constant light (LL) is represented by a thick blue line. Examples of individual cell gene expression profiles under LD and LL are represented by thin grey lines. When cultures are transferred to LL, cells get strongly desynchronized and their individual gene expression profiles become out of phase. This results in a strong reduction in the amplitude of the culture average gene expression profile although individual gene expression profiles maintain the same amplitude. (B) Culture average gene expression profile under LD and DD is represented by a thick blue line. Examples of individual cell gene expression profiles under LD and DD are represented by thin grey lines. When cultures are transferred to DD, cells get moderately desynchronized and their individual gene expression profiles become out of phase. This results in a slight reduction in the amplitude of the culture average gene expression profile although individual gene expression profiles maintain the same amplitude.

Under free running conditions rhythmicity is maintained in different proportions depending on the photoperiod of entrainment

As it was described in the introduction, circadian processes are self-sustained and maintain their rhythmicity even when the given zeitgeber become constant. Following that definition, circadian genes can be detected and discerned from light or dark responding ones using our data generated under free-running conditions. One of the main observations is that the maintenance of rhythmic expression profiles is dependent on the photoperiod of entrainment.

Although genes with rhythmic expression profiles under LD (6201 rhythmic genes) and SD conditions (6104 rhythmic genes) are almost coincident (Fig. 20-A), their rhythmicity is not maintained equally under free running conditions. Specifically, we found 2804 genes (36.57% of the entire genome) with a previous LD entrainment that maintain their rhythmicity under constant light (LL) conditions (Fig. 23-A). But the number of genes with a previous SD entrainment maintaining their rhythmicity under LL conditions decrease to 1526 (19.9% of the entire genome) (Fig. 23-C). However, 4006 genes with a previous SD entrainment and 3311 genes with a previous LD entrainment maintain their rhythmicity only under constant dark conditions (DD) (Fig. 23-A,C). It suggests that rhythmic expression under SD conditions is very dependent on the presence of a long period of dark whereas rhythmic expression under LD conditions due to the presence of a short period of dark is better maintained under continuous light.

Regulatory mechanisms are often composed of large networks influenced by a wide range of inputs. Circadian clocks are strongly influenced by external environmental signals but there exists a complex interplay between the clock and cell physiology as well (Mazzoccoli et al., 2020; Morris et al., 2020). Genes maintaining their rhythmic expression profiles only under LL or DD are only partially regulated by diurnal changes in the circadian clock. They are also influenced by other regulatory mechanisms as light (Fig. 23-B) or darkness (Fig. 21-D).

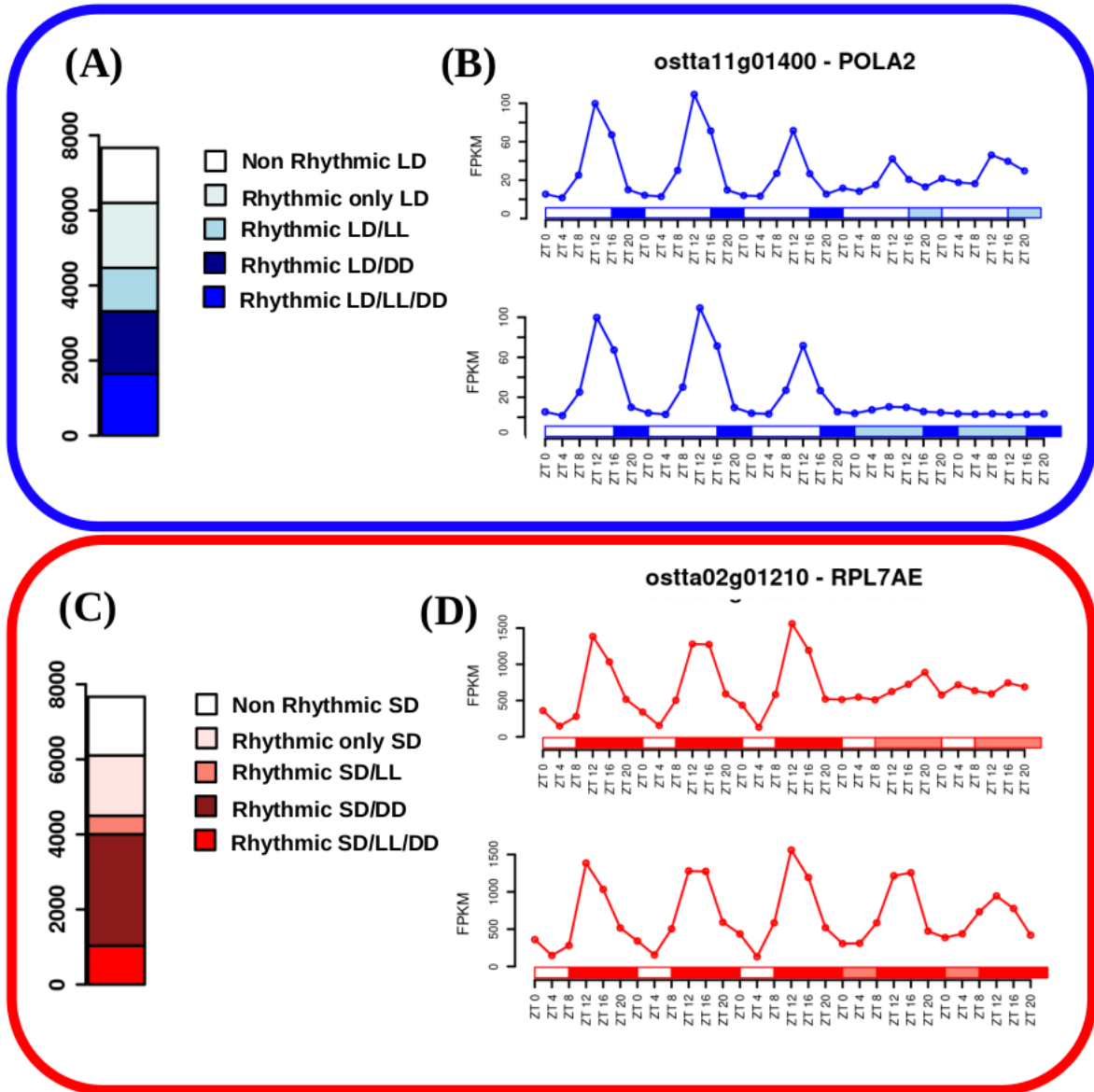


Figure 23: Rhythmicity maintenance under free-running conditions: (C) Barplot representing with blue colors different rhythmic gene sets under LD conditions. From bottom to top: circadian genes exhibiting rhythmicity under LD, constant light (LL) and constant dark (DD); rhythmic genes under LD and DD requiring a dark input; rhythmic genes under LD and LL requiring a light input; rhythmic genes only under LD and non-rhythmic genes. (D) Gene expression profiles under LD, LL and DD of DNA polymerase alpha subunit B (*ostta11g01400*, *POLA2*). *POLA2* illustrates that specific genes involved in DNA replication require light maintaining rhythmicity under LL whereas being strongly repressed under DD. (E) Barplot representing with red colors different rhythmic gene sets under SD conditions. From bottom to top: circadian genes exhibiting rhythmicity under SD, LL and DD; rhythmic genes under SD and DD requiring a dark input; rhythmic genes under SD and LL requiring a light input; rhythmic genes only under SD and non-rhythmic genes. (F) Gene expression profiles under SD, LL and DD of Ribosomal protein L7Ae (*ostta02g01210*, *RPL7AE*). *RPL7AE* illustrates that specific genes involved in translation require dark maintaining rhythmicity under DD whereas presenting flat expression levels under LL.

For example, one of the enriched processes in the set of genes that maintain their rhythmicity only under LL is the DNA replication (ANEXO). It agrees with previous cell cycle studies in other microalgae like *Euglena* (Kato & Nam, 2021) and *Chlamydomonas* (Donnan & John, 1983; Zones et al., 2015) as well as *Ostreococcus* (Moulager et al., 2007, 2010). They suggest that cell cycle have a strong circadian clock regulation as well as G1 phase is light-dependent due to the need of light to grow in photosynthetic organisms, and it will explain why DNA replication genes need a light input to maintain rhythmicity.

Also, the main enriched processes in set of genes that maintain their rhythmicity only under DD are RNA processing and ribosome biogenesis (ANEXO). These processes, that are known have a complex regulatory mechanism influenced by the circadian clock as well as other regulatory machinery, are commonly programmed at the transcriptomic level to take place during the night so translation of other proteins can be achieved during the day (Merchante et al., 2017). It is logical that a dark input is needed to maintain rhythmicity of those genes since their activation is dark-dependent.

In addition, comparison of circadian genes (that maintain their rhythmic expression profiles under both DD and LL) with previous LD entrainment or SD entrainment allow us the identification of what is called *bona fide* circadian genes (Fig. 24-A). *Bona fide* circadian rhythms are the ones maintained under every condition (both photoperiods of entrainment and both free-running conditions) and are mainly regulated by diurnal changes in the circadian clock. In our data, there are only 350 genes (comprising 4.6% of the entire *Ostreococcus* genome) that don't present either a flat or noisy profile under any of the studied conditions.

In previous work, RuBisCO activase (RCA) and RuBisCO small subunit (RBCS) mRNA were quantified in *Arabidopsis* under a light dark cycle, constant light and constant darkness conditions (Pilgrim & McClung, 1993). Their results are in agreement with our transcriptomic data in *Ostreococcus*, where the gene expression profile of RuBisCO activase (ostta04g02510, RCA) under the different conditions exemplifies how *bona fide* circadian genes maintain their rhythmicity (Fig. 24-B).

A functional enrichment analysis over this set of genes shows that they are mainly involved in biological processes like photosynthesis, chlorophyll metabolic/biosynthetic process and chloroplast organization among others (Fig. 24-C). Some of those processes are known to present a circadian physiological activity in plants and microalgae like *Euglena*, but there is

a lack of confirmation of this observation at the transcriptomic level in most cases (Cumming & Wagner, 1968; Noordally & Millar, 2015; Panter et al., 2019). Understanding the key evolutionary position of *Ostreococcus tauri* in the green lineage, this results suggests that those are the processes purely transcriptionally regulated by circadian clocks since early in the evolution of the green lineage.

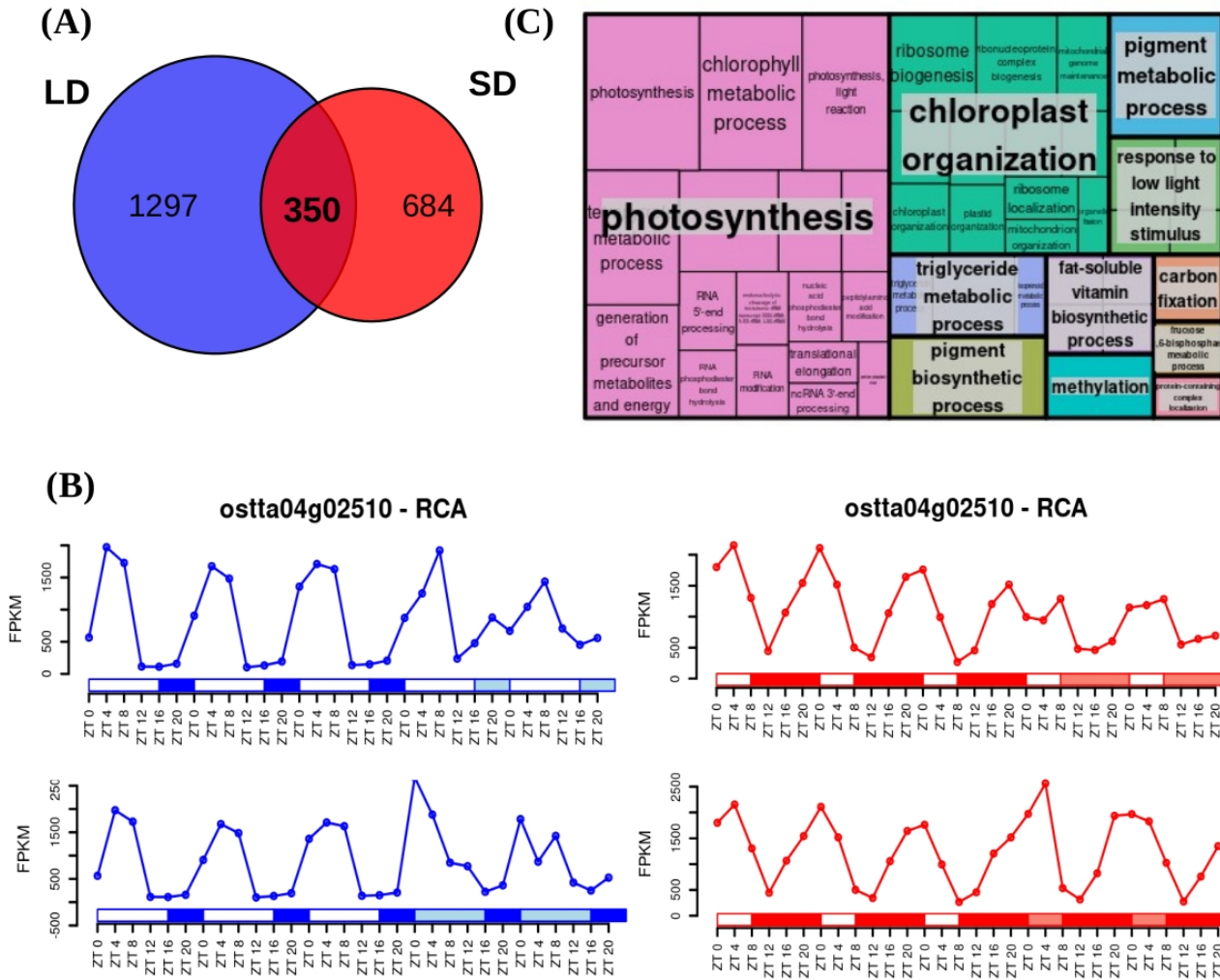


Figura 24: Identification of bona fide circadian genes and their functional enrichment analysis: (A) Venn diagram comparing circadian genes identified after LD entrainment (blue circle) and after SD entrainment (red circle). Only a reduced number of genes are identified as bona fide circadian maintaining rhythmicity under the free running conditions LL and DD after both LD and SD entrainments. (B) Gene expression profiles under LD, SD, LL and DD of RuBisCO Activase (*ostta04g02510*, RCA) exemplifying bona fide circadian genes that maintain rhythmicity under light/dark cycles as well as free running conditions. (C) Treemap summarizing the biological processes significantly enriched over the bona fide circadian genes or rhythmic genes under LD, SD, LL and DD. Rectangle sizes represent significance levels. Semantically similar biological processes are grouped together into the same colored rectangles. The most representative biological process is shown for each rectangle.

Transcriptomic characterization of seasonal effects over gene expression profiles

Seasonal changes induce changes in amplitude and phase over gene expression profiles.

R package circacompare is used to study the global effect of the photoperiod over the amplitude and phase of rhythmic expression profiles. Changes in amplitude and phase offsets of biological rhythms dependent of photoperiods have been already described in mammals like human and others (Messager et al., 2000; Sumová et al., 2003; Van Dongen et al., 1997; Wucher et al., 2022), as well as in plants and microalgae (Flis et al., 2016; Panter et al., 2019; Serrano et al., 2009). The photoperiod inducing an increase in amplitude is different depending on the organism. Specifically, when biological rhythms are studied globally in *Arabidopsis thaliana*, they show phase offsets as an adaptation to changes in photoperiod but differences in amplitude are not observed (Flis et al., 2016). A similar effect is observed in *Chlamydomonas* (Serrano et al., 2009). In both studies, differences in amplitude are only found in some biological rhythms when they are studied individually. For example, the rhythmic expression profile of CrCO show an increase of amplitude under SD conditions as well as a negative phase shift.

However, in *Ostreococcus* transcriptome, we found global changes over the amplitude. Specifically, SD amplitudes are significantly reduced with respect to LD according to a p-value of $1.16e10^{-111}$ computed using Mann-Whitney-Wilcoxon (Fig. 25-A). A high number of rhythmic genes (2036 genes) exhibit a significant decrease in the amplitude of their rhythmic expression profiles. Whereas, only 123 significantly increase their amplitude in short day when compared to long day conditions. This suggests a possibly decline in culture synchrony under SD, accordingly to the previous similar synchronization observed between DD and SD conditions (Fig.21-D).

Negative phase shift or phase anticipation is also globally observed over the transcriptome of *Ostreococcus*, in agreement with what has been described in *Arabidopsis* and *Chlamydomonas*. Specifically, 3424 genes comprising 64.95% of the rhythmic genes exhibited a significantly anticipated phase under short day conditions when compared to long day conditions. Phase anticipation are apparent under SD since gene phases are mostly reached around SD midnight (ZT12 to ZT16) whereas, under LD, phases are uniformly distributed from LD dusk (ZT12) to the end of the night (Fig. 25-B). Only a low number of rhythmic

genes exhibit their phase or maximum level of expression during the light period in LD and SD. The main activity at the transcriptomic level takes place during the night in *Ostreococcus*, which is in agreement with the similarities between *Ostreococcus* transcriptome and nocturnal animals activity (Fig. 21-22).

Cyclin B (ostta01g06150, CYCB) and Delta-9 acyl-lipid desaturase 1 (ostta01g00790, ADS1) are two examples of genes exhibiting the typical phase anticipation and amplitude reduction under short day conditions when compared to long day conditions (Fig. 25-B).

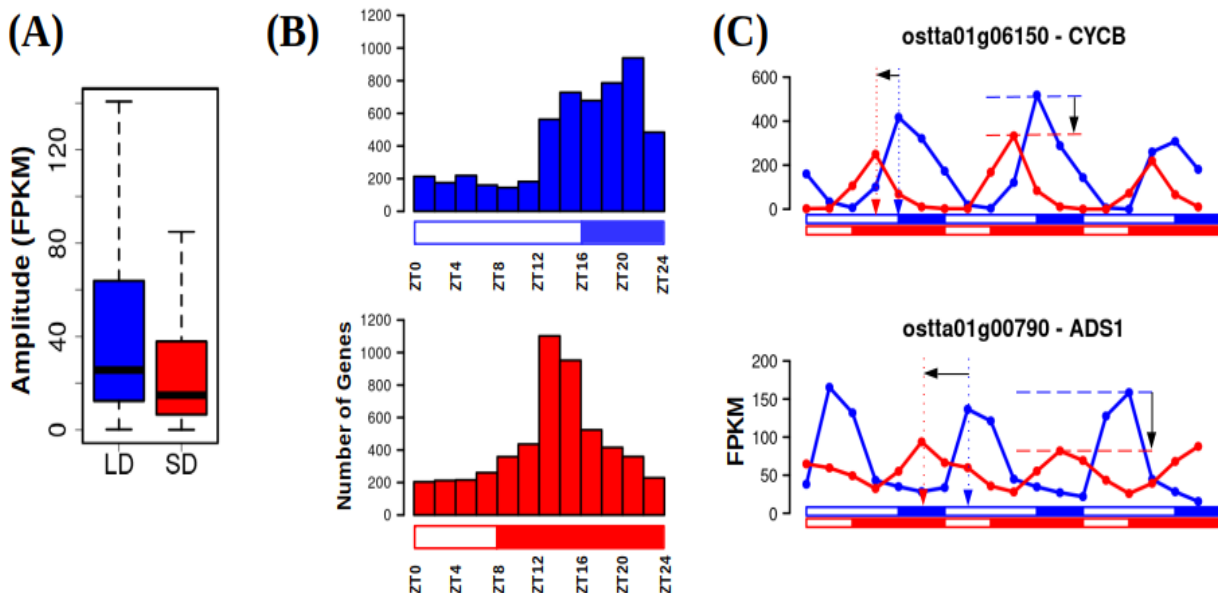


Figure 25: Photoperiod changes cause amplitude reductions and phase shifts over gene expression profiles. (A) Boxplot representing rhythmic genes amplitude or maximum expression level reached under LD and under SD. SD amplitudes are significantly reduced with respect to LD according to a p -value of 1.16×10^{-111} computed using Mann-Whitney-Wilcoxon test possibly due to a decline in culture synchrony under SD. (B) Histograms showing the distribution of the number of genes with phase or maximum expression level at specific time points during the day under LD conditions (blue, top) and SD conditions (red, bottom). Backward phase shifts are apparent under SD when gene phases are mostly reached around SD midnight ZT12 to ZT16 whereas, under LD, phases are uniformly distributed from dusk (ZT12) to the end of the night. (C) Gene expression profiles under LD (blue line) and SD (red line) of Cyclin B (ostta01g06150, CYCB, top) and Delta-9 acyl-lipid desaturase 1 (ostta01g00790, ADS1, bottom). Blue and red vertical dotted arrows mark LD and SD phases. Horizontal black arrow represents backward phase shifts under SD when compared to LD. Blue and red horizontal dashed lines mark LD and SD amplitudes. Vertical black arrows represent the reductions in amplitude under SD with respect to LD.

Seasonal changes promote the emergence of 12 h period cycles

When comparing SD and LD conditions, another significant phenomenon affects the transcriptome of *Ostreococcus*. Under LD conditions almost every rhythmic gene (5825 genes covering 75.97% of the entire genome) reaches its maximum level of expression once a day, presenting one single peak each 24h in their expression profile (Fig. 26-D, E). Under SD conditions the number of genes presenting one single peak of expression per day decrease to 4249 (55.41% of the entire genome). Also, an increasing number of genes, namely 1855 genes, present a more complex rhythmic expression profile with two peaks of expression per day (every 12 h) (Fig. 26-D, E).

Biological rhythms with 12 h periods (two peaks per day) have been described from marine organisms to mammals including humans. It is hypothesized that 12 h rhythm of gene expression and metabolism in terrestrial organisms is reminiscent of the ~ 12 h circatidal rhythms of coastal and estuarine organisms (Ballance & Zhu, 2021). The maintenance of 12 h rhythms after evolving to live on land is hypothesized to provide an advantage in the adaptation to metabolic stress that peak at transition periods during the diurnal cycle (Pan et al., 2020; B. Zhu et al., 2017).

There are other bimodal rhythms (presenting two peaks per day but which periods are different to 12h) that are maintained under free running conditions and have been observed in animals (Binkley & Mosher, 1985; Foà & Bertolucci, 2001; Kyorku & Brady, 1994; Prabhakaran & Sheeba, 2012; Watanabe et al., 2007), plants (Hayes et al., 2010; Van Gelderen, 2020) and some microalgae like Euglena (Mohabir & Edmunds, 1999). However, they are described by specific processes, genes or compounds abundance, they've never been observed as a global effect in the transcriptome. Season cycles were thought to have some effect over some of these cycles but in the majority of the studies different photoperiods weren't studied or there weren't any difference between them (Prabhakaran & Sheeba, 2012). There is only an observation of a bimodal biological rhythm observed in ruin lizards that is apparently strongly dependent on photoperiod and is also maintained under free-runnig conditions (Foà & Bertolucci, 2001).

However, the 12 h cycles emerging under shorter photoperiods have gone mostly unnoticed and thus there isn't an hypothesis about its biological role yet, although they can be found reanalyzing already published transcriptomic data. As an example, this phenomenon

is found in an already published microarray set of data generated from cultures of *Ostreococcus tauri* under 12 h of light-12 h of dark cycle (Monnier et al., 2010). Most of the rhythmic genes presented rhythmic expression profiles with a 24 hours period and, thus, a single expression peak. However, 1171 genes presented rhythmic expression pattern with an apparent period of 12 hours (two peaks of expression per day). This photoperiod can be considered an intermediate step between the two extreme photoperiods studied (LD and SD) and, indeed, the data show an intermediate number of genes with two peaks of expression per day. Also in agreement with our results, this effect can be found in data generated from other organisms like *Chlamydomonas* under neutral day (Zones et al., 2015). That means, that at least in *Ostreococcus* (and possibly other microalgae) there is an increasing number of genes that reach their maximum level of expression twice a day (every 12h) as the photoperiod get shorter although its biological role isn't clear yet.

Ostreococcus is a marine organism, so the maintenance of these 12 h rhythms under free running condition is also studied in order to discard a possibly circatidal rhythm. Nevertheless, 12 h period rhythmic gene expression profiles (two peaks of expression per day) in *Ostreococcus* transcriptome under SD are not maintained under free-running conditions. One of the peaks of expression is maintained only under constant light and the other one only under constant darkness (Fig. 26-C).

Since bimodal circadian rhythms (with periods equal or not to 12 h) have been probed to be maintained under free-running conditions, our results suggest that the seasonal effect observed over the transcriptome of *Ostreococcus* isn't a self-sustained 12 h rhythm, but a combination of two distinct rhythmic profiles: one depending on the photoperiod (maintaining its rhythmicity only under LL) and another apparently depending on the skotoperiod (maintaining its rhythmicity only under DD). A simulation of both distinct rhythmic profiles can be illustrated using Cicacompare parametrization of gene expression profiles maintained under DD and LL and, indeed, a perfect coincidence with the peaks described under the dark/light cycle is observed (Fig. 26-C).

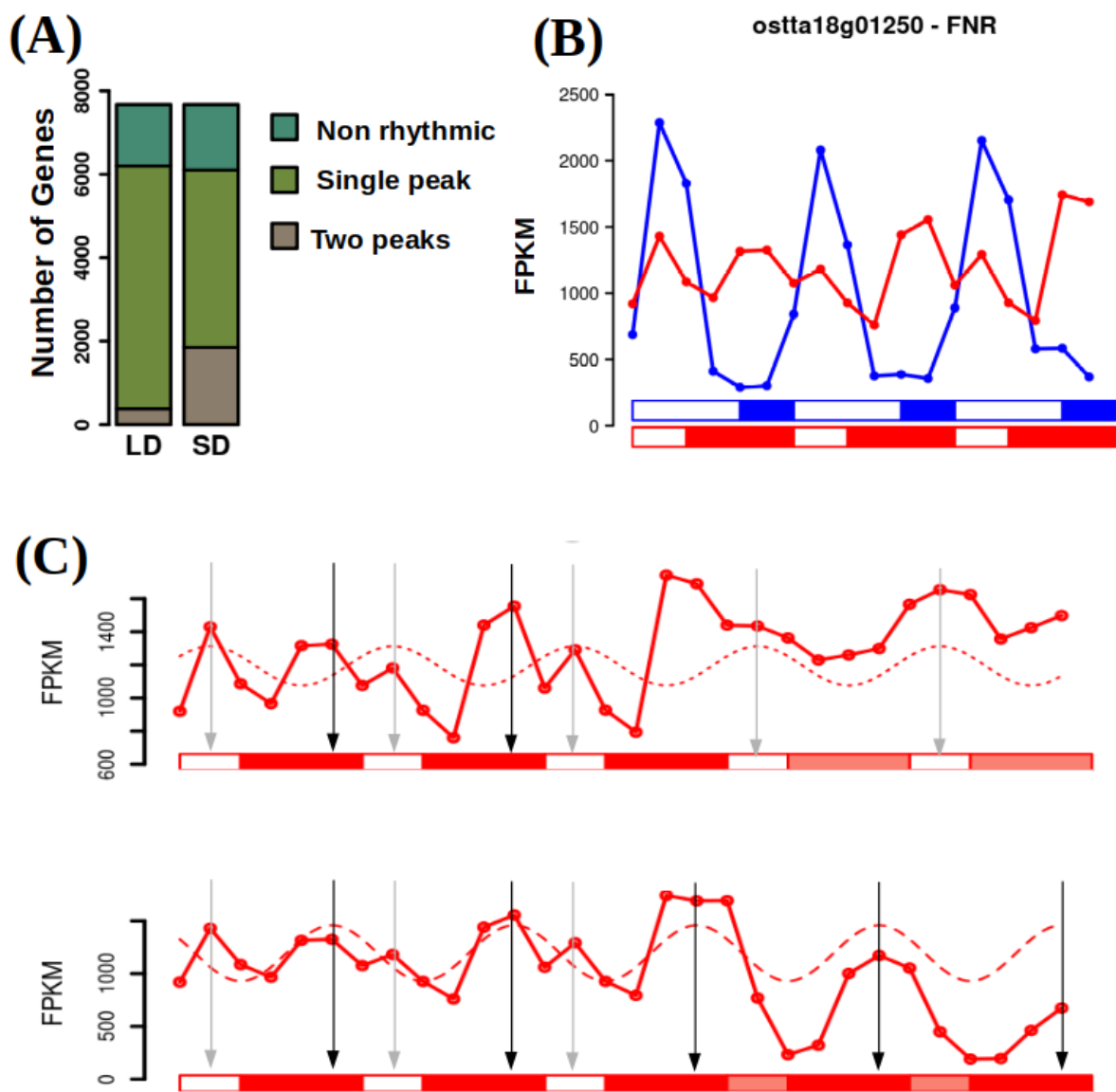


Figure 26: Emergence of 12 h period rhythmic expression profiles under SD. (A) Barplot representing in different green colors the number of non rhythmic, single peak rhythmic and two peaks rhythmic genes under LD and SD conditions. An increase in the number of two peaks rhythmic genes is observed as the photoperiod shortens. (E) Gene expression profiles under LD (blue line) and SD (red line) of Ferredoxin-NADP⁺ reductase (*ostta18g01250*, FNR). This gene illustrates how specific single peak rhythmic expression patterns under LD conditions become two peaks rhythmic expression profiles under SD conditions. (F) Gene expression profiles under SD and free running conditions consisting of constant light (LL) or constant dark (DD) of Ferredoxin-NADP⁺ reductase (*ostta18g01250*, FNR). This gene exemplifies how two peaks expression patterns under SD conditions could emerge as the combination of two distinct rhythmic profiles. One depending on the photoperiod (dotted line) with phase marked with a grey vertical arrow maintaining its rhythmicity only under LL (top). Another expression profile is apparent depending on the skotoperiod (dashed line) with phase marked with a black vertical arrow maintaining its rhythmicity only under DD (bottom).

Seasonal cycles induced distinct temporal transcriptional programs organizing biological processes during diurnal cycles

Genes are clustered together depending on their phase or time of maximum expression level. A functional enrichment analysis of the resulting clusters of genes show which cellular processes are activated at the transcriptomic level in each time point (supp 8 y 9). Focusing on the most enriched processes in each time point, a clear transcriptional temporal map of *Ostreococcus* under each photoperiod is illustrated in Fig. 27.

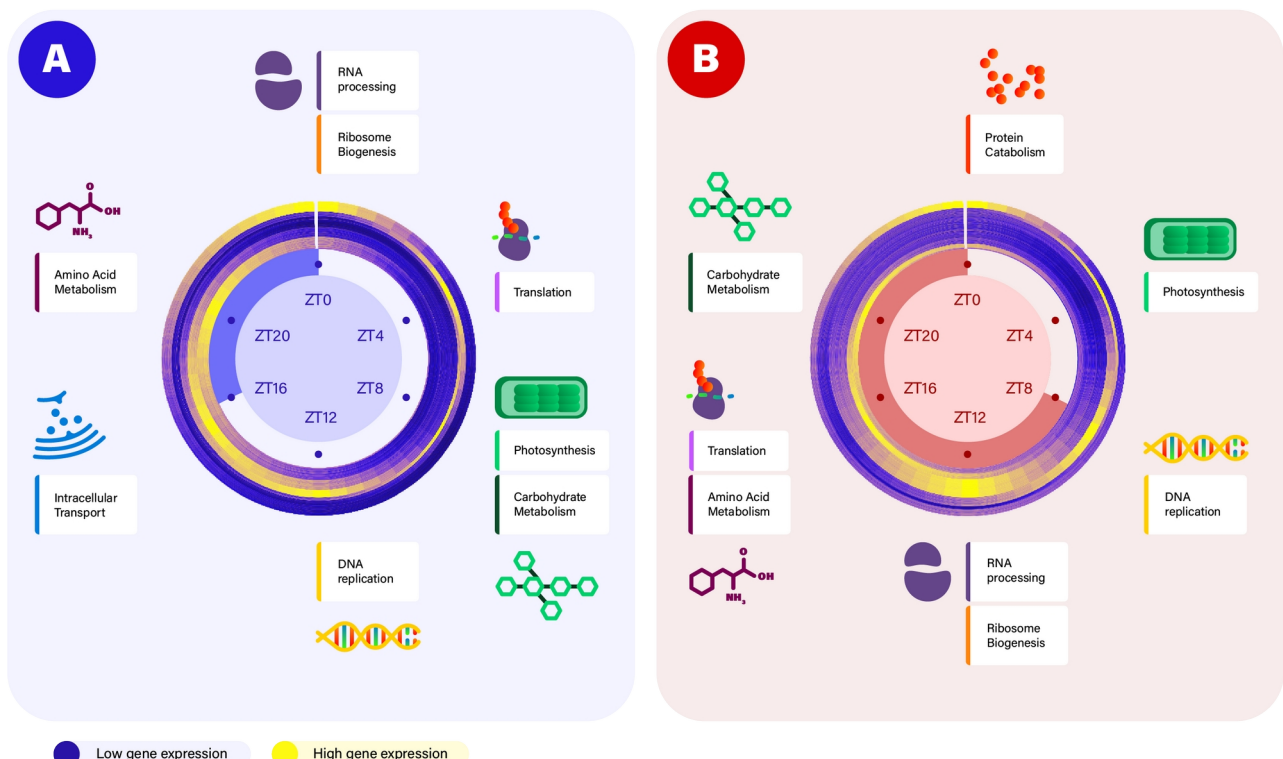


Figure 27: Summary of the transcriptional temporal program of *Ostreococcus tauri* under LD and SD conditions. (A) Circular heatmap representing the temporal organization of gene expression profiles under LD conditions. Dark blue stands for low expression whereas yellow represents high expression. Genes are clustered depending on their phase or time of maximum expression where genes with phase at ZT0 are located in the outer circle and genes with phase at subsequent ZTs are placed sequentially into inner circles. Biological enriched processes in the gene set with phase at each specific time point are depicting capturing the temporal transcriptional program over diurnal cycles under LD conditions. (B) Similarly, circular heatmap representing the temporal organization of the diurnal transcriptional program under SD conditions. A shift as well as a re-arrangement is observed in the SD diurnal transcriptional program when compared to the one inferred for LD.

On one hand, *Ostreococcus tauri* during summer days (Fig. 27-A), seems to activate genes involved in RNA processing and ribosome biogenesis at dawn (ZT0). Examples for such genes are U3 small nucleolar RNA-associated protein 14 (*ostta04g00770*, *Utp14*) or the Ribosome Biogenesis Factor BMS1 (*ostta05g01080*, *BMS1*) (Supp 8). During the first

part of the morning (ZT4) *Ostreococcus* transcriptome is almost completely focused in genes involved in translation, such as eukaryotic Initiation Factor 2 (ostta03g02100, eIF2) and translation elongation factor P (ostta03g03015, YeiP). The genes mainly involved in photosynthesis but also in carbohydrate metabolism reach their maximum level of expression during the the midday, when the maximum irradiance is reached (ZT8). Some of those genes are subunits of both photosystems: ostta01g03170 (PsbP), ostta02g00580 (PsaL), ostta02g02560 (PsbX), ostta02g03860 (PsaE), ostta04g01790 (PsaF), ostta05g04560 (PsbR), etc. Then, during the afternoon (ZT12), the activation of genes involved in DNA replication takes place. Some minichromosome maintenance proteins (ostta01g02580 and ostta05g01680 which corresponds to MCM6 and MCM9, respectively) are found, as well as the proliferating cell nuclear antigen (PCNA) which is central to the DNA replication process. Intracellular transport and cellular respiration are the two most prominent biological processes whose genes reach their maximum expression level at dusk (ZT16) under LD conditions. Genes like lysophospholipases (ostta01g04440, CLC) or nucleoporins (ostta14g02210, Nup133) are some examples for this time point. Finally, during midnight *Ostreococcus* focuses on expressing genes involved mainly in cellular aminoacid metabolic process, like 3-Deoxy-D-arabinoheptulosonate 7-phosphate (DAHP) synthase (ostta06g03270) which encodes the first enzyme in the biosynthesis of the amino acids phenylalanine, tyrosine and tryptophan.

On the other hand, under SD conditions, the most prominent biological process whose genes reach their maximum expression level at dawn (ZT0) is protein catabolism. Examples for such genes are *Signal transduction Histidine Kinase* (ostta09g02190, HK), or *Ubiquitin Fusion Degradation protein* (ostta09g00750, UFD). In agreement with what was observed in LD, genes having their peak of expression during midday (which in SD takes place at ZT4, maximum irradiance) are involved in photosynthesis. Once again, genes encoding photosystems subunits are clustered together in this time point. Under SD conditions, dusk takes place at ZT8 and the genes involved in DNA replication show their maximum level of expression during this time point. The same genes used as an example in LD are found also in SD but anticipating their peak of expression 4 h. Then, RNA processing and ribosome biogenesis are the two most prominent biological processes early during the night (ZT12) under SD conditions, showing a delay of 12 h compared with LD temporal program. Also genes involved in translation show a 12h delay reaching its maximum ex-

pression level during midnight (ZT16). Under LD photoperiod, genes involved in aminoacids metabolic process reach their maximum expression level at ZT20, 8h before genes involved in translation did (ZT4). However, under SD photoperiod genes involved in both processes seems to reach their maximum expression level at the same time. The opposite situation is observed with the genes involved in photosynthesis and the ones involved in carbohydrate metabolism. They reach their maximum expression level at the same time under LD (ZT8), but they take place at two different times under SD: the ones involved in photosynthesis maintain their maximum level of expression at the maximum irradiance hours (which correspond to ZT4 in SD) but the ones involved in carbohydrate metabolism reach their maximum expression level 12 h later (after midnight at ZT20). This suggests that phase shifts globally observed over the transcriptome of *Ostreococcus tauri* as an adaptation to photoperiods, not only consist in anticipating or delaying processes but also in a rearrangement of the complete temporal program.

Chapter 3: Proteomic analysis of diurnal and seasonal cycles in *Ostreococcus tauri*

SWATH proteomics allow us not only to quantify but also to identify proteins in *Ostreococcus tauri* proteome. Our proteomics analysis has reached a proteome coverage of 40%, detecting proteins from all the different cell components (Fig. 28).

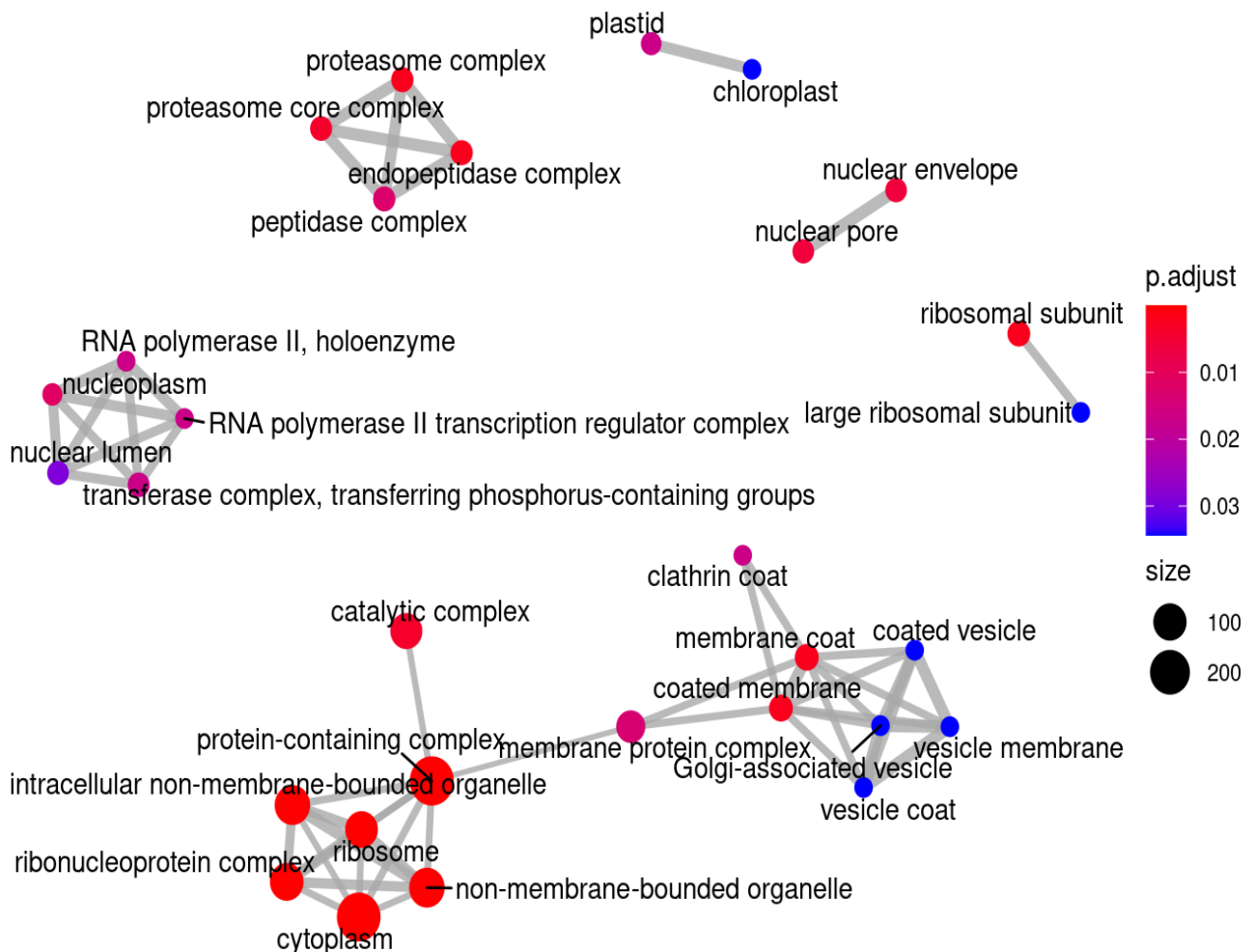


Figure 28: **Our proteomics data cover all cell components.** Enrichment map representing the cellular components or organelle significantly covered by the proteins detected in our data. Dots or nodes sizes represent the number of proteins identified located in the corresponding organelle. A blue to red gradient is used to represent the level of significance. Lines or edges link dots or nodes representing related organelle.

Furthermore, since our data is obtained from 3 technical replicates of each biological replicate (3 light/dark cycles), it can be observed that the global distribution of each group of 3 technical replicates is similar (Fig. 29-A). The differences observed over the global distribu-

tion of different groups of technical replicates are solved with log₂ quantile normalization of the data, ensuring data comparability (Fig. 29-B).

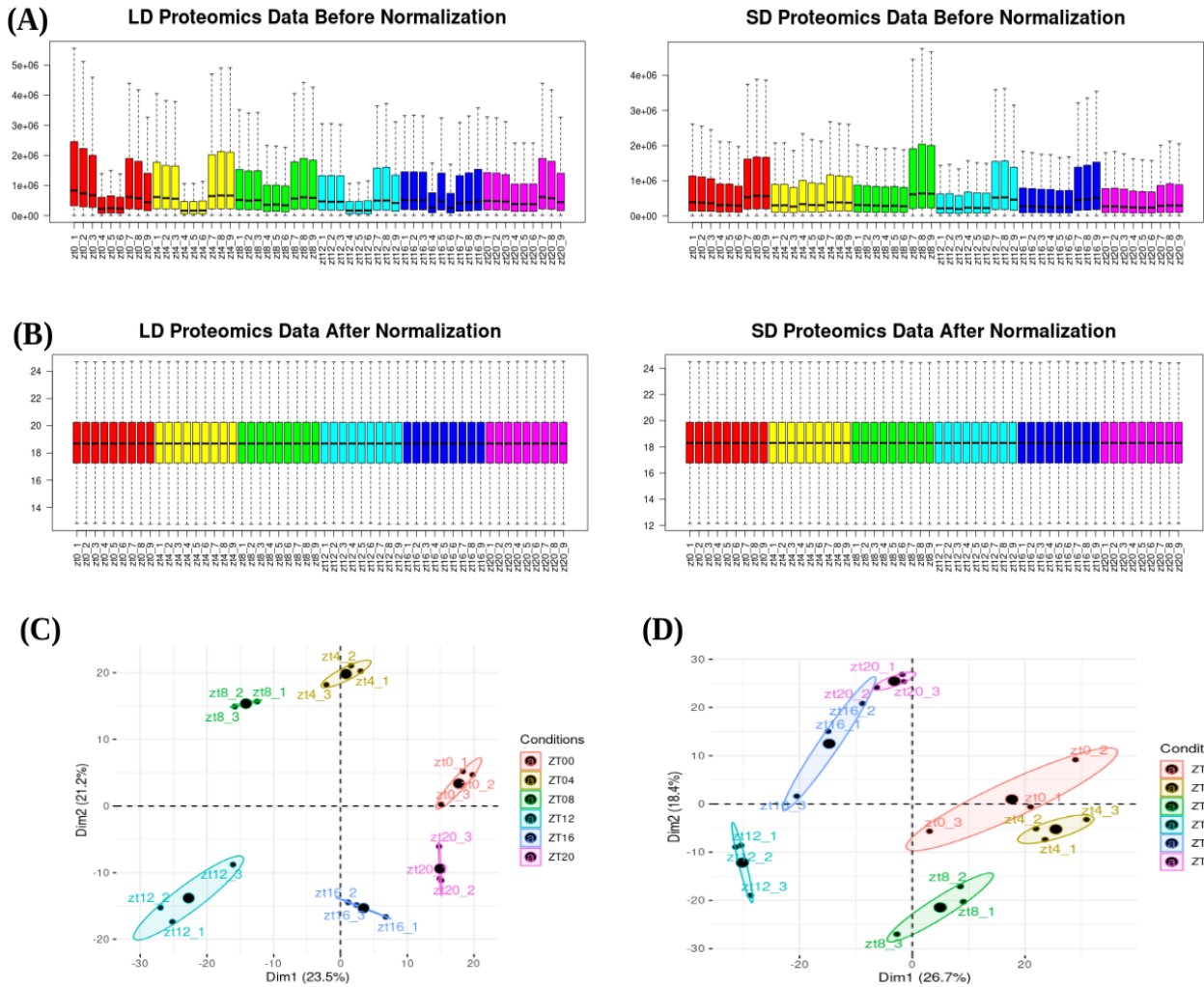


Figure 29: Proteomic data normalization and reliability. (A) Boxplots representing global distributions (before normalization) of protein abundances over the three technical replicates of the six time points corresponding to three consecutive days under long day conditions on the left and under short day conditions on the right. (B) Boxplot representing global distributions after normalization. (C) Principal Component Analysis of the time point global rhythmic proteomes under LD conditions. Small dots correspond to the 2D projection of each time point global rhythmic proteome. Big dots correspond to the average of the three replicates 2D projections for each time point. Ellipses mark the 95% confidence regions corresponding to each time point global rhythmic proteome. A clear circular distribution emerges capturing the cycling structure in diurnal rhythmic LD proteomes. (D) Principal Component Analysis of the time point global rhythmic proteomes under SD conditions. Points and ellipses are used as described before.

In order to obtain a deeper understanding of the underlying structure in our data a principal components analysis was performed separately over the LD (Fig. 28- C) and SD (Fig. 28-

D) rhythmic proteomes. Under LD conditions, the proteomes corresponding to the same time point in the three different days tightly cluster together globally constituting a circular structure. Nonetheless, under SD conditions more variability is observed but the circular structure is still maintained, in contrast to what was observed with SD transcriptomes. Also, the high similarity between the transcriptomes corresponding to ZT0 and ZT20 under SD conditions that is not present in SD proteomes corresponding to those time points. This suggests that during the night starts the transcription of genes which encoding proteins are needed during light , while at the proteomic level, those proteins are present during the light period and, thus, there isn't a clear similarity between night and morning proteomes.

In overall, these results support that our experimental design grants good quality data and a high level of synchronization in our rhythmic proteomic data allowing us to proceed to the identification and comparison of proteins under LD and SD conditions.

Proteomic characterization of diurnal rhythmic abundance profiles

Phase offsets and a decrease in rhythmicity are observed when proteomic and transcriptomic data are compared

The same analysis executed with transcriptomic data, using the R package RAIN, is also executed with proteomic data. In long day proteomic data, only 928 proteins (comprising approximately 32% of the total proteins detected) present diurnal periodic rhythmic expression patterns (FIGX-A). An increase in rhythmicity is observed in short day proteomic data, detecting 1442 rhythmic proteins comprising 44% of the proteins detected (FIGX-B). However, independently from the photoperiod, the rhythmicity levels present in the proteome are much lower than the ones observed in the transcriptome of *Ostreococcus tauri*.*(en el paper de gerben tienen un 67% de proteinas ritmicas en ND, lo menciono?)* Transcripts rhythmic expression profiles do not seem to always lead to a rhythmic protein abundance profile. This phenomenon highlight the relevance of multiomics integration, since transcripts behavior cannot be extrapolated to proteins or cellular processes, neither vice versa. Rhythmic transcripts which encoding proteins maintain their abundance levels constant among diurnal changes have been a paradox in chronobiology research. Currently, protein degradation process is commonly used to unify transcriptomic and proteomic data(citar rhythmic degradation y quizas el de gerben degradation). This hypothesis sug-

gest that rhythmic transcripts are needed to maintain a constant abundance level of the encoding protein when its degradation process is rhythmic. In that way, cells have to cyclic supply new transcripts to balance protein synthesis/degradation ratio.

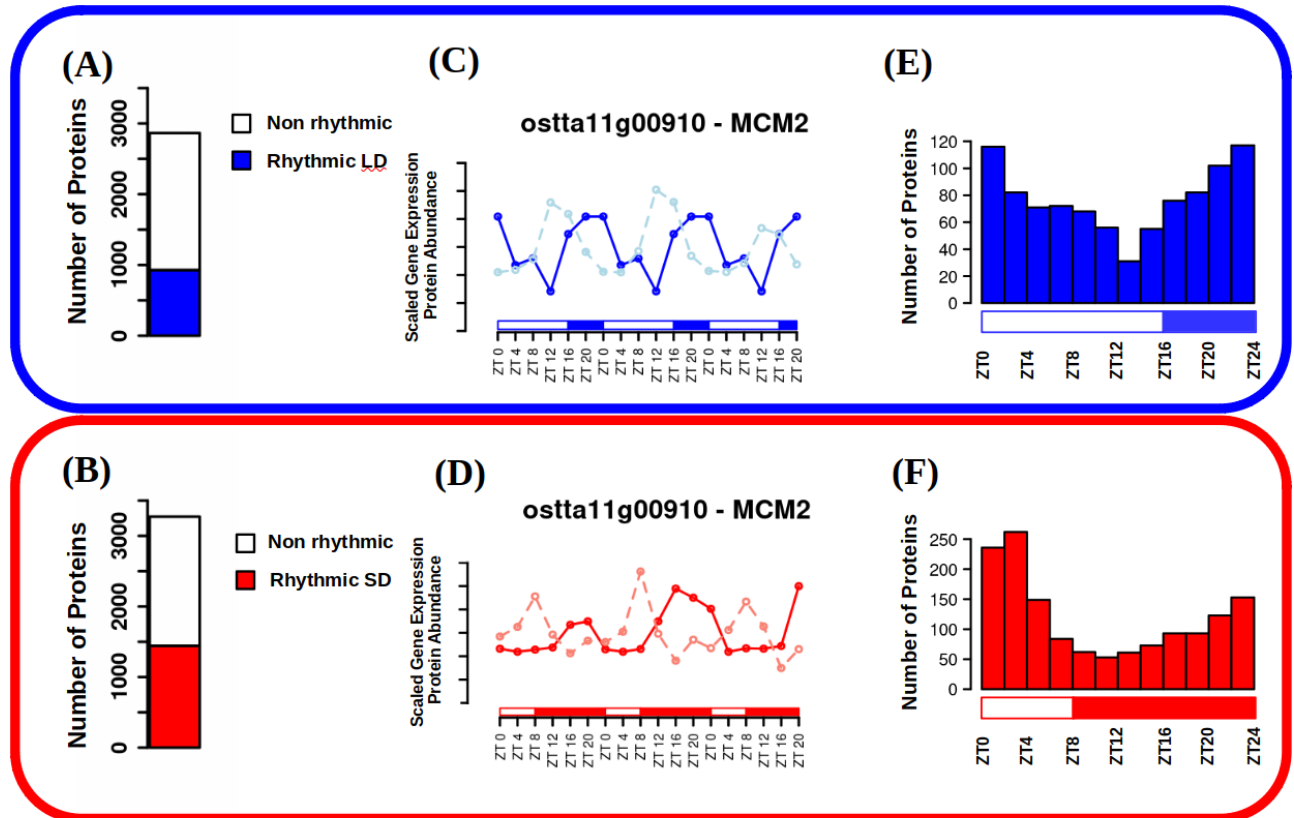


Figure 30: Proteome rhythmicity under alternating light/dark cycles and integration with the transcriptome. (A-B) Barplots representing the number of identified proteins under long day conditions and under short day conditions. The number of rhythmic proteins under LD conditions is represented in blue and under SD conditions in red. Non rhythmic proteins are represented in white. (C-D) Protein abundance profiles under LD (blue) and SD (red) conditions represented together with gene expression profiles under LD (light blue) and SD (light red) conditions for Minichromosome Maintenance 2 (*ostta11g00910*, MCM2). (E-F) Histograms showing the distribution of the number of proteins with phase or maximum abundance at specific time points under LD conditions (blue) and SD conditions (red).

In agreement with previous chronobiology results in other organisms (mismo paper), when protein rhythmic abundance profiles are compared with transcripts rhythmic expression profiles, it is observed a clear phase offset (FIG-C). It suggests that protein translation takes place few hours after gene expression. In our data, while the majority of the transcripts have their maximum expression level during night hours in both photoperiods, the majority of the rhythmic proteins present their maximum abundance level during light hours (FIGX-D). It suggests that the transcriptome of *Ostreococcus tauri* present a nocturnal ac-

tivity while its proteome present a clear diurnal activity. This observation is in agreement with the effects of free-running conditions over the transcriptome of *Ostreococcus tauri*, which were similar with the ones described in the activity of nocturnal organisms.

Proteomic characterization of seasonal effects over the protein abundance profiles

The effects of seasons over the wave parameters in the transcriptome are also found in the proteome of Ostreococcus tauri

As it was executed in the transcriptomic analysis, the R package circacompare is used to study the global effect of the photoperiod over the amplitude and phase of rhythmic abundance profiles of proteins as well. In the previous chapter, it was mentioned that changes in amplitude and phase offsets of biological rhythms dependent of photoperiods have been already described in a wide range of organisms. The effects observed over the transcriptome are also found on the proteome of *Ostreococcus tauri*.

In contrast to our transcriptomic data, when LD and SD rhythmic proteomes are compared globally, there is not a clear increase in the amplitude of the waves described by proteins abundance profiles. However, 57% of the detected rhythmic proteins (that maintain their rhythmicity under both photoperiods) present an increase in amplitude, being significant on 45% of them. This could be directly caused by the decline of synchrony observed over SD transcriptome and/or a decline of synchrony of post-traductional rhythms under shorter photoperiods.

Negative phase shift or phase anticipation is observed over the proteome of *Ostreococcus*, in agreement with what has been described in our transcriptomic data. Specifically, 53% of the detected rhythmic proteins exhibit an anticipated phase under short day conditions when compared to long day conditions, being significant in 60% of them. Phase anticipation are apparent under SD since protein phases are mostly reached around SD light period (from ZT0 to ZT8) whereas, under LD, phases are more uniformly distributed from LD night (ZT16-ZT20) to the end of the maximum irradiance hours (ZT4-ZT8) (Fig. 30-E,F).

These results suggest that seasonal effects over amplitude and phase are more severe over the transcriptome than the proteome of *Ostreococcus tauri*. However, the same

changes are found in a considerable portion of the rhythmic proteins detected. In order to further study this results, the correlation between rhythmic gene expression profiles and proteins abundance profiles is tested (Fig. 31). Whereas the original rhythmic protein abundance and gene expression profiles are negative correlated with a value of -0.34 between, a high positive correlation of 0.84 is observed between the phased aligned profiles, globally (Fig. 31-A). It suggests that the rhythmic wave described by a gene expression and its encoding protein abundance are almost identical, except for their phase offsets (Fig. 31-B,C).

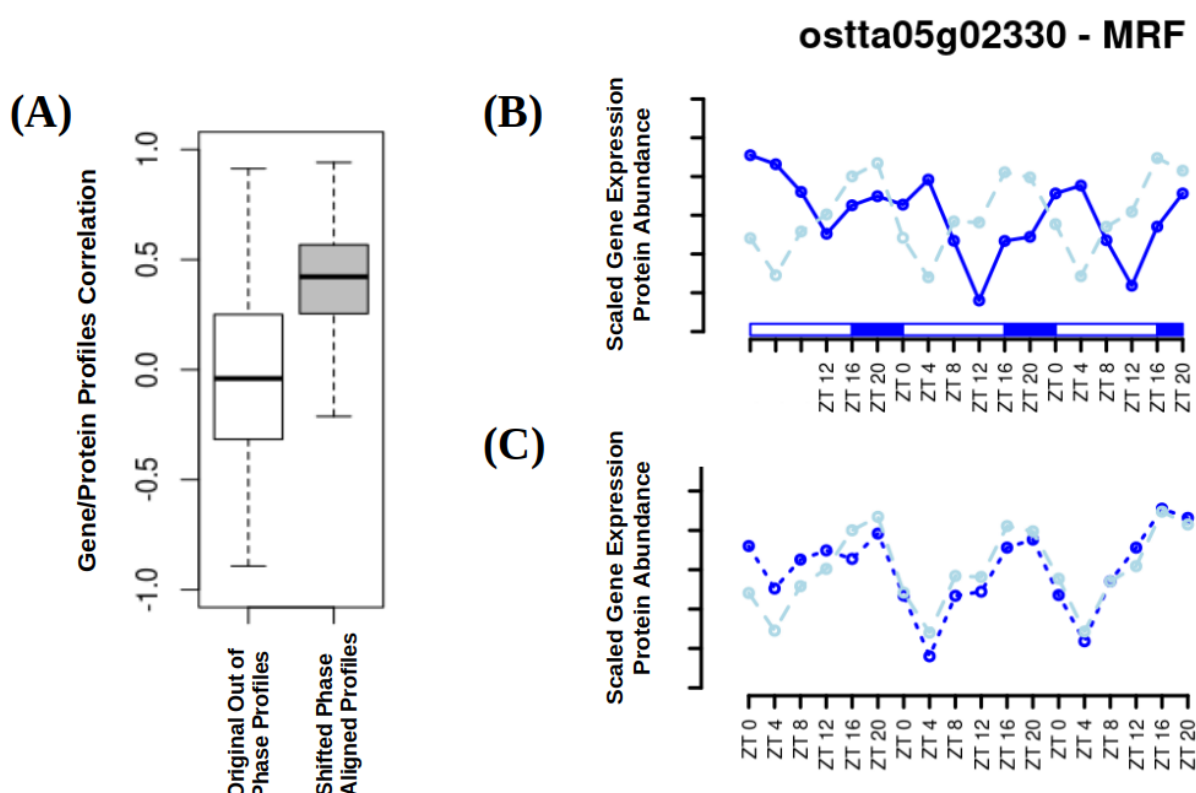


Figure 31: Protein/gene correlation analysis. (A) Boxplots representing the global distribution of the correlations between protein abundance and gene expression profiles (white box) and shifted aligned profiles with coincident phases (grey). (B) Protein abundance (continuous blue line) and gene expression (dashed light blue line) profiles under LD conditions for MA3 domain-containing translation Regulatory Factor (*ostta05g02330*, MRF). (C) Phase aligned protein abundance (dotted blue line) and gene expression (dashed light blue line) profiles.

Phase offsets between genes and proteins involved in the same biological process are adjusted by seasons

In order to obtain a deeper understanding of gene/protein phase offsets, an extensive analysis of its correlation with different factors and protein properties is executed.

One of the possible hypothesis is that gene/protein offsets depend on proteins properties computed from their sequences such as amino acid composition, charge and hydrophobicity. However, no relation is apparent between any protein index and protein/gene offsets (ANEXO).

Another of the possible hypothesis is that gene/protein offsets depend on the time when the maximum level of expression of the encoding gene is reached (gene phase). So, for example, a gene that reaches its maximum level of expression during the morning could take less time to translate than a gene which peak of expression takes place in the middle of the night. However, in our LD data, no significant differences are found when comparing gene/protein offsets of different genes sets with specific phases (Fig. 32-A). Whereas, in our SD data, genes with phases during the skotoperiod (dark period, ZT8, ZT12, ZT16 and ZT20) present significantly longer offsets when compared to those genes with phases during the photoperiod (light period, ZT0 and ZT4) according to Mann-Whitney-Wilcoxon test (Fig. 32-B).

Furthermore, gene/protein offsets affected by seasons cycles is considered as a possible phenomenon. In fact, global protein/gene offsets are significantly longer under SD conditions with respect to LD conditions according to a p-value of 1.2×10^{-9} computed using Mann-Whitney-Wilcoxon test (Fig. 32-C). This phenomenon can also be easily noticed when comparing gene/protein offsets of gene sets involved in the same biological function. For example, following GO terms functional annotation, the genes and proteins involved in DNA replication (associated with the term GO:0006260), show a significant increase in the offset observed between expression and translation under SD conditions (Fig. 32-D). Although the increase in this offset is observed globally, it does not affect equally to every gene/protein, as it is represented in (Fig. 32-D). It suggests that seasonal cycles adjust the offset between gene expression and translation depending on the function they are involved in.

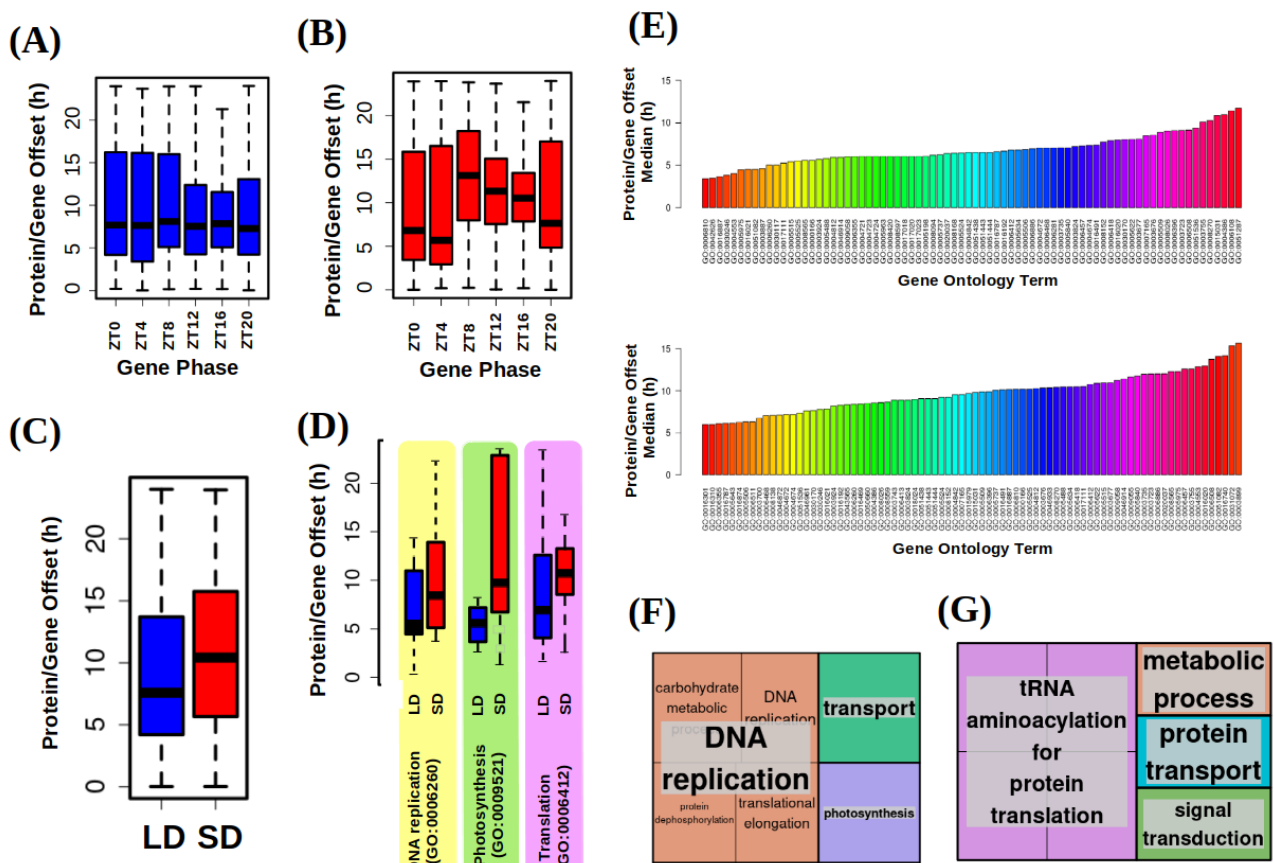


Figure 32: Gene/protein offsets analysis. (A) Boxplot representing protein/gene offsets under LD conditions for different gene sets with specific phases or maximum expression time points. There is no significant differences. (B) Boxplot representing protein/gene offsets under SD conditions for different gene sets with specific phases or maximum expression time points. Differences are significant according to Mann-Whitney-Wilcoxon test. (C) Boxplot representing the offset in hours between protein abundance and gene expression phases under LD (blue) and SD (red) conditions. Differences are significant according to a p-value of 1.2×10^{-9} computed using Mann-Whitney-Wilcoxon test. (D) Boxplot illustrating how genes involved in different biological processes according to their gene ontology (GO) annotation present distinct protein/gene offsets that are longer under SD (red) than LD (blue) conditions. DNA replication (GO:0006260), photosynthesis (GO:0009521) and translation (GO:0006412) are chosen as examples exhibiting short and long protein/gene offsets. (E) Median protein/gene offset for gene sets annotated with the same Gene Ontology (GO) term under LD conditions (top) and SD conditions (bottom). Different biological processes identified by specific GO terms present distinct short or long protein/gene offsets. (F) Treemaps summarizing the biological processes with shortest protein/gene offsets and (G) with longest protein/gene offsets. Semantically similar biological processes are grouped together into the same colored rectangles. The most representative biological processes are shown for each rectangle.

A deeper analysis of gene/protein offsets for gene sets annotated with the same GO term, shows how the different biological functions present distinct short or long offsets under both photoperiods (Fig 32-E). For example, one of the biological processes with the long-

est time between gene expression and translation is related with translation (Fig. 32-F). This result is in agreement with the transcriptional temporal program of *Ostreococcus tauri* illustrated in the previous chapter. Genes involved in translation reach their maximum level of expression during midnight in SD conditions, 8h before dawn. *Ostreococcus tauri* severely reorganize its transcriptional temporal program taking in count not only the current photoperiod but also the different gene/proteins offsets that each biological function presents. In that way, it ensures that proteins will be ready in the exact time they are needed. This could be a possible explanation of why the LD and SD transcriptional temporal programs are not just shifted, but differently arranged.

Furthermore, one of the processes with the shortest time between gene expression and translation is photosynthesis. Some proteins involved in photosynthesis present a high rate of change (CITA?), which can be preserved with short times between gene expression and translation. Also, once again in agreement with our transcriptomic data, genes involved in photosynthesis reach their maximum of expression during high irradiance hours under both photoperiods, so a short delay between gene expression and translation is needed to get the proteins ready when they are needed the most. Photosynthesis and other processes are further analyzed in the next chapter, where an integration of transcriptomics, proteomics and physiological data is presented.

Chapter 4: Diurnal and seasonal multi-omic integration with physiological data.

In the last two chapters, biological rhythms described by proteins and mRNAs have been deeply analyzed and discussed. One of the main results has been the observed temporal offset between transcripts and proteins, which has shown the relevance of multi-omic integration to unveil the complete molecular mechanisms of interest. Since it is the main goal of this thesis, the integration of physiological measurements with multi-omic data is presented as the final step to deeply understand how biological processes are regulated by diurnal and seasonal cycles.

Cell Division Cycle (CDC) of *Ostreococcus tauri* under diurnal and seasonal cycles

Cell division cycle is a biological process that controls the proliferation of cells (from unicellular organisms division to tissue renewal) and it is highly conserved through eukaryotes. The influence of diurnal cycles upon cell division have been studied in a wide range of phyla, from plants and microalgae like *Chlamydomonas*, *Euglena* and *Gonyaulax* (Bruce, 1970; Edmunds & Laval-Martin, 2019; Fung-Uceda et al., 2018; Homma & Hastings, 1989) to mice and humans (Fu et al., 2005; Matsuo et al., 2003). However, the confirmation that circadian regulation controls cell division has been a controversy topic in some organisms, such as one of the main microalgae model organisms, *Chlamydomonas reinhardtii*. While some studies concluded that cell division cycle of this microalgae was under circadian regulation (Bruce, 1970), some other concluded that the daily periodicity observed was caused by a cyclic energy status linked to the circadian regulation of photosynthesis (Spu-dich & Sager, 1980). Nowadays it is known that this biological rhythm present evidences of being directly regulated by the clock, as usually persist in free-running conditions and is able to be entrained by different photoperiods independent of the photosynthetic capacity. In agreement with the RNA-seq data of this thesis, cell division cycle have a complex regulatory mechanism which consist of a strong circadian clock regulation as well as a light-dependence since it is the main energy source in photosynthetic organisms (Goto & Johnson, 1995; Hagiwara et al., 2002; Moulager et al., 2007, 2010). Furthermore, *Ostreococcus tauri* transcriptome seems to accomplish these characteristics. As it was mentioned in Chapter 2, its DNA replication genes need a light input to maintain rhythmicity under free-

running conditions (ANEXO). Cell division cycle of *Ostreococcus* consists of the typical phases of a simple binary fission. First, a G1 phase which is dependent on light-energy status. During this phase the cell grows and commitment takes place (Moulager et al., 2007). In cell division cycle studies, the term commitment refers to the moment when the cell, taking into consideration its energy status, decides whether is ready or not to continue with the progression of the cell division cycle. Once cells are committed, cell division is not impaired by darkness. If commitment is achieved, G1 phase is followed by the S phase where DNA replication takes place. S phase is usually gated several hours after sunrise (Moulager et al., 2007, 2010). Once DNA replication is completed, cells enter to the final G2|M phase where they prepare themselves for cell division (G2) and achieve mitosis (M). These two last phases are usually treated as one because they are the shortest ones and, thus, the most difficult to detect and discern. In all eukaryotes, the progression of cells throughout the phases of the cell division cycle is controlled by cyclins and cyclin-dependent kinases (CDKs). *Ostreococcus tauri* has got a extremely reduced set of cyclins and CDKs, presenting only a single copy of each gene (Robbens et al., 2005). Also, in *Ostreococcus* genome are found a canonical cell division control protein 25 (CDC25), which is not present in plants (Khadaroo et al., 2004), and a plant-specific CDKB (Corellou et al., 2005).

In the previous chapters, genes and proteins involved in DNA replication (S phase) have been highlighted in several analyses. Specifically, DNA replication is one of the enriched processes in the set of genes that need a light input to maintain rhythmicity, as well as one of the processes with the shortest time between gene expression and translation. Those results from multi-omics analyses are integrated with physiologic data in this chapter. This integration unveil the adaptation of the cell division cycle of *Ostreococcus* to different seasons and contributes to dissect the molecular mechanisms of circadian regulation of cell division in microalgae.

Temporal program of cell division cycle under summer and winter photoperiod

The phases from the cell division cycle have been detected by estimating the DNA content of cells using flux cytometry and chloroplast division have been observed under the fluorescence microscope, as described in Materials and Methods. The same rhythmicity analysis, also described in Materials and Methods, carried out with the transcriptomic and pro-

teomic data, is also achieved using cytometry data generated from the three days in a row under light-dark cycles.

Under summer photoperiod, G1, S and G2|M phases present significant rhythmic profiles with p-values of 2.96×10^{-6} , 3.84×10^{-4} and 0.017, respectively. Whereas under winter photoperiod, only G1 and S phases present significant rhythmic profiles with p-values of 3.08×10^{-3} and 0.067, respectively. In agreement with our transcriptomic and proteomic analyses, a decrease in synchronization manifested as a reduction in amplitude is observed under winter photoperiod (Fig 33-A). The reduction in amplitude is so drastic in the G2|M phase that RAIN is not able to detect a rhythmic profile. This suggest that cell division cycles of each individual cell in the culture are more synchronized during summer photoperiod. Also, there is a significant anticipation of the phase described by this biological rhythm, suggesting that cell division cycle is shifted ~4h between seasons as well as a lower percentage of committed cells under winter photoperiod. ([añadir boxplot mostrando estas diferencias?](#))

The mean percentage of cells involved in G1, S and G2|M phases are calculated for each time point. These data are used to illustrate a temporal program of the cell division cycle of *Ostreococcus* under both photoperiods (Fig. 33- B,C). Under summer photoperiod, G1 phase takes place during the light hours, the maximum percentage of cells in this phase are detected around ZT8 (coinciding with the maximum irradiance hours). After commitment, the percentage of cells in G1 phase decrease while the percentage of cells in S phase increase. The majority of cells are in S phase around and after sunset (between ZT16 and ZT20). From that moment, the percentage of cells in G2|M phase increase gradually as they successfully duplicate its DNA. The transition from G2|M phase to G1, which indicates that cell division has been achieved, takes place around ZT4. This suggest that cell division in *Ostreococcus* takes place after sunrise in summer conditions (Fig. 33-B).

Under winter photoperiod, in agreement with what has been observed in summer photoperiod, G1 phase coincide with the maximum irradiance hours (corresponding to ZT4 in this photoperiod) and the S phase takes place 4h hours after sunset (corresponding to ZT8 in this photoperiod). However, the G2|M phase present not only an adjustment to the photoperiod, but a reorganization in order to anticipate the small number of light hours ahead. During winter photoperiod, G2|M phase takes place only during the night. Right when the

sun rises, cell division is achieved so cells are ready to grow during the morning. It suggest that cell division cycle, as it is strongly influenced by the circadian clock, can anticipate cyclic changes like the short time of light in winter photoperiods. To anticipate it, the circadian clock ensures that all cells enter G1 phase right during sunrise so any hour of light is wasted (Fig. 33-A). This anticipation is also observed in chloroplast division. Under summer photoperiod, chloroplast duplication is achieved during the last part of the night (ZT20) (Fig. 33-D) and during ZT16 under winter photoperiods. Before sunrise, there are already a substantial number of cells with only one chloroplast during winter photoperiods (Fig. 33-E).

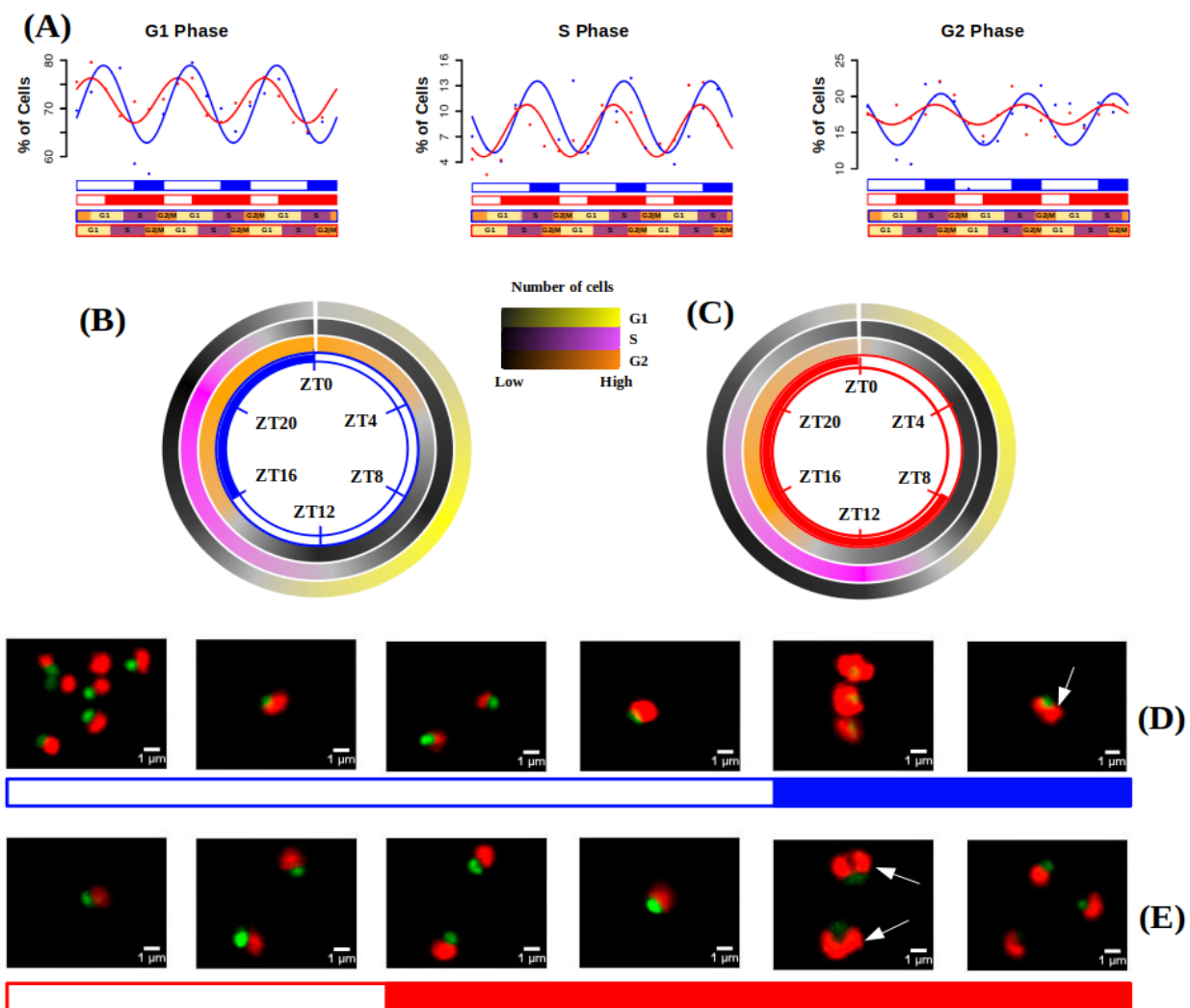


Figure 33. Cell division cycle of *Ostreococcus tauri* under summer and winter photoperiod. (A) Percentage of cells in G1, S and G2|M phases during the three days of sampling. Points correspond to real data and lines represent waves approximations made by Circacompare during the rhythmicity analysis. (B-C) Circular heatmap representing mean percentage of cells in G1, S and G2|M phases during summer and winter photoperiod, respectively. (D-E) Pictures of cells under the fluorescence microscope. Each picture correspond to a different time point of summer and winter photoperiod, respectively. Nucleus are dyed and they fluorescence in green, chloroplast in red.

Integration of cell division cycle program with transcriptomic and proteomic data.

Ostreococcus tauri annotated genes involved in cell cycle are organized in three different groups in order to mark in which phase of the cell cycle they are present. This organization is represented in ANEXO (meter en anexo o aquí como tabla?) following the current cell cycle model in plants (Carneiro et al., 2021).

Cyclin A and CDKA are transcribed and translated during G1, thus, they are considered as proteins related to G1 phase which are needed to enter to S phase. Transcription factors like E2F and Dp as well as other proteins (Rb, cell division control protein 6 and ORCs) also act during G1 phase regulating the activation of genes related to the S phase. Cyclin B and CDKB transcript/proteins levels are maintained during the S phase, in conjunction with the generation of polymerases and replication related proteins (MCM complexes, replication factors, PCNA, primases, helicases, ligases, etc). Finally, Cyclin D marks the beginning of G2|M phase as well as subunits of the anaphase-promoting complex (APC) and cell division control proteins (CDC20 and CDC25) (Moulager et al., 2007, 2010; Robbins et al., 2005).

Their gene expression and protein abundance profiles are compared with the % of cells in the phase of the cycle they are involved in (Fig. 34). Besides the gene-protein offset, a general offset between protein abundance and the execution of their physiological role is observed. This offset is longer in phases as G1 or G2 (Fig. 34- A,C). During the S phase, as soon as the proteins are available the biological process is executed (Fig. 34- B). It could be explained by the experimental design followed, since proteins selected are directly involved in DNA replication and flow cytometry directly estimates cell division phases based in the DNA content of populations.

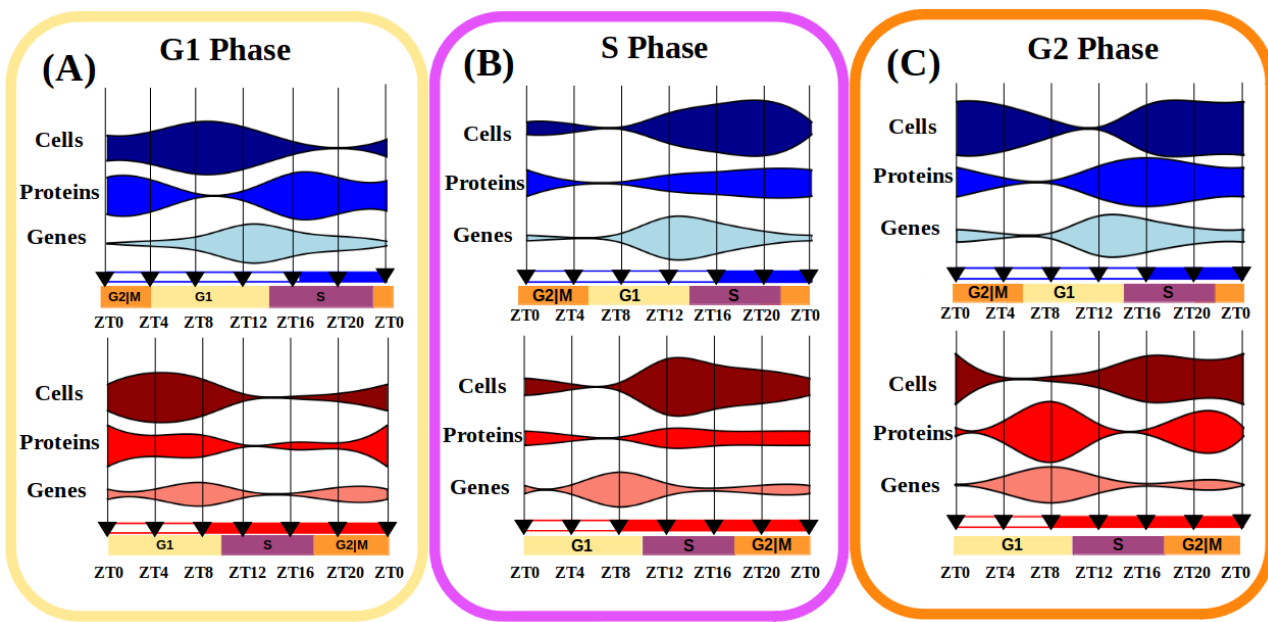


Figure 34: Integration of gene expression, protein abundance and cell population profiles for each phase of the cell cycle. Violin plots represent the three biological levels studied: “Genes” for transcriptomic data, “Proteins” for proteomic data and “Cells” for DNA content estimation by flow cytometry. (A) Involves G1 phase related data, (B) for S phase and (C) for G2 phase.

The transcriptomic and proteomic data for cyclins and CDKs found in *Ostreococcus* are in agreement with the current cell cycle model for plants (Fig. 35). For both summer and winter photoperiods, the transcription of Cyclin A gene takes place during G1 phase and it is the first cyclin to be activated. Cyclin A is suggested to be purely regulated by the circadian clock since it has been probed to be independent of the metabolic status (Moulager et al., 2010). In agreement with previous transcriptomic analysis (Carneiro et al., 2021; Moulager et al., 2007), Cyclin A expression is followed by Cyclin B expression during the S phase (Fig 35-A).

Cyclins proteins are not detected in our proteomic analysis, however CDKA and CDKB proteins are detected and their abundance profiles are in agreement with the proposed model. CDKA transcript reaches its maximum level of expression during G1, which causes an increase of CDKA protein abundance by the second part of G1 phase (Fig. 35-B) allowing, with CyclinA, the progression of the cell cycle to the S phase. During the S phase, CDKB protein abundance level reaches its maximum (Fig. 35- C), being coincident with Cyclin B transcript. Cyclin D transcript levels are low under both photoperiods, but their maximum level of expression are coincident with G2|M phase (Fig. 35-A). **Por qué sube tanto la CycA en SD?**

FTSZ transcript and protein profiles are presented in order to achieve a deeper understanding of the chloroplast division in *Ostreococcus*. FTSZ is a key protein of the chloroplast division machinery that has been conserved from its cyanobacterial ancestors (FtsZ in chloroplast division: Structure, function and evolution). Chloroplast division is considered to take place during sunrise in summer photoperiod and 4h before sunrise in winter photoperiod (Fig. 33- D,E), which is in agreement with the protein abundance profiles of FTSZ in both photoperiods (Fig. 35-D) **En realidad SD no coincide muy bien no? merece la pena poner las graficas de FTSZ?**

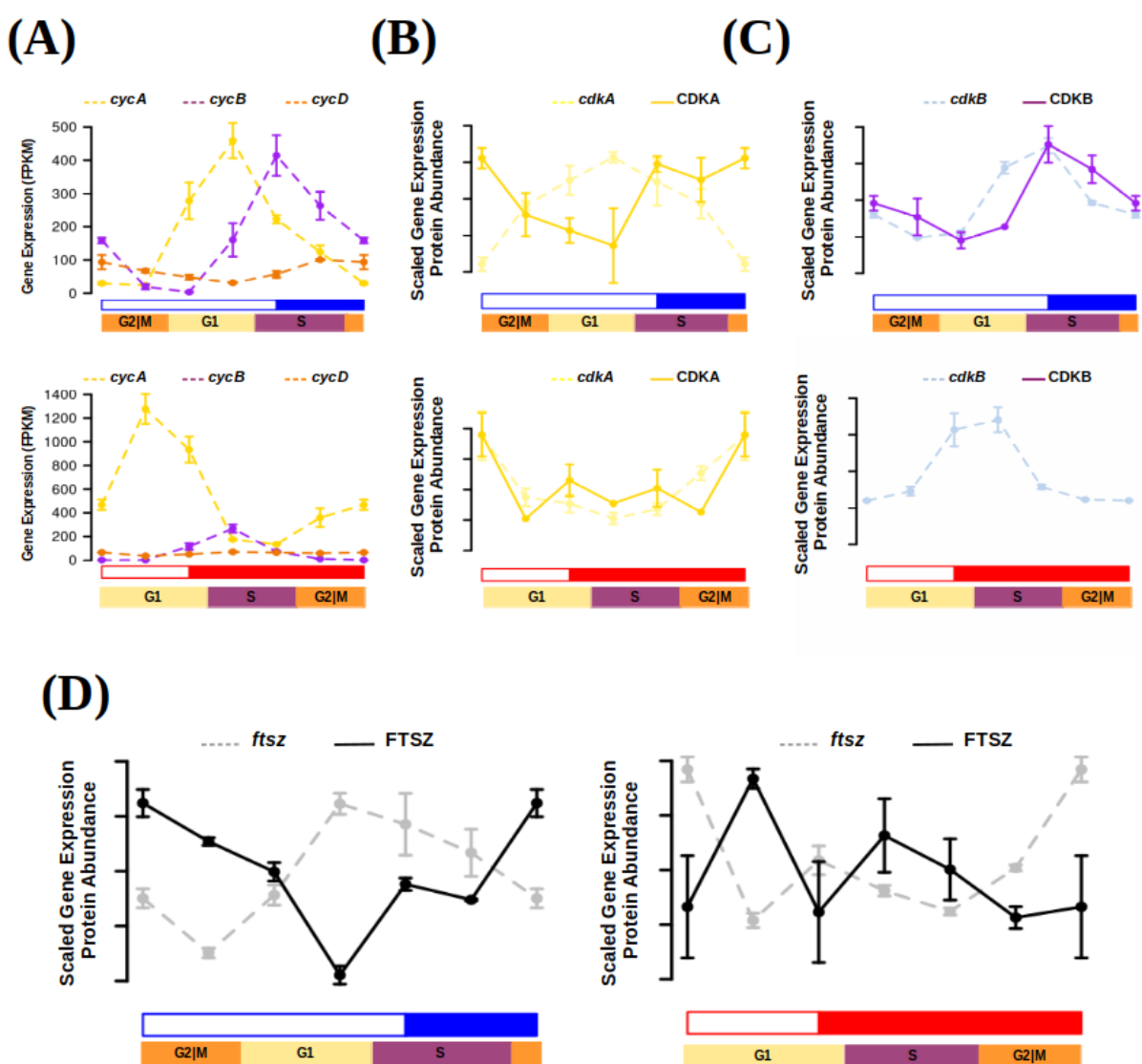


Figure 35: Transcript and protein abundance profiles of the main cell cycle proteins under summer and winter photoperiod in *Ostreococcus tauri*. (A) Expression level of cyclins A (yellow), B (purple) and D (orange) genes are represented with discontinued lines under summer (blue) and winter (red) photoperiods. Transcript (discontinued line) and protein (solid line) abundances of CDKA are represented in yellow (B), CDKB in purple (C) and FTSZ in black (D).

Diurnal and seasonal rhythm of photosynthesis in *Ostreococcus tauri*

Photosynthesis is the process that allow plants to use light as their main energy source. It consumes H₂O and produces O₂ (which is released to the atmosphere), ATP (which is used as energy in the main cellular processes), and NADPH (which is used as reducing agent needed in the Calvin cycle to fix CO₂ from the atmosphere and synthesize carbon compounds).

In the genome of *Ostreococcus tauri*, all the essential proteins involved in photosynthesis electron transport chain and carbon fixation are present, but with a lower number of copies compared with other plants and microalgae. The light-harvesting complexes of *Ostreococcus* are singular: light-harvesting complex proteins associated with photosystem I (LHC_I) are present but LHC_{II} are lacking. Instead, a prasinophyte-specific chrolophyll-binding proteins are found (Blanc-Mathieu et al., 2014; Derelle et al., 2006). It suggest that LHC_I is present in the green lineage since earlier (Six et al., 2005).

Understanding how photosynthesis is adapted to diurnal and seasonal cycles can contribute to develop systems where plant productivity is increased, which is a relevant topic of great importance in agriculture. Circadian regulation of this process was first described in marine algae, when circadian oscillations of oxygen production were observed for the first time (Dodd et al., 2014; Sweeney & Haxo, 1961). After that discovery, circadian oscillations of more physiological phenomena related to photosynthesis (such as chloroplast ATP concentration, electron transport rate, starch content or photosynthesis efficiency) have been also described in microalgae (Mackenzie & Morse, 2011; Ral et al., 2006; Sorek et al., 2013; Sweeney & Haxo, 1961). Furthermore, circadian oscillations in physiological measurements related to photosynthesis are also found in plants, even in the ones with agriculture interest (Feugier & Satake, 2013; Lonergan, 1981; Tucker et al., 2004). Nowadays, omics techniques have enable to elucidate that genes involved in photosynthesis and carbon fixation describe oscillations with a 24h period in microalgae and plants (Ferrari et al., 2019). In addition, this thesis describes for the first time how rhythmic expression profiles of the genes involved in the complete metabolic pathway are maintained under different photoperiods and free-running conditions (constant light and constant darkness) in a photosynthetic organism.

During the previous chapters, photosynthesis have been highlighted several times. First, the genes involved in photosynthesis have been described as *bona fide* circadian genes in Chapter 4, since their rhythmic expression profile is maintained during both summer and winter photoperiod and free-running conditions. Moreover, in Chapter 5, photosynthesis have been found as one of the processes with the shortest offset between gene expression and translation in *Ostreococcus tauri*. Those results from multi-omics analyses are now integrated with photosynthetic efficiency measurements under both photoperiods. This integration unveil the adaptation of photosynthesis and related processes like carbon fixation and starch metabolism in *Ostreococcus* to different seasons and contributes to dissect the conserved circadian regulation mechanisms controlling photosynthetic productivity in the green lineage.

Rhythmic oscillations of photosynthetic efficiency under summer and winter photoperiod

Photosynthesis efficiency has been calculated by estimating chlorophyll fluorescence parameter Fv/Fm, which is used as a common measure of PSII performance. The same rhythmicity analysis carried out with the transcriptomic, proteomic and cytometry data is also achieved with Fv/Fm measurements obtained from three consecutive days under light-dark cycles (summer and winter photoperiods). Data generation and analysis methods are described in detail in Materials and Methods.

Under summer photoperiod, Fv/Fm measurements present a clear rhythmic profile with a 24h period, with a p-value of 3.5×10^{-7} (Fig. 36-A). The maximum level of Fv/Fm takes place periodically every 24h during the maximum irradiance hours (around ZT8 in summer photoperiod). It suggests that photosystems are at their higher performance by that time of the day and, thus, photosynthesis efficiency. Whereas under winter photoperiod, it is described a rhythmic profile with two increments in the Fv/Fm value (Fig. 36-B). Both peaks in Fv/Fm rhythmic profile are significantly repeated periodically every 12h with a p-value of 0.01. One peak is in agreement with the summer Fv/Fm rhythmic profile and it takes place during the maximum irradiance hours (ZT4 in winter photoperiod). The other peak correspond to a smaller increment of Fv/Fm value that takes place more than 8h before sunrise. It means that photosynthesis machinery is prepared in anticipation during the night as a circadian response to the few hours of light during winter photoperiod. These results suggest

that *Ostreococcus tauri* is able to anticipate cyclic changes in photoperiod, which is a signal of strong circadian regulation of photosynthesis machinery.

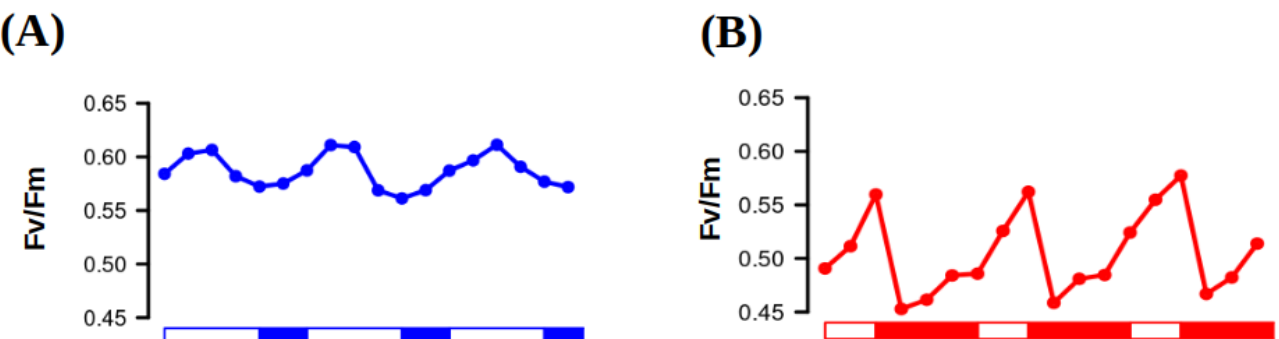


Figure 36. Photosynthesis efficiency rhythmic oscillations. F_v/F_m oscillating values used as an estimation of PSII performance and, thus, photosynthesis efficiency under three consecutive days of summer (A) and winter (B) photoperiods.

Integration of photosynthesis efficiency rhythmic profile with multi-omic data

F_v/F_m rhythmic profiles are integrated with the proteomics and transcriptomics data of the PSII, PSI and chlorophyll binding proteins (ANEXO con las proteinas consideradas o tabla aquí?). During summer photoperiod, those photosynthesis proteins are maintained at the same abundance levels during the light hours. However, the F_v/F_m levels are not equally maintained during the light hours as proteins do. Instead, the best photosynthesis efficiency (higher F_v/F_m levels) is observed when transcription of photosynthesis genes is taking place (Fig. 37-A). It suggest that, during summer photoperiod, there is not a significant temporal offset between gene-protein-physiological measurement. Genes are translated as soon as they are transcribed and photosynthesis efficiency increase as proteins are *de-novo* synthesized. During winter photoperiod, as it was mentioned in Chapter 3, the gene-protein offset become larger. Gene expression and *de-novo* synthesis of proteins are not taking place simultaneously as they apparently do during summer photoperiod. In agreement, maximum level of photosynthesis efficiency takes place few hours after the maximum expression level (Fig. 37-B). In addition, rhythmic profiles with 12h period (2 peaks every 24h) under winter photoperiod are not only observed in F_v/F_m measurements, but also at the transcriptomic level. Photosynthesis genes present two peaks of expression per day, as many other genes do under winter photoperiod (Fig. 26-A). In this case, one of the expression peaks takes place during the first part of the morning, increas-

ing photosynthetic efficiency during the maximum irradiance hours. Whereas the second peak of expression takes place during the night hours, preparing the photosynthesis machinery with anticipation to sunrise. It suggest that photosynthesis machinery anticipation to photoperiod is transcriptionally regulated in *Ostreococcus tauri* and, probably, since early in the green lineage.

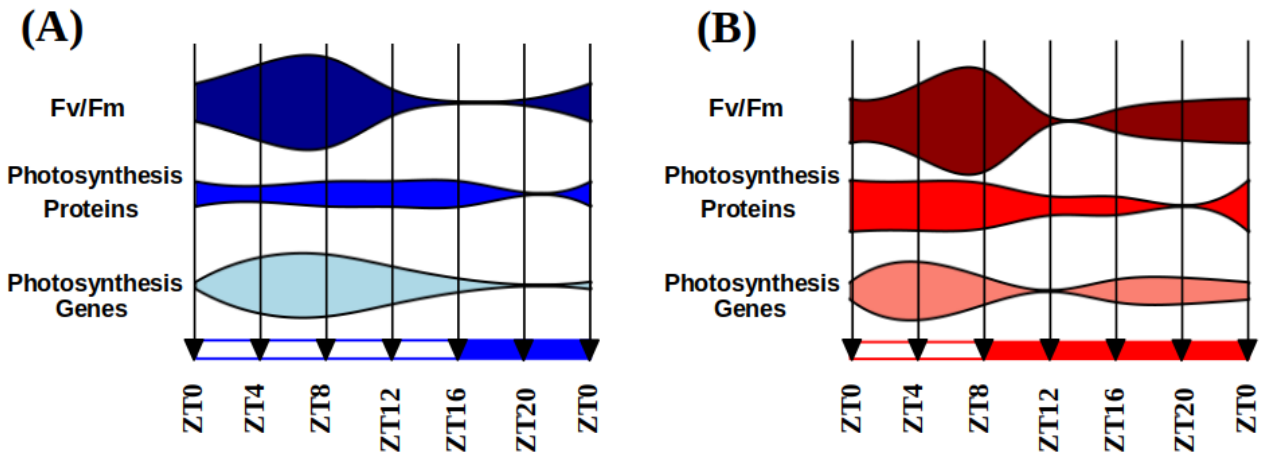


Figure 37. Integration of Fv/Fm oscillations with multi-omic data. Fv/Fm measurents are integrated with multi-omic data from proteins related with photosynthesis efficiency under summer (A) and winter (B) photoperiod.

Only a reduced number of proteins with a clear role on photosynthesis efficiency were included in the previous results in order to correctly correlate their profiles. However, photosynthesis is a process where a huge amount of different proteins are involved and different metabolic pathways strongly depend on its execution. Photosynthesis is executed by an electron transport chain that consist of three big protein complexes (Photosystem II, cytochrome b6f, Photosystem I) that use electrons obtained from hydrolysis to generate NADPH. The protons accumulated inside the lumen during electron transport are released by the ATPase producing also ATP. NADPH and ATP are needed to fix CO₂ and generate carbon compounds in the Calvin cycle. Those carbon compounds can be accumulated as a reservoir of starch. In higher plants, the circadian clock participates in the coordination of different physiological processes like photosynthesis, carbon fixation and starch biosynthesis (de los Reyes, Romero-Campero, Teresa Ruiz, et al., 2017; Farré & Weise, 2012; Graf et al., 2010). Multi-omics data presented in this thesis allow generate a complete picture of how these processes respond and anticipate to seasonal and diurnal cycles in *Ostreococcus tauri*.

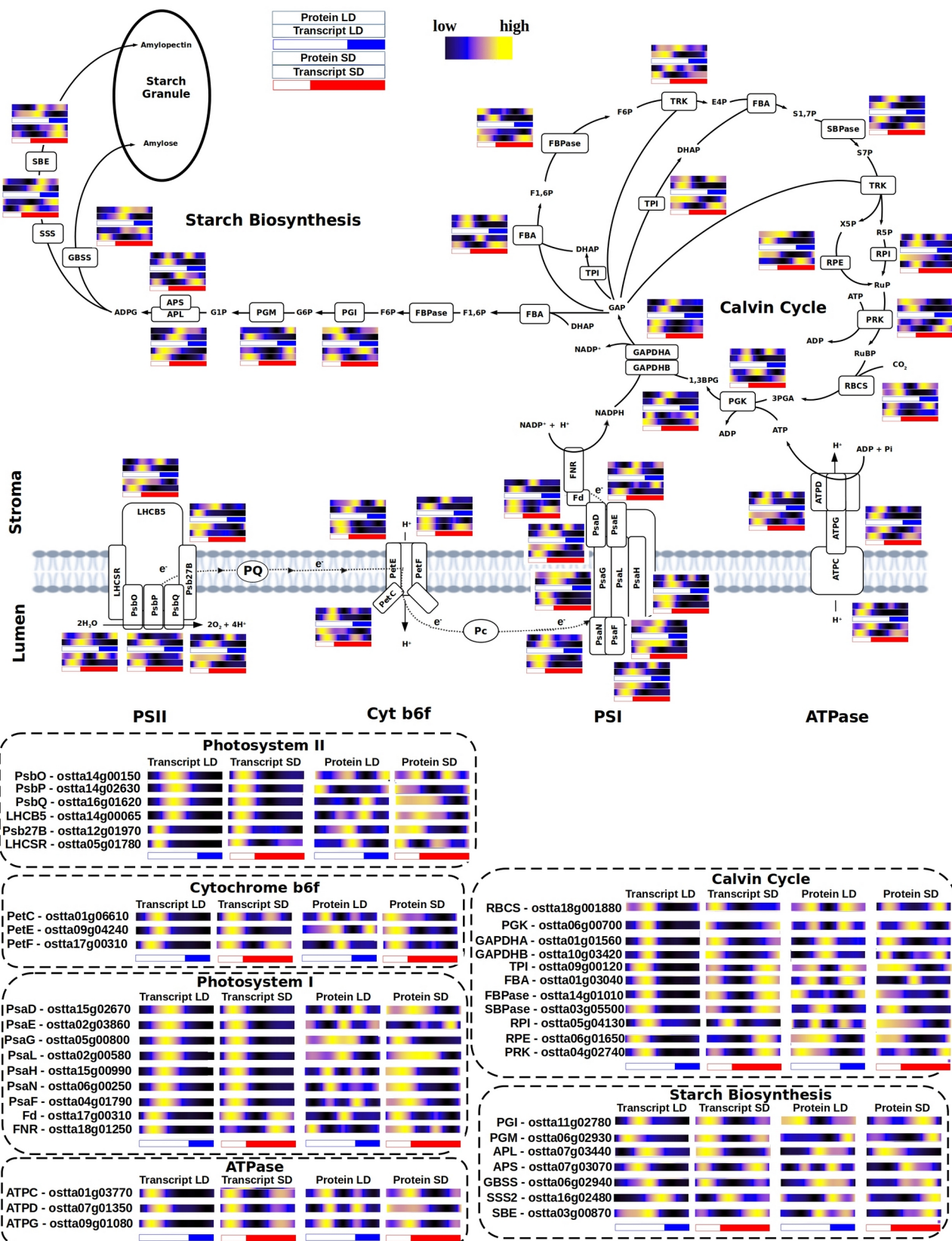


Figure 38. Integration of multi-omic data of enzymes and proteins involved in photosynthesis, Calvin cycle and starch biosynthesis.

Genes involved photosynthesis electron transport chain and Calvin cycle are uniformly expressed early in the morning during both summer and winter photoperiod. The expression of those genes early in the morning seems to be conserved independently of the photoperiod, since it has been also observed in *Ostreococcus* under 12h of light and 12h of dark (Monnier et al., 2010). However, the already mentioned rhythmic profiles with 12h period (2 peaks of expression per day) are described by numerous genes involved in both processes during winter photoperiod (Fig. 38). The anticipation to the short light period during winter photoperiod is not only reflected on photosynthesis efficiency (Fig. 36-37). Instead, it is found systematically in the complete metabolic interaction of both processes.

In addition, protein abundance rhythmic profiles with 12h period are observed under summer photoperiod. This phenomenon has been previously observed in RuBisCO small sub-unit (RBCS) protein abundance profile in plants ([CITA pedir a fran](#)), our multi-omics integration show that this phenomenon is present systematically in the Calvin cycle enzymes, as well as some proteins from the photosynthesis electron transport chain. Also, these 12h period profiles are not transcriptomically regulated, since its encoding transcripts describe one peak of expression per day. The mRNA rhythmic profiles of some enzymes from the Calvin cycle are in agreement with previously published data in plants (Pilgrim & McClung, 1993), so it suggest that a strong post-translation regulatory mechanism is causing this 12h period profile in proteins involved in photosynthesis during long photoperiods in both microalgae and plants.

Integration of starch content diel oscillations with multi-omic data

There exist an influx of carbon compounds obtained from the Calvin cycle that are accumulated inside cells as starch. The accumulation and degradation of starch have been described to be circadian regulated since a periodic oscillation of its content is observed in photosynthetic organisms as *Chlamydomonas* and *Arabidopsis*, as well as a rhythmic gene expression profile of the enzymes involved in the process (Flis et al., 2019; Ral et al., 2006; Sulpice et al., 2014). Starch content in *Ostreococcus tauri* under diurnal cycles is also rhythmic with a 24h period (Fig. 39), reaching its maximum starch content at the high irradiance hours under both summer and winter photoperiods. *Chlamydomonas* reaches its maximum starch content few hours after sunset (Ral et al., 2006), while *Arabidopsis* plants reach it exactly at sunset (Feugier & Satake, 2013). In both cases, starch starts to

accumulate during the light hours, until amylase (AMY) enzymes are activated and its degradation starts. Starch content is a result of a controlled balance between its degradation (where AMY is involved) and its synthesis (where APL is involved). In *Ostreococcus tauri*, AMY (ostta10g00260) protein abundance starts to increase right after the high irradiance hours, coinciding with the beginning of starch degradation. Whereas, APL (ostta07g03440) protein abundance seems to increase in order to counter the degradation of starch during the night hours and avoid carbon starvation (Fig. 39-B). In plants, starch degradation during winter photoperiods has been described to be executed more slowly than during summer photoperiod (Feugier & Satake, 2013; Sulpice et al., 2014), which is in agreement with the results presented in this thesis (Fig. 39-A). In addition, both APL and AMY protein abundance profiles are strongly coincident with their gene expression profile with a ~4h offset, showing that starch synthesis-degradation balance is possibly transcriptomically regulated. These results suggest that there is not a conserved starch content temporal program throughout the green lineage as it has been observed with other biological processes in this thesis. However, a strong transcriptomic circadian regulation and seasonal adaptation seems to be conserved.

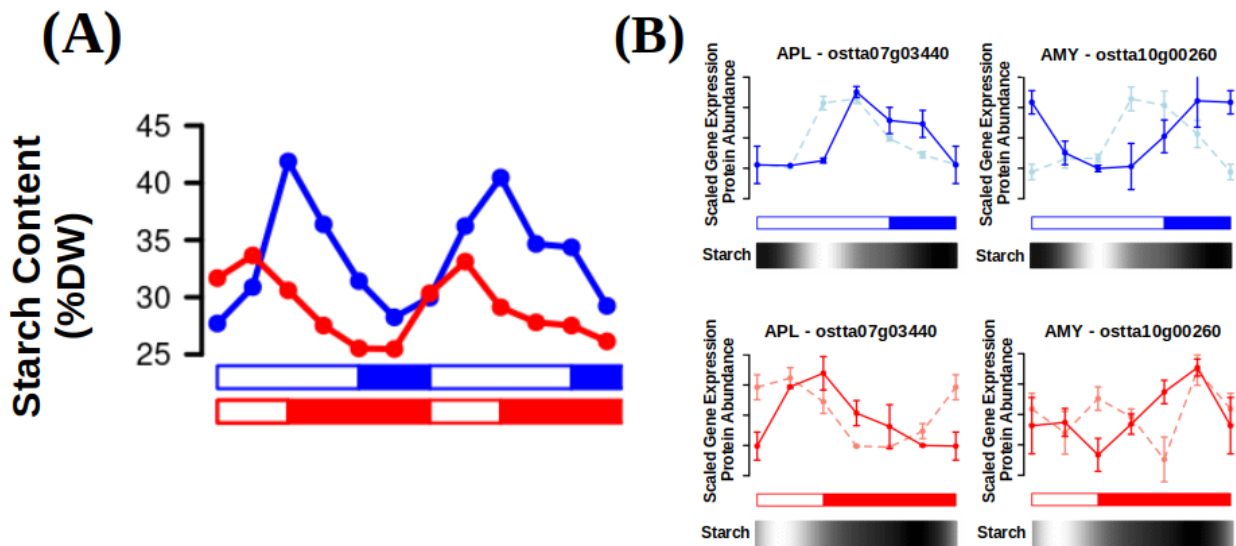


Figure 39. Starch content periodic oscillations coincide with main enzymes involved in starch synthesis and degradation.

More metabolic pathways of *Ostreococcus tauri* showing periodic oscillations under diurnal and seasonal cycles

Carotenoids biosynthesis in Ostreococcus tauri under diurnal and seasonal cycles

Carotenoid are a group of isoprenoid pigments that are present in microalgae and plants. Some of these pigments are associated with light harvesting complexes and play a crucial role in photosynthesis by absorbing light energy and transferring it to chlorophyll. Carotenoids also act as antioxidants, protecting the organism from damage caused by excess light or environmental stress (García-Plazaola et al., 2017; T. Sun et al., 2022). Carotenoids are produced and accumulated at the most appropriate time to maximize their benefits for the organism. In fact, expression of genes involved in carotenoid biosynthesis are regulated by the circadian clock in plants and algae (Covington et al., 2008; García-Plazaola et al., 2017; Pan et al., 2009; T. H. Sun et al., 2010; Zhang et al., 2022).

In addition to their role in photosynthesis, carotenoids also have significant nutritional value for humans. Some carotenoids, such as β -carotene and α -carotene, can be converted into vitamin A, which is essential for vision and the immune system. These and other carotenoids as astaxanthin have also been shown to have potential health benefits, such as reducing the risk of certain types of cancer and heart disease (Eggersdorfer & Wyss, 2018).

Industrial production of carotenoids involves the large-scale cultivation of photosynthetic microorganisms such as algae. They are tipically grown outdoors in large ponds or in closed photobioreactors. In the last two decades, numerous research groups have been studying growth conditions, microalgae metabolism and optimizing photobioreactors design in order to maximize carotenoids production while minimizing costs (Del Campo et al., 2004; Hoys et al., 2021; Sierra et al., 2008). Since they are cultivated outdoors, understanding how carotenoids biosynthesis oscillates under diurnal and seasonal cycles is crucial to ensure the maximum carotenoids content at harvesting time, as well as to find possible gene and proteins targets. However, the possible influence of the circadian clock on carotenoids production optimization still remains unkown due to a lack of research of the topic. This thesis work aims to contribute to elucidate the circadian regulatory mechanism of carotenoids biosynthesis in order to enhance plants and microalgae industry optimization.

Integration of multi-omics data with oscillations described by carotenoids content in *Ostreococcus tauri* under diurnal and seasonal cycles

Ostreococcus tauri is rich in widely distributed carotenoids like violaxanthin, antheraxanthin or zeaxanthin. Carotenoids specific of Mamiellophyceae like micromonal, uriolide or prasinoxanthin are also found in this prasinophyte, being prasinoxanthin the most abundant (Egeland et al., 1995; Guyon et al., 2018; Six et al., 2009). Its genome present genes encoding for the Methylerythritol 4-phosphate (MEP) pathway (Derelle et al., 2006; L. Zhao et al., 2013), which derives pyruvate to the production of geranyl pyrophosphate (GPP), the main carotenoid precursor. The carotenogenesis pathway starts with the enzyme phytoene synthase (PSY) and consist of two different branches: β -branch, including the xanthophylls cycle; and α -branch, including the main antenna carotenoids in prasinophyte which biosynthesis pathways are still unknown (Guyon et al., 2018; Six et al., 2009).

Carotenoids content during diurnal cycles under both summer and winter photoperiods have been estimated from HPLC profiles, as described in Materials and Methods. The same rhythmicity analysis carried out with the omic data was also achieved using the estimated carotenoids content generated from the three consecutive days under light-dark cycles.

Under both summer and winter photoperiods, all carotenoids describe rhythmic abundance profiles with periods of 24h, with a p-value lower than 0.05. With the exception of lutein and violaxanthin, that do not maintain their rhythmicity under winter photoperiod. In general, fluctuations on carotenoids content during winter photoperiod seem to less drastic. (Fig. 40-A).

Oscillating carotenoids content are in agreement with the transcriptomic and proteomic data generated. The generation of geranyl pyrophosphate is crucial for carotenogenesis, the most of the enzymes involved in MEP pathway present a high protein abundance level with anticipation during the night under both summer and winter photoperiod. The enzymes involved in the first steps of the carotenogenesis, from the generation of phytoene with PSY to the fork created by LCYE/ β , have their maximum protein abundance level during the light hours during summer photoperiod. During winter photoperiod, a clear anticipation of those enzymes can be observed, which describe their maximum abundance level just before sunrise. Also the profiles of the enzymes involved in the xanthophylls cycle are in agreement with zeaxanthin and violaxanthin contents. Under summer photoperiod, the

maximum protein abundance of violaxanthin de-epoxidase (VDE) match the increasing zeaxanthin content during the light hours, as well as the maximum abundance of zeaxanthin epoxidase (ZEP) match the increasing content of violaxanthin during the dark hours. A similar phenomenon is observed during winter photoperiod, where VDE is present during the light hours and ZEP during the dark hours (Fig. 40-B). However, there is not a significant amount of zeaxanthin being accumulated under winter photoperiods, instead, a high level of violaxanthin without drastic variations is maintained during diurnal cycles (Fig. 40-A). Xanthophylls cycle is not enhancing the production of zeaxanthin due to a lack of high irradiance stress during winter photoperiod, as it has been observed in *Ostreococcus* and others prasinophytes under low irradiance stress conditions (Böhme et al., 2002; Guyon et al., 2018; Six et al., 2009). In general, the enzymes of the β -branch pathway are coordinated to be present at a specific time of the day. Early in the morning β CH gene is expressed, sequentially followed by ZEP and VDE in that specific order under both photoperiods (Fig. 40-B). It suggests that β -branch carotenoids are transcriptionally regulated to sequentially achieve their roles at the right time.

Pigment synthesis on the α -branch biosynthesis pathway described a similar behavior to the one presented in β -branch pathway. Although the α -branch biosynthesis pathway is still unknown, there are some hypothesis that are supported by our results in *Ostreococcus* (Egeland et al., 1997). A *Mantoniella squamata* carotenoid content study linked the accumulation of luthein to irradiance stress and its following conversion to prasinoxanthin when the stress condition is over (Böhme et al., 2002). These results are in agreement with the observed lack of luthein content during winter photoperiod in *Ostreococcus*, as well as the observed accumulation of luthein during the light hours of the summer photoperiod and the following increment of prasinoxanthin content after sunset.

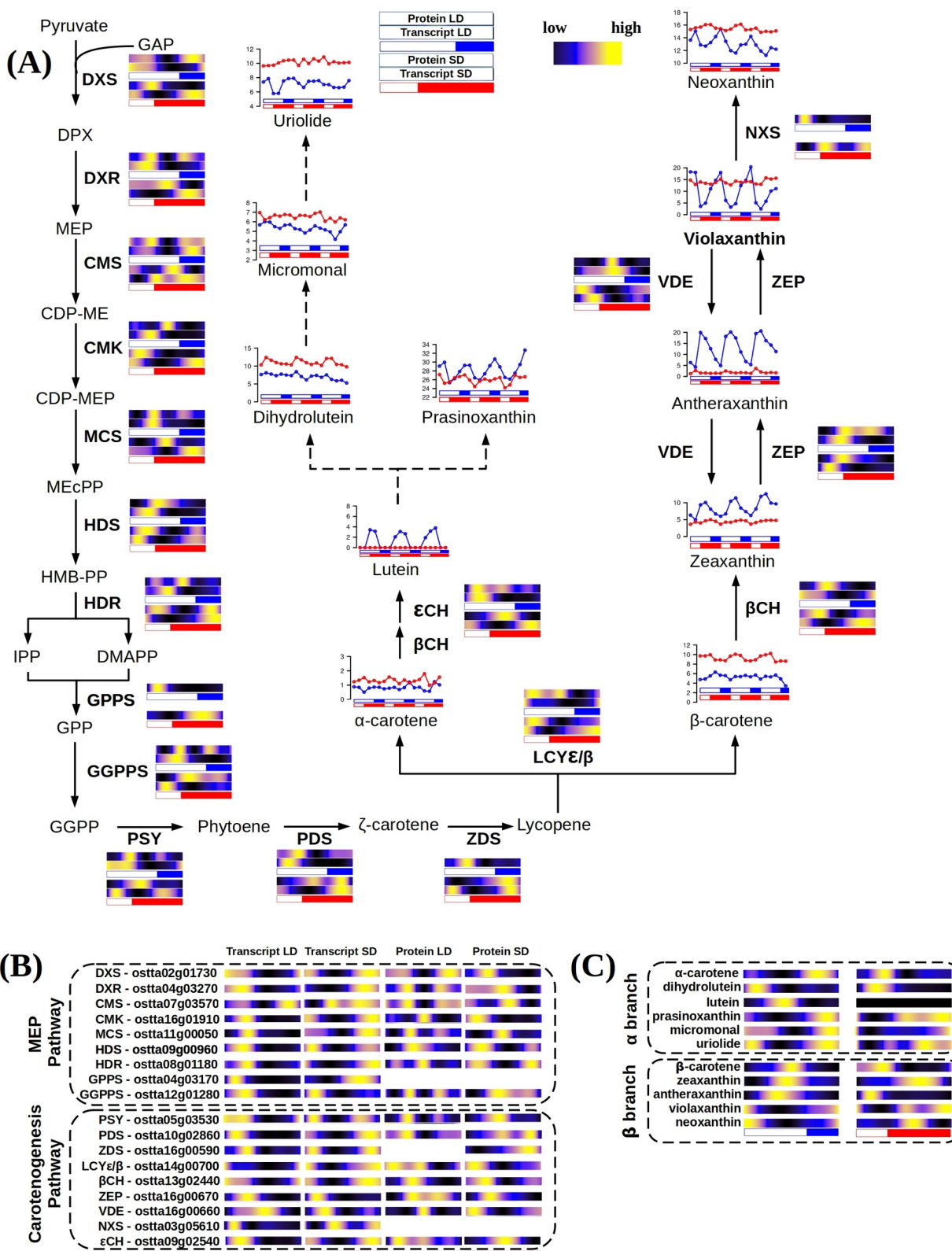


Figure 40. Integration of multi-omics data from the complete carotenoids biosynthesis pathway and carotenoids content of *Ostreococcus tauri*. (A) Schematic MEP pathway and carotenogenesis pathways according to (Egeland et al., 1997). (B) Organized visualization of multi-omic data from enzymes involved in both MEP and carotenogenesis pathways. (voy a guitar la C, me parece muy repetitivo)

Overall, those results suggest that *Ostreococcus tauri* carotenogenesis present the common characteristics of processes regulated by the circadian clock, as being able to adapt to different photoperiods and present an anticipation to diurnal cyclic changes. This hypothesis is very likely true for other prasinophytes as well, since their carotenoids content behavior under irradiance stress seems to be very similar (Böhme et al., 2002; Egeland et al., 1997; Guyon et al., 2018; Six et al., 2009).

Nitrate assimilation under diurnal and seasonal cycles in Ostreococcus tauri

As it has been discussed previously, photosynthetic organisms accumulate reserves during the light hours to support growth at night. Circadian regulation of C reserves as starch content diel oscillations have been already discussed in this work. However, the macroelement nitrogen is also an essential component in biomolecules of great importance for living beings. The most abundant form of nitrogen in the atmosphere or dissolved in water ecosystems is inaccessible for microalgae, it can only be used by fixing bacteria like *Synechococcus*. However, resource acquisition is critical to survival and nitrogen is, in fact, a major limiting nutrient of marine phytoplankton (Barros et al., 2005; Mittag, 2001; Sanz-Luque et al., 2015). *O. tauri* seems to have developed competitive mechanisms to ensure nitrogen assimilation in the marine ecosystem. *Ostreococcus* can grow on nitrate, ammonium, and urea, and complete sets of genes allowing transport and assimilation of these substrates have been identified in its genome (Blanc-Mathieu et al., 2014; Derelle et al., 2006). Specifically, in the growth medium used during this work, nitrate was used as nitrogen source. Nitrite reductase (NIR) enzyme of *Ostreococcus* has two additional redox domains that allow this enzyme to use NAD(P)H directly as reducing agent, improving nitrogen assimilation process (Derelle et al., 2006).

In the previous chapters of this thesis, nitrate assimilation has been identified as one of the biological processes which genes and proteins present significant rhythmic profiles under diurnal cycles, as well as one of the processes with larger offset between gene expression and translation. Here, enzymatic activities of two of the main enzymes involved in nitrate assimilation is presented and integrated with multi-omic data from enzymes involved in the complete pathway.

Integration of key enzyme activities from nitrate assimilation pathway with multi-omic data

Although the nitrate assimilation pathway from nitrate to amino acid is relatively simple, its regulation to ensure an optimal nutrient assimilation coupled to changing environmental factors is more complex. Nitrate is first transported into the cell, where a nitrate reductase (NR) achieve its reduction to nitrite. Nitrite is transported into the chloroplast where it is reduced to ammonium by a nitrite reductase (NiR). Finally, ammonium is incorporated to carbon compounds by the glutamine synthetase enzyme (GS) (Sanz-Luque et al., 2015).

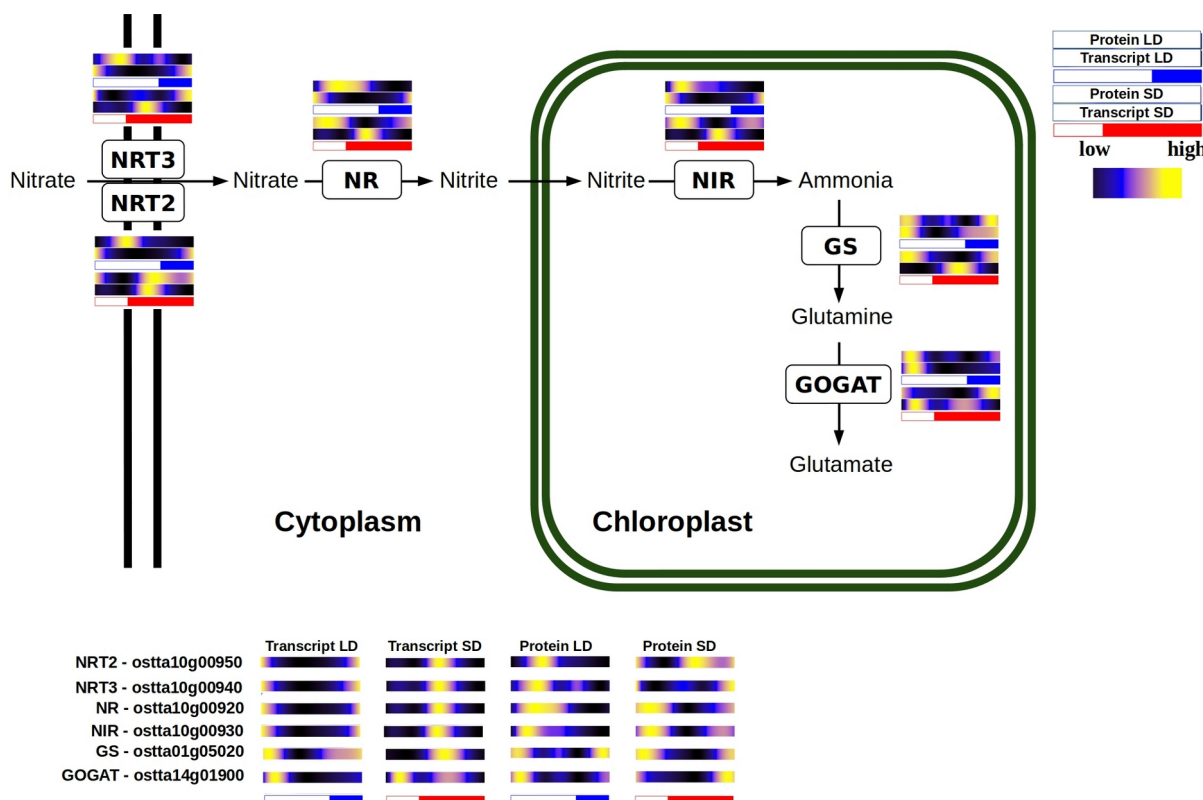


Figure 41: Multi-omics integration of nitrate assimilation pathway.

Circadian oscillations in expression and activity of the first enzyme of this pathway (NR) have been described in *Arabidopsis* and other crop plants as maize or tomato (Lillo et al., 2001; Lillo & Ruoff, 1989; Tucker et al., 2004; Z. Yang & Midmore, 2005). In addition, light is apparently an important factor for NR to maintain its rhythmic behavior. Rhythms in NR activity or NR gene expression profiles were shown to persist only in continuous light but not in darkness in plants (Lillo et al., 2001; Lillo & Ruoff, 1989). These results are in agreement with the transcriptomic data obtained in this work, where NR gene expression rhyth-

mic profiles are maintained only under light-dark cycles and constant light. This transcriptomic behavior is also present in others enzymes involved in this pathway (Fig. 41).

Genes involved in this pathway reach their maximum level of expression few hours before sunrise during summer photoperiod, presenting a clear anticipation to the light period. This anticipation become larger in winter photoperiod, where these genes reach their maximum expression level in the first part of the night (Fig. 41).

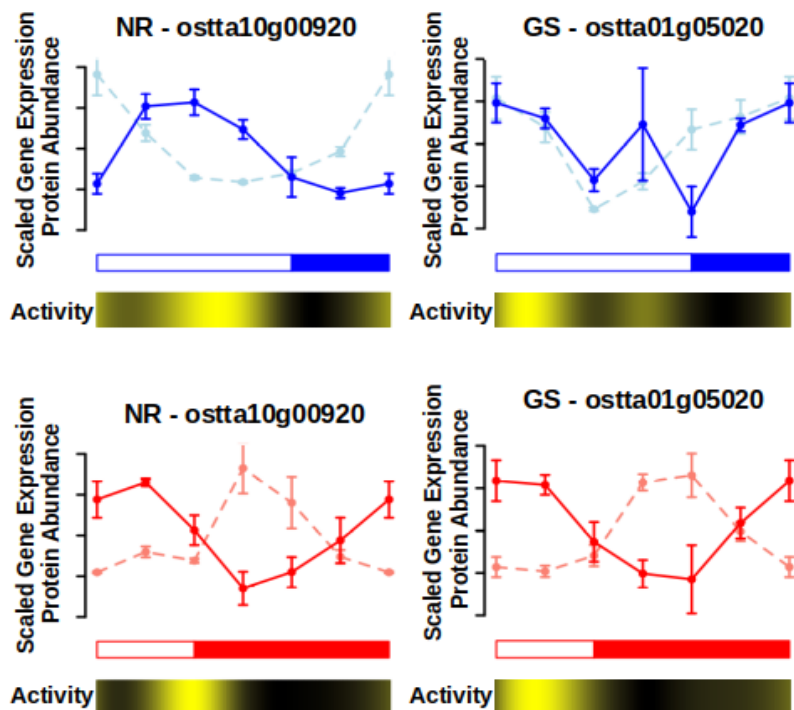


Figure 42. NR and GS rhythmic activity compared with its proteomic and transcriptomic data generated.

Protein abundance profiles are coincident with gene expression profiles except for the 8-16h offset observed in the enzymes from this pathway (Fig. 42). Enzymatic activities of NR and GS presented a significant rhythmic profile with a p-value lower than 0.05 and there is an almost non-existent offset between their protein abundance profile and their activity.

The huge transcriptomic anticipation observed is adjusted by the clock taking in count the large offset between gene expression and translation described by the enzymes involved in this pathway. In fact, although genes are transcribed at different times under winter and summer photoperiod, proteins reach their maximum abundance level around sunrise in both cases (Fig. 41). This is a clear example of how *Ostreococcus* adjust its transcriptional

program in order to ensure the presence of proteins at the exact right time, in spite of their specific translation offset.

Bibliography

- Abascal, F., Acosta, R., Addleman, N. J., Adrian, J., Afzal, V., Aken, B., Akiyama, J. A., Jammal, O. Al, Amrhein, H., Anderson, S. M., Andrews, G. R., Antoshechkin, I., Ardlie, K. G., Armstrong, J., Astley, M., Banerjee, B., Barkal, A. A., Barnes, I. H. A., Barozzi, I., ... Myers, R. M. (2020). Perspectives on ENCODE. In *Nature* (Vol. 583, Issue 7818). <https://doi.org/10.1038/s41586-020-2449-8>
- Abinandan, S., Subashchandrabose, S. R., Venkateswarlu, K., & Megharaj, M. (2018). Nutrient removal and biomass production: advances in microalgal biotechnology for wastewater treatment. *Critical Reviews in Biotechnology*, 38(8), 1244–1260. <https://doi.org/10.1080/07388551.2018.1472066>
- Ajjawi, I., Verruto, J., Aqui, M., Soriaga, L. B., Coppersmith, J., Kwok, K., Peach, L., Orchard, E., Kalb, R., Xu, W., Carlson, T. J., Francis, K., Konigsfeld, K., Bartalis, J., Schultz, A., Lambert, W., Schwartz, A. S., Brown, R., & Moellering, E. R. (2017). Lipid production in *Nannochloropsis gaditana* is doubled by decreasing expression of a single transcriptional regulator. *Nature Biotechnology*, 35, 647–652. <https://doi.org/10.1038/nbt.3865>
- Andreatta, G., & Tessmar-Raible, K. (2020). The Still Dark Side of the Moon: Molecular Mechanisms of Lunar-Controlled Rhythms and Clocks. In *Journal of Molecular Biology* (Vol. 432, Issue 12). <https://doi.org/10.1016/j.jmb.2020.03.009>
- Ashburner, M., Ball, C. A., Blake, J. A., Botstein, D., Butler, H., Cherry, J. M., Davis, A. P., Dolinski, K., Dwight, S. S., Eppig, J. T., Harris, M. A., Hill, D. P., Issel-Tarver, L., Kasarskis, A., Lewis, S., Matese, J. C., Richardson, J. E., Ringwald, M., Rubin, G. M.,

- & Sherlock, G. (2000). Gene ontology: Tool for the unification of biology. *Nature Genetics*, 25, 25–29. <https://doi.org/10.1038/75556>
- Bachy, C., Wittmers, F., Muschiol, J., Hamilton, M., Henrissat, B., & Worden, A. Z. (2022). The Land-Sea Connection: Insights Into the Plant Lineage from a Green Algal Perspective. In *Annual Review of Plant Biology* (Vol. 73). <https://doi.org/10.1146/annurev-arplant-071921-100530>
- Ballance, H., & Zhu, B. (2021). Revealing the hidden reality of the mammalian 12-h ultradian rhythms. *Cellular and Molecular Life Sciences*, 78(7), 3127–3140. <https://doi.org/10.1007/s0018-020-03730-5>
- Barros, M. P., Pinto, E., Sigaud-Kutner, T. C. S., Cardozo, K. H. M., & Colepicolo, P. (2005). Rhythmicity and oxidative/nitrosative stress in algae. *Biological Rhythm Research*, 36(1–2). <https://doi.org/10.1080/09291010400028666>
- Bartoszewicz, R., Chmielewska, D., Domoń, M., & Barbacka-Surowiak, G. (2010). Influence of short-term constant light on phase shift of mouse circadian locomotor activity rhythm induced by agonist and antagonist of serotonin. *Biological Rhythm Research*, 41(4). <https://doi.org/10.1080/09291010903018016>
- Becker, B., & Marin, B. (2009). Streptophyte algae and the origin of embryophytes. *Annals of Botany*, 103(7), 999–1004. <https://doi.org/10.1093/aob/mcp044>
- Benites, L. F., Buccini, F., Sanchez-Brosseau, S., Grimsley, N., Vandepoele, K., & Pi-ganeau, G. (2021). Evolutionary Genomics of Sex-Related Chromosomes at the Base of the Green Lineage. *Genome Biology and Evolution*, 13(10). <https://doi.org/10.1093/gbe/evab216>
- Berube, P. M., Biller, S. J., Hackl, T., Hogle, S. L., Satinsky, B. M., Becker, J. W., Braakman, R., Collins, S. B., Kelly, L., Berta-Thompson, J., Coe, A., Bergauer, K., Bouman, H. A., Browning, T. J., De Corte, D., Hassler, C., Hulata, Y., Jacquot, J. E., Maas, E. W., ... Chisholm, S. W. (2018). Data descriptor: Single cell genomes of Prochlorococcus, Synechococcus, and sympatric microbes from diverse marine environments. *Scientific Data*, 5. <https://doi.org/10.1038/sdata.2018.154>
- Biebach, H., Falk, H., & Krebs, J. R. (1991). The Effect of Constant Light and Phase Shifts on a Learned Time-Place Association in Garden Warblers (*Sylvia borin*): Hourglass or Circadian Clock? *Journal of Biological Rhythms*, 6(4). <https://doi.org/10.1177/074873049100600406>
- Binkley, S., & Mosher, K. (1985). Direct and circadian control of sparrow behavior by light and dark. *Physiology and Behavior*, 35(5). [https://doi.org/10.1016/0031-9384\(85\)90413-5](https://doi.org/10.1016/0031-9384(85)90413-5)

- Blaby, I. K., Blaby-Haas, C. E., Tourasse, N., Hom, E. F. Y., Lopez, D., Aksoy, M., Grossman, A., Umen, J., Dutcher, S., Porter, M., King, S., Witman, G. B., Stanke, M., Harris, E. H., Goodstein, D., Grimwood, J., Schmutz, J., Vallon, O., Merchant, S. S., & Prochnik, S. (2014). The Chlamydomonas genome project: A decade on. In *Trends in Plant Science* (Vol. 19, Issue 10). <https://doi.org/10.1016/j.tplants.2014.05.008>
- Blanc-Mathieu, R., Verhelst, B., Derelle, E., Rombauts, S., Bouget, F.-Y., Carré, I., Château, A., Eyre-Walker, A., Grimsley, N., Moreau, H., Piégu, B., Rivals, E., Schackwitz, W., Van de Peer, Y., & Piganeau, G. (2014). An improved genome of the model marine alga Ostreococcus tauri unfolds by assessing Illumina de novo assemblies. *BMC Genomics*, 15(1), 1103. <https://doi.org/10.1186/1471-2164-15-1103>
- Blanc, G., Agarkova, I., Grimwood, J., Kuo, A., Brueggeman, A., Dunigan, D. D., Gurnon, J., Ladunga, I., Lindquist, E., Lucas, S., Pangilinan, J., Pröschold, T., Salamov, A., Schmutz, J., Weeks, D., Yamada, T., Lomsadze, A., Borodovsky, M., Claverie, J. M., ... Van Etten, J. L. (2012). The genome of the polar eukaryotic microalga Coccomyxa subellipsoidea reveals traits of cold adaptation. *Genome Biology*, 13(5). <https://doi.org/10.1186/gb-2012-13-5-r39>
- Böhme, K., Wilhelm, C., & Goss, R. (2002). Light regulation of carotenoid biosynthesis in the prasinophycean alga Mantoniella squamata. *Photochemical and Photobiological Sciences*, 1(8). <https://doi.org/10.1039/b204965c>
- Borowitzka, M. A. (2013). High-value products from microalgae-their development and commercialisation. *Journal of Applied Phycology*, 25(3), 743–756. <https://doi.org/10.1007/s10811-013-9983-9>
- Bowler, C., Allen, A. E., Badger, J. H., Grimwood, J., Jabbari, K., Kuo, A., Maheswari, U., Martens, C., Maumus, F., Otillar, R. P., Rayko, E., Salamov, A., Vandepoele, K., Beszteri, B., Gruber, A., Heijde, M., Katinka, M., Mock, T., Valentin, K., ... Grigoriev, I. V. (2008). The Phaeodactylum genome reveals the evolutionary history of diatom genomes. *Nature*, 456(7219). <https://doi.org/10.1038/nature07410>
- Brandoli, C., Petri, C., Egea-Cortines, M., & Weiss, J. (2020). Gigantea: Uncovering new functions in flower development. In *Genes* (Vol. 11, Issue 10, pp. 1–15). MDPI AG. <https://doi.org/10.3390/genes11101142>
- Bray, N. L., Pimentel, H., Melsted, P., & Pachter, L. (2016). Near-optimal probabilistic RNA-seq quantification. *Nature Biotechnology*, 34(5). <https://doi.org/10.1038/nbt.3519>
- Bruce, V. G. (1970). The biological clock in Chlamydomonas reinhardtii. *J Protozool*, 17, 328–334. <https://doi.org/https://doi.org/10.1111/j.1550-7408.1970.tb02380.x>
- Carbon, S., Douglass, E., Dunn, N., Good, B., Harris, N. L., Lewis, S. E., Mungall, C. J., Basu, S., Chisholm, R. L., Dodson, R. J., Hartline, E., Fey, P., Thomas, P. D., Albou, L. P., Ebert, D., Kesling, M. J., Mi, H., Muruganujan, A., Huang, X., ... Westerfield, M.

- (2019). The Gene Ontology Resource: 20 years and still GOing strong. *Nucleic Acids Research*, 47(D1), D330–D338. <https://doi.org/10.1093/nar/gky1055>
- Carbon, S., Ireland, A., Mungall, C. J., Shu, S., Marshall, B., Lewis, S., Lomax, J., Mungall, C., Hitz, B., Balakrishnan, R., Dolan, M., Wood, V., Hong, E., & Gaudet, P. (2009). AmiGO: Online access to ontology and annotation data. *Bioinformatics*, 25(2), 288–289. <https://doi.org/10.1093/bioinformatics/btn615>
- Carlson, M., & Pagès, H. (2019). *AnnotationForge: Tools for building SQLite-based annotation data packages* (1.26.0.).
- Carneiro, A. K., Montessoro, P. da F., Fusaro, A. F., Araújo, B. G., & Hemerly, A. S. (2021). Plant cdks—driving the cell cycle through climate change. In *Plants* (Vol. 10, Issue 9). <https://doi.org/10.3390/plants10091804>
- Chapman, R. L. (2013). Algae: The world's most important “plants”—an introduction. *Mitigation and Adaptation Strategies for Global Change*, 18(1). <https://doi.org/10.1007/s11027-010-9255-9>
- Chen, H., Li, T., & Wang, Q. (2019). Ten years of algal biofuel and bioproducts: gains and pains. *Planta*, 249(1), 195–219. <https://doi.org/10.1007/s00425-018-3066-8>
- Chen, M. X., Zhang, Y., Fernie, A. R., Liu, Y. G., & Zhu, F. Y. (2021). SWATH-MS-Based Proteomics: Strategies and Applications in Plants. In *Trends in Biotechnology* (Vol. 39, Issue 5, pp. 433–437). Elsevier Ltd. <https://doi.org/10.1016/j.tibtech.2020.09.002>
- Cheng, S., Xian, W., Fu, Y., Marin, B., Keller, J., Wu, T., Sun, W., Li, X., Xu, Y., Zhang, Y., Wittek, S., Reder, T., Günther, G., Gontcharov, A., Wang, S., Li, L., Liu, X., Wang, J., Yang, H., ... Melkonian, M. (2019). Genomes of Subaerial Zygnematophyceae Provide Insights into Land Plant Evolution. *Cell*, 179(5). <https://doi.org/10.1016/j.cell.2019.10.019>
- Cock, J. M., & Coelho, S. M. (2011). Algal models in plant biology. In *Journal of Experimental Botany* (Vol. 62, Issue 8). <https://doi.org/10.1093/jxb/err117>
- Coleto-Alcudia, V., & Vega-Rodríguez, M. A. (2020). Artificial Bee Colony algorithm based on Dominance (ABCD) for a hybrid gene selection method. *Knowledge-Based Systems*, 205. <https://doi.org/10.1016/j.knosys.2020.106323>
- Collado-Fabbri, S., Vaulot, D., & Ulloa, O. (2011). Structure and seasonal dynamics of the eukaryotic picophytoplankton community in a wind-driven coastal upwelling ecosystem. *Limnology and Oceanography*, 56(6). <https://doi.org/10.4319/lo.2011.56.6.2334>
- Corellou, F., Camasses, A., Ligat, L., Peaucellier, G., & Bouget, F. Y. (2005). Atypical regulation of a green lineage-specific B-type cyclin-dependent kinase. *Plant Physiology*, 138(3). <https://doi.org/10.1104/pp.105.059626>

- Correa, A., & Bell-Pedersen, D. (2002). Distinct signaling pathways from the circadian clock participate in regulation of rhythmic conidiospore development in *Neurospora crassa*. *Eukaryotic Cell*, 1(2). <https://doi.org/10.1128/EC.1.2.273-280.2002>
- Corteggiani Carpinelli, E., Telatin, A., Vitulo, N., Forcato, C., D'Angelo, M., Schiavon, R., Vezzi, A., Giacometti, G. M., Morosinotto, T., & Valle, G. (2014). Chromosome scale genome assembly and transcriptome profiling of *nannochloropsis gaditana* in nitrogen depletion. *Molecular Plant*, 7(2). <https://doi.org/10.1093/mp/sst120>
- Covington, M. F., Maloof, J. N., Straume, M., Kay, S. A., & Harmer, S. L. (2008). Global transcriptome analysis reveals circadian regulation of key pathways in plant growth and development. *Genome Biology*, 9(8). <https://doi.org/10.1186/gb-2008-9-8-r130>
- Craig, R. J., Hasan, A. R., Ness, R. W., & Keightley, P. D. (2021). Comparative genomics of Chlamydomonas. *Plant Cell*, 33(4). <https://doi.org/10.1093/plcell/koab026>
- Cui, Y., Thomas-Hall, S. R., & Schenk, P. M. (2019). Phaeodactylum tricornutum microalgae as a rich source of omega-3 oil: Progress in lipid induction techniques towards industry adoption. In *Food Chemistry* (Vol. 297). <https://doi.org/10.1016/j.foodchem.2019.06.004>
- Cumming, B. G., & Wagner, E. (1968). Rhythmic Processes in Plants. *Annual Review of Plant Physiology*, 19(1). <https://doi.org/10.1146/annurev.pp.19.060168.002121>
- De Keersmaecker, S. C. J., Thijss, I. M. V., Vanderleyden, J., & Marchal, K. (2006). Integration of omics data: How well does it work for bacteria? In *Molecular Microbiology* (Vol. 62, Issue 5). <https://doi.org/10.1111/j.1365-2958.2006.05453.x>
- de los Reyes, P., Romero-Campero, F. J., Ruiz, M. T., Romero, J. M., & Valverde, F. (2017). Evolution of Daily Gene Co-expression Patterns from Algae to Plants. *Frontiers in Plant Science*. <https://doi.org/10.3389/fpls.2017.01217>
- de los Reyes, P., Romero-Campero, F. J., Teresa Ruiz, M., Romero, J. M., & Valverde, F. (2017). Evolution of daily gene co-expression patterns from algae to plants. *Frontiers in Plant Science*, 8(July), 1–22. <https://doi.org/10.3389/fpls.2017.01217>
- De Mairan, J. J. . (1729). Observation Botanique. *Histoire de l'Academie Royale Des Sciences*.
- Del Campo, J. A., Rodríguez, H., Moreno, J., Vargas, M. Á., Rivas, J., & Guerrero, M. G. (2004). Accumulation of astaxanthin and lutein in *Chlorella zofingiensis* (Chlorophyta). *Applied Microbiology and Biotechnology*, 64(6). <https://doi.org/10.1007/s00253-003-1510-5>
- Demir-Hilton, E., Sudek, S., Cuvelier, M. L., Gentemann, C. L., Zehr, J. P., & Worden, A. Z. (2011). Global distribution patterns of distinct clades of the photosynthetic picoeukaryote *Ostreococcus*. *ISME Journal*, 5(7). <https://doi.org/10.1038/ismej.2010.209>

- Derelle, E., Ferraz, C., Rombauts, S., Rouze, P., Worden, A. Z., Robbens, S., Partensky, F., Degroeve, S., Echeynie, S., Cooke, R., Saeys, Y., Wuyts, J., Jabbari, K., Bowler, C., Panaud, O., Piegu, B., Ball, S. G., Ral, J.-P., Bouget, F.-Y., ... Moreau, H. (2006). Genome analysis of the smallest free-living eukaryote *Ostreococcus tauri* unveils many unique features. *Proceedings of the National Academy of Sciences*, 103(31), 11647–11652. <https://doi.org/10.1073/pnas.0604795103>
- Ditz, B., Boekhoudt, J. G., Aliee, H., Theis, F. J., Nawijn, M., Brandsma, C.-A., Hiemstra, P. S., Timens, W., Tew, G. W., Grimaldeston, M. A., Neighbors, M., Guryev, V., van den Berge, M., & Faiz, A. (2021). Comparison of genome-wide gene expression profiling by RNA Sequencing versus microarray in bronchial biopsies of COPD patients before and after inhaled corticosteroid treatment: does it provide new insights? *ERJ Open Research*, 7(2), 00104–02021. <https://doi.org/10.1183/23120541.00104-2021>
- Dodd, A. N., Kusakina, J., Hall, A., Gould, P. D., & Hanaoka, M. (2014). The circadian regulation of photosynthesis. In *Photosynthesis Research* (Vol. 119, Issues 1–2). <https://doi.org/10.1007/s11120-013-9811-8>
- Donnan, L., & John, P. C. L. (1983). Cell cycle control by timer and sizer in Chlamydomonas. *Nature*, 304(5927). <https://doi.org/10.1038/304630a0>
- Edmunds, L. N. (1983). Chronobiology at the cellular and molecular levels: Models and mechanisms for circadian timekeeping. *American Journal of Anatomy*, 168(4). <https://doi.org/10.1002/aja.1001680404>
- Edmunds, L. N., & Laval-Martin, D. L. (2019). Cell Division Cycles And Circadian Oscillators In Euglena. In *Intracellular space as oligogenetic ecosystem. Proceedings*. <https://doi.org/10.1515/9783110841237-033>
- Edwards, K. D., Akman, O. E., Knox, K., Lumsden, P. J., Thomson, A. W., Brown, P. E., Pokhilko, A., Kozma-Bognar, L., Nagy, F., Rand, D. A., & Millar, A. J. (2010). Quantitative analysis of regulatory flexibility under changing environmental conditions. *Molecular Systems Biology*, 6. <https://doi.org/10.1038/msb.2010.81>
- Eelderink-Chen, Z., Bosman, J., Sartor, F., Dodd, A. N., Kovács, Á. T., & Merrow, M. (2021). A circadian clock in a nonphotosynthetic prokaryote. *Science Advances*, 7(2). <https://doi.org/10.1126/sciadv.abe2086>
- Egeland, E. S., Eikrem, W., Throndsen, J., Wilhelm, C., Zapata, M., & Liaaen-Jensen, S. (1995). Carotenoids from further prasinophytes. In *Biochemical Systematics and Ecology* (Vol. 23, Issues 7–8). [https://doi.org/10.1016/0305-1978\(95\)00075-5](https://doi.org/10.1016/0305-1978(95)00075-5)
- Egeland, E. S., Guillard, R. R. L., & Liaaen-Jensen, S. (1997). Additional carotenoid prototype representatives and a general chemosystematic evaluation of carotenoids in Prasinophyceae (Chlorophyta). *Phytochemistry*. [https://doi.org/10.1016/S0031-9422\(96\)00650-4](https://doi.org/10.1016/S0031-9422(96)00650-4)

- Eggersdorfer, M., & Wyss, A. (2018). Carotenoids in human nutrition and health. In *Archives of Biochemistry and Biophysics* (Vol. 652). <https://doi.org/10.1016/j.abb.2018.06.001>
- El Gamal, A. A. (2010). Biological importance of marine algae. *Saudi Pharmaceutical Journal*, 18(1), 1–25. <https://doi.org/10.1016/j.jps.2009.12.001>
- Engel, S. R., Dietrich, F. S., Fisk, D. G., Binkley, G., Balakrishnan, R., Costanzo, M. C., Dwight, S. S., Hitz, B. C., Karra, K., Nash, R. S., Weng, S., Wong, E. D., Lloyd, P., Skrzypek, M. S., Miyasato, S. R., Simison, M., & Cherry, J. M. (2014). The Reference Genome Sequence of *Saccharomyces cerevisiae*: Then and Now. *G3: Genes, Genomes, Genetics*, 4(3). <https://doi.org/10.1534/g3.113.008995>
- Evans, D. R. (1961). Biological Clocks. Volume XXV. Cold Spring Harbor Symposia on Quantitative Biology. . *The Quarterly Review of Biology*, 36(3). <https://doi.org/10.1086/403447>
- Farré, E. M., & Weise, S. E. (2012). The interactions between the circadian clock and primary metabolism. In *Current Opinion in Plant Biology* (Vol. 15, Issue 3). <https://doi.org/10.1016/j.pbi.2012.01.013>
- Fauré-Fremiet, E. (1951). The tidal rhythm of the diatom *Hantzschia amphioxys*. *Biological Bulletin*, 100(3), 173–177.
- Ferrari, C., Proost, S., Janowski, M., Becker, J., Nikoloski, Z., Bhattacharya, D., Price, D., Tohge, T., Bar-Even, A., Fernie, A., Stitt, M., & Mutwil, M. (2019). Kingdom-wide comparison reveals the evolution of diurnal gene expression in Archaeplastida. In *Nature Communications*. <https://doi.org/10.1038/s41467-019-08703-2>
- Feugier, F. G., & Satake, A. (2013). Dynamical feedback between circadian clock and sucrose availability explains adaptive response of starch metabolism to various photoperiods. *Frontiers in Plant Science*, 3(JAN). <https://doi.org/10.3389/fpls.2012.00305>
- Flis, A., Mengin, V., Ivakov, A. A., Mugford, S. T., Hubberten, H. M., Encke, B., Krohn, N., Höhne, M., Feil, R., Hoefgen, R., Lunn, J. E., Millar, A. J., Smith, A. M., Sulpice, R., & Stitt, M. (2019). Multiple circadian clock outputs regulate diel turnover of carbon and nitrogen reserves. *Plant Cell and Environment*, 42(2). <https://doi.org/10.1111/pce.13440>
- Flis, A., Sulpice, R., Seaton, D. D., Ivakov, A. A., Liput, M., Abel, C., Millar, A. J., & Stitt, M. (2016). Photoperiod-dependent changes in the phase of core clock transcripts and global transcriptional outputs at dawn and dusk in *Arabidopsis*. *Plant Cell and Environment*, 39(9). <https://doi.org/10.1111/pce.12754>

- Foà, A., & Bertolucci, C. (2001). Temperature cycles induce a bimodal activity pattern in ruin lizards: Masking or clock-controlled event? A seasonal problem. *Journal of Biological Rhythms*, 16(6). <https://doi.org/10.1177/074873001129002268>
- Frazee, A. C., Pertea, G., Jaffe, A. E., Langmead, B., Salzberg, S. L., & Leek, J. T. (2015). Ballgown bridges the gap between transcriptome assembly and expression analysis. *Nature Biotechnology*, 33, 243. <https://doi.org/10.1038/nbt.3172>
- Fu, L., Patel, M. S., Bradley, A., Wagner, E. F., & Karsenty, G. (2005). The molecular clock mediates leptin-regulated bone formation. *Cell*, 122(5). <https://doi.org/10.1016/j.cell.2005.06.028>
- Fung-Uceda, J., Lee, K., Seo, P. J., Polyn, S., De Veylder, L., & Mas, P. (2018). The Circadian Clock Sets the Time of DNA Replication Licensing to Regulate Growth in Arabidopsis. *Developmental Cell*, 45(1). <https://doi.org/10.1016/j.devcel.2018.02.022>
- Galperin, M. Y., Wolf, Y. I., Makarova, K. S., Alvarez, R. V., Landsman, D., & Koonin, E. V. (2021). COG database update: Focus on microbial diversity, model organisms, and widespread pathogens. *Nucleic Acids Research*, 49(D1). <https://doi.org/10.1093/nar/gkaa1018>
- García-Cubero, R., Moreno-Fernández, J., & García-González, M. (2018). Potential of Chlorella vulgaris to Abate Flue Gas. *Waste and Biomass Valorization*, 9(11), 2015–2019. <https://doi.org/10.1007/s12649-017-9987-9>
- García-Domínguez, M., & Florencio, F. J. (1997). Nitrogen availability and electron transport control the expression of glnB gene (encoding PII protein) in the cyanobacterium Synechocystis sp. PCC 6803. *Plant Molecular Biology*, 35(6). <https://doi.org/10.1023/A:1005846626187>
- García-Plazaola, J. I., Fernández-Marín, B., Ferrio, J. P., Alday, J. G., Hoch, G., Landais, D., Milcu, A., Tissue, D. T., Voltas, J., Gessler, A., Roy, J., & Resco de Dios, V. (2017). Endogenous circadian rhythms in pigment composition induce changes in photochemical efficiency in plant canopies. *Plant Cell and Environment*, 40(7). <https://doi.org/10.1111/pce.12909>
- Gaspar, J. M. (2018). Improved peak-calling with MACS2. *BioRxiv*.
- Goodstein, D. M., Shu, S., Howson, R., Neupane, R., Hayes, R. D., Fazo, J., Mitros, T., Dirks, W., Hellsten, U., Putnam, N., & Rokhsar, D. S. (2012). Phytozome: A comparative platform for green plant genomics. *Nucleic Acids Research*, 40(D1), D1178–D1186. <https://doi.org/10.1093/nar/gkr944>
- Goto, K., & Johnson, C. H. (1995). Is the cell division cycle gated by a circadian clock? The case of Chlamydomonas reinhardtii. *Journal of Cell Biology*, 129(4). <https://doi.org/10.1083/jcb.129.4.1061>

- Graf, A., Schlereth, A., Stitt, M., & Smith, A. M. (2010). Circadian control of carbohydrate availability for growth in *Arabidopsis* plants at night. *Proceedings of the National Academy of Sciences*, 107(20), 9458–9463. <https://doi.org/10.1073/pnas.0914299107>
- Granados-Fuentes, D., Tseng, A., & Herzog, E. D. (2006). A circadian clock in the olfactory bulb controls olfactory responsiveness. *Journal of Neuroscience*, 26(47). <https://doi.org/10.1523/JNEUROSCI.3445-06.2006>
- Grigoriev, I. V., Hayes, R. D., Calhoun, S., Kamel, B., Wang, A., Ahrendt, S., Dusheyko, S., Nikitin, R., Mondo, S. J., Salamov, A., Shabalov, I., & Kuo, A. (2021). PhycoCosm, a comparative algal genomics resource. *Nucleic Acids Research*, 49(D1). <https://doi.org/10.1093/nar/gkaa898>
- Guyon, J.-B., Vergé, V., Schatt, P., Lozano, J.-C., Liennard, M., & Bouget, F.-Y. (2018). Comparative Analysis of Culture Conditions for the Optimization of Carotenoid Production in Several Strains of the Picoeukaryote *Ostreococcus*. *Marine Drugs*, 16(3). <https://doi.org/10.3390/md16030076>
- Hagiwara, S., Bolige, A., Zhang, Y., Takahashi, M., Yamagishi, A., & Goto, K. (2002). Circadian Gating of Photoinduction of Commitment to Cell-cycle Transitions in Relation to Photoperiodic Control of Cell Reproduction in *Euglena*. *Photochemistry and Photobiology*, 76(1). [https://doi.org/10.1562/0031-8655\(2002\)076<0105:cgopoc>2.0.co;2](https://doi.org/10.1562/0031-8655(2002)076<0105:cgopoc>2.0.co;2)
- Hayes, K. R., Beatty, M., Meng, X., Simmons, C. R., Habben, J. E., & Danilevskaya, O. N. (2010). Maize global transcriptomics reveals pervasive leaf diurnal rhythms but rhythms in developing ears are largely limited to the core oscillator. *PLoS ONE*, 5(9). <https://doi.org/10.1371/journal.pone.0012887>
- Henderson, G. P., Gan, L., & Jensen, G. J. (2012). 3-D Ultrastructure of *O. tauri*: Electron Cryotomography of an Entire Eukaryotic Cell. *PLoS ONE*, 2(1). <https://doi.org/10.1371/journal.pone.0000749>
- Homma, K., & Hastings, J. W. (1989). The S phase is discrete and is controlled by the circadian clock in the marine dinoflagellate *Gonyaulax polyedra*. *Experimental Cell Research*, 182(2). [https://doi.org/10.1016/0014-4827\(89\)90265-6](https://doi.org/10.1016/0014-4827(89)90265-6)
- Hori, K., Maruyama, F., Fujisawa, T., Togashi, T., Yamamoto, N., Seo, M., Sato, S., Yamada, T., Mori, H., Tajima, N., Moriyama, T., Ikeuchi, M., Watanabe, M., Wada, H., Kobayashi, K., Saito, M., Masuda, T., Sasaki-Sekimoto, Y., Mashiguchi, K., ... Ohta, H. (2014). *Klebsormidium flaccidum* genome reveals primary factors for plant terrestrial adaptation. *Nature Communications*, 5. <https://doi.org/10.1038/ncomms4978>
- Howe, K. L., Achuthan, P., Allen, J., Allen, J., Alvarez-Jarreta, J., Ridwan Amode, M., Armean, I. M., Azov, A. G., Bennett, R., Bhai, J., Billis, K., Boddu, S., Charkhchi, M., Cummins, C., da Rin Fioretto, L., Davidson, C., Dodiya, K., El Houdaigui, B., Fatima,

- R., ... Flicek, P. (2021). Ensembl 2021. *Nucleic Acids Research*, 49(D1). <https://doi.org/10.1093/nar/gkaa942>
- Hoys, C., Romero-Losada, A. B., del Río, E., Guerrero, M. G., Romero-Campero, F. J., & García-González, M. (2021). Unveiling the underlying molecular basis of astaxanthin accumulation in Haematococcus through integrative metabolomic-transcriptomic analysis. *Bioresource Technology*, 332. <https://doi.org/10.1016/j.biortech.2021.125150>
- Hundahl, C. A., Fahrenkrug, J., Hay-Schmidt, A., Georg, B., Faltoft, B., & Hannibal, J. (2012). Circadian behaviour in neuroglobin deficient mice. *PLoS ONE*, 7(4). <https://doi.org/10.1371/journal.pone.0034462>
- Ideker, T., Galitski, T., & Hood, L. (2001). A new approach to decoding life: Systems biology. In *Annual Review of Genomics and Human Genetics* (Vol. 2). <https://doi.org/10.1146/annurev.genom.2.1.343>
- Imai, R., Makino, H., Katoh, T., Kimura, T., Kurita, T., Hokamura, K., Umemura, K., & Nakajima, Y. (2020). Desflurane anesthesia shifts the circadian rhythm phase depending on the time of day of anesthesia. *Scientific Reports*, 10(1). <https://doi.org/10.1038/s41598-020-75434-6>
- Jamers, A., Blust, R., & De Coen, W. (2009). Omics in algae: Paving the way for a systems biological understanding of algal stress phenomena? In *Aquatic Toxicology* (Vol. 92, Issue 3). <https://doi.org/10.1016/j.aquatox.2009.02.012>
- Joyce, A. R., & Palsson, B. (2006). The model organism as a system: Integrating “omics” data sets. In *Nature Reviews Molecular Cell Biology* (Vol. 7, Issue 3). <https://doi.org/10.1038/nrm1857>
- Kanehisa, M., Sato, Y., Kawashima, M., Furumichi, M., & Tanabe, M. (2016). KEGG as a reference resource for gene and protein annotation. *Nucleic Acids Research*, 44(D1), D457–D462. <https://doi.org/10.1093/nar/gkv1070>
- Karahalil, B. (2016). Overview of Systems Biology and Omics Technologies. *Current Medicinal Chemistry*, 23(37), 4221–4230. <https://doi.org/10.2174/0929867323666160926150617>
- Kato, S., & Nam, H. G. (2021). The cell division cycle of euglena gracilis indicates that the level of circadian plasticity to the external light regime changes in prolonged-stationary cultures. *Plants*, 10(7). <https://doi.org/10.3390/plants10071475>
- Kester, D. R., Duedall, I. W., Connors, D. N., & Pytkowicz, R. M. (1967). PREPARATION OF ARTIFICIAL SEAWATER. *Limnology and Oceanography*, 12(1), 176–179. <https://doi.org/10.4319/LO.1967.12.1.0176>
- Khadaroo, B., Robbens, S., Ferraz, C., Derelle, E., Eychenié, S., Cooke, R., Peaucellier, G., Delsenay, M., Demaille, J., Van De Peer, Y., Picard, A., & Moreau, H. (2004). The

- first green lineage cdc25 dual-specificity phosphatase. *Cell Cycle*, 3(4). <https://doi.org/10.4161/cc.3.4.815>
- Kim, D., Langmead, B., & Salzberg, S. L. (2015). HISAT: A fast spliced aligner with low memory requirements. *Nature Methods*, 12, 357–360. <https://doi.org/10.1038/nmeth.3317>
- Klante, G., & Steinlechner, S. (1994). Light Irradiance and Wavelength as Seasonal Cues for Djungarian Hamsters. *Biological Rhythm Research*, 25(4). <https://doi.org/10.1080/09291019409360310>
- Konopka, R. J., & Benzer, S. (1971). Clock mutants of *Drosophila melanogaster*. *Proceedings of the National Academy of Sciences of the United States of America*, 68(9). <https://doi.org/10.1073/pnas.68.9.2112>
- Krumholz, E. W., Yang, H., Weisenhorn, P., Henry, C. S., & Libourel, I. G. L. (2012). Genome-wide metabolic network reconstruction of the picoalga *Ostreococcus*. *Journal of Experimental Botany*, 63(6), 2353–2362. <https://doi.org/10.1093/jxb/err407>
- Kuhlman, S. J., Craig, L. M., & Duffy, J. F. (2018). Introduction to chronobiology. *Cold Spring Harbor Perspectives in Biology*, 10(9). <https://doi.org/10.1101/cshperspect.a033613>
- Kyorku, C., & Brady, J. (1994). A free-running bimodal circadian rhythm in the tsetse fly *Glossina longipennis*. *Journal of Insect Physiology*, 40(1). [https://doi.org/10.1016/0022-1910\(94\)90112-0](https://doi.org/10.1016/0022-1910(94)90112-0)
- Lamesch, P., Berardini, T. Z., Li, D., Swarbreck, D., Wilks, C., Sasidharan, R., Muller, R., Dreher, K., Alexander, D. L., Garcia-Hernandez, M., Karthikeyan, A. S., Lee, C. H., Nelson, W. D., Ploetz, L., Singh, S., Wensel, A., & Huala, E. (2012). The Arabidopsis Information Resource (TAIR): Improved gene annotation and new tools. *Nucleic Acids Research*, 40(D1). <https://doi.org/10.1093/nar/gkr1090>
- Langmead, B., & Salzberg, S. L. (2012). Fast gapped-read alignment with Bowtie 2. *Nature Methods*, 9(4). <https://doi.org/10.1038/nmeth.1923>
- Lawrence, M., Huber, W., Pagès, H., Aboyoun, P., Carlson, M., Gentleman, R., Morgan, M. T., & Carey, V. J. (2013). Software for Computing and Annotating Genomic Ranges. *PLoS Computational Biology*, 9(8). <https://doi.org/10.1371/journal.pcbi.1003118>
- Le Bihan, T., Martin, S. F., Chirnside, E. S., van Ooijen, G., Barrios-Llerena, M. E., O'Neill, J. S., Shliaha, P. V., Kerr, L. E., & Millar, A. J. (2011). Shotgun proteomic analysis of the unicellular alga *Ostreococcus tauri*. *Journal of Proteomics*, 74(10). <https://doi.org/10.1016/j.jprot.2011.05.028>

- Lebert, M., Porst, M., & Häder, D. P. (1999). Circadian rhythm of gravitaxis in Euglena gracilis. *Journal of Plant Physiology*, 155(3). [https://doi.org/10.1016/S0176-1617\(99\)80115-1](https://doi.org/10.1016/S0176-1617(99)80115-1)
- Leconte, J., Benites, L. F., Vannier, T., Wincker, P., Piganeau, G., & Jaillon, O. (2020). Genome resolved biogeography of mamiellales. *Genes*, 11(1). <https://doi.org/10.3390/genes11010066>
- Lelandais, G., Scheiber, I., Paz-Yepes, J., Lozano, J.-C., Botebol, H., Pilátová, J., Žárský, V., Léger, T., Blaiseau, P.-L., Bowler, C., Bouget, F.-Y., Camadro, J.-M., Sutak, R., & Lesuisse, E. (2016). Ostreococcus tauri is a new model green alga for studying iron metabolism in eukaryotic phytoplankton. *BMC Genomics*, 17(1), 319. <https://doi.org/10.1186/s12864-016-2666-6>
- Leliaert, F., Smith, D. R., Moreau, H., Herron, M. D., Verbruggen, H., Delwiche, C. F., & De Clerck, O. (2012). Phylogeny and Molecular Evolution of the Green Algae. *Critical Reviews in Plant Sciences*, 31(1). <https://doi.org/10.1080/07352689.2011.615705>
- Leliaert, F., Verbruggen, H., & Zechman, F. W. (2011). Into the deep: New discoveries at the base of the green plant phylogeny. In *BioEssays* (Vol. 33, Issue 9). <https://doi.org/10.1002/bies.201100035>
- Lillo, C., Meyer, C., & Ruoff, P. (2001). The nitrate reductase circadian system. The central clock dogma contra multiple oscillatory feedback loops. In *Plant Physiology* (Vol. 125, Issue 4). <https://doi.org/10.1104/pp.125.4.1554>
- Lillo, C., & Ruoff, P. (1989). An unusually rapid light-induced nitrate reductase mRNA pulse and circadian oscillations. *Naturwissenschaften*, 76(11). <https://doi.org/10.1007/BF00374129>
- Lonergan, T. A. (1981). A Circadian Rhythm in the Rate of Light-Induced Electron Flow in Three Leguminous Species. *Plant Physiology*, 68(5). <https://doi.org/10.1104/pp.68.5.1041>
- Lopez, D., Casero, D., Cokus, S. J., Merchant, S. S., & Pellegrini, M. (2011). Algal Functional Annotation Tool: A web-based analysis suite to functionally interpret large gene lists using integrated annotation and expression data. *BMC Bioinformatics*, 12, 282. <https://doi.org/10.1186/1471-2105-12-282>
- Ludwig, C., Gillet, L., Rosenberger, G., Amon, S., Collins, B. C., & Aebersold, R. (2018). Data-independent acquisition-based SWATH - MS for quantitative proteomics: a tutorial. *Molecular Systems Biology*, 14(8). <https://doi.org/10.15252/msb.20178126>
- Mackenzie, T. D. B., & Morse, D. (2011). Circadian photosynthetic reductant flow in the dinoflagellate Lingulodinium is limited by carbon availability. *Plant, Cell and Environment*, 34(4). <https://doi.org/10.1111/j.1365-3040.2010.02271.x>

- Masseroli, M., Martucci, D., & Pincioli, F. (2004). GFINDer: Genome Function INtegrated Discoverer through dynamic annotation, statistical analysis, and mining. *Nucleic Acids Research*, 32(WEB SERVER ISS.). <https://doi.org/10.1093/nar/gkh432>
- Matsuo, T., Yamaguchi, S., Mitsui, S., Emi, A., Shimoda, F., & Okamura, H. (2003). Control mechanism of the circadian clock for timing of cell division in vivo. *Science*, 302(5643). <https://doi.org/10.1126/science.1086271>
- Mazzocchi, F. (2012). Complexity and the reductionism-holism debate in systems biology. *Wiley Interdisciplinary Reviews: Systems Biology and Medicine*, 4(5), 413–427. <https://doi.org/10.1002/wsbm.1181>
- Mazzoccoli, G., Vinciguerra, M., Carbone, A., & Relógio, A. (2020). The circadian clock, the immune system, and viral infections: The intricate relationship between biological time and host-virus interaction. In *Pathogens* (Vol. 9, Issue 2). <https://doi.org/10.3390/pathogens9020083>
- McClung, C. R. (2006). Plant circadian rhythms. In *Plant Cell* (Vol. 18, Issue 4). <https://doi.org/10.1105/tpc.106.040980>
- Merchant, S. S., Prochnik, S. E., Vallon, O., Harris, E. H., Karpowicz, S. J., Witman, G. B., Terry, A., Salamov, A., Fritz-Laylin, L. K., Maréchal-Drouard, L., Marshall, W. F., Qu, L. H., Nelson, D. R., Sanderfoot, A. A., Spalding, M. H., Kapitonov, V. V., Ren, Q., Ferris, P., Lindquist, E., ... Zhou, K. (2007). The Chlamydomonas genome reveals the evolution of key animal and plant functions. *Science*, 318(5848). <https://doi.org/10.1126/science.1143609>
- Merchante, C., Stepanova, A. N., & Alonso, J. M. (2017). Translation regulation in plants: an interesting past, an exciting present and a promising future. *Plant Journal*, 90(4). <https://doi.org/10.1111/tpj.13520>
- Mermet, J., Yeung, J., & Naef, F. (2017). Systems chronobiology: Global analysis of gene regulation in a 24-hour periodic world. *Cold Spring Harbor Perspectives in Biology*, 9(3). <https://doi.org/10.1101/cshperspect.a028720>
- Merrow, M., Spoelstra, K., & Roenneberg, T. (2005). The circadian cycle: Daily rhythms from behaviour to genes. In *EMBO Reports* (Vol. 6, Issue 10). <https://doi.org/10.1038/sj.embo.7400541>
- Messager, S., Hazlerigg, D. G., Mercer, J. G., & Morgan, P. J. (2000). Photoperiod differentially regulates the expression of Per1 and ICER in the pars tuberalis and the suprachiasmatic nucleus of the Siberian hamster. *European Journal of Neuroscience*, 12(8). <https://doi.org/10.1046/j.1460-9568.2000.00174.x>
- Mi, H., Ebert, D., Muruganujan, A., Mills, C., Albou, L. P., Mushayamaha, T., & Thomas, P. D. (2021). PANTHER version 16: A revised family classification, tree-based classifica-

- tion tool, enhancer regions and extensive API. *Nucleic Acids Research*, 49(D1). <https://doi.org/10.1093/nar/gkaa1106>
- Mistry, J., Chuguransky, S., Williams, L., Qureshi, M., Salazar, G. A., Sonnhammer, E. L. L., Tosatto, S. C. E., Paladin, L., Raj, S., Richardson, L. J., Finn, R. D., & Bateman, A. (2021). Pfam: The protein families database in 2021. *Nucleic Acids Research*, 49(D1). <https://doi.org/10.1093/nar/gkaa913>
- Mittag, M. (2001). Circadian rhythms in microalgae. *International Review of Cytology*, 206. [https://doi.org/10.1016/S0074-7696\(01\)06023-5](https://doi.org/10.1016/S0074-7696(01)06023-5)
- Mohabir, G., & Edmunds, L. N. (1999). Circadian clock regulation of the bimodal rhythm of cyclic AMP in wild-type Euglena. *Cellular Signalling*, 11(2). [https://doi.org/10.1016/S0898-6568\(98\)00046-1](https://doi.org/10.1016/S0898-6568(98)00046-1)
- Monnier, A., Liverani, S., Bouvet, R., Jesson, B., Smith, J. Q., Mosser, J., Corellou, F., & Bouget, F. Y. (2010). Orchestrated transcription of biological processes in the marine picoeukaryote Ostreococcus exposed to light/dark cycles. *BMC Genomics*, 11(1). <https://doi.org/10.1186/1471-2164-11-192>
- Moreau, H., Grimsley, N., Derelle, E., Ferraz, C., Escande, M.L., Eychené, S., Cooke, R., Piganneau, G., Desdevises, Y., Bellec, L. (1995). A new marine picoeukaryote: *Ostreococcus tauri* gen. et sp. nov. (*Chlorophyta, Prasinophyceae*). 34(4), 285–292.
- Moreau, H., Verhelst, B., Couloux, A., Derelle, E., Rombauts, S., Grimsley, N., Van Bel, M., Poulain, J., Katinka, M., Hohmann-Marriott, M. F., Piganneau, G., Rouzé, P., Da Silva, C., Wincker, P., Van de Peer, Y., & Vandepoele, K. (2012). Gene functionalities and genome structure in Bathycoccus prasinos reflect cellular specializations at the base of the green lineage. *Genome Biology*, 13(8). <https://doi.org/10.1186/gb-2012-13-8-r74>
- Morimoto, D., Yoshida, T., & Sawayama, S. (2020). Draft Genome Sequence of the Astaxanthin-Producing Microalga Haematococcus lacustris Strain NIES-144. *Microbiology Resource Announcements*, 9(23). <https://doi.org/10.1128/mra.00128-20>
- Moriya, Y., Itoh, M., Okuda, S., Yoshizawa, A. C., & Kanehisa, M. (2007). KAAS: An automatic genome annotation and pathway reconstruction server. *Nucleic Acids Research*, 35(SUPPL.2), 182–185. <https://doi.org/10.1093/nar/gkm321>
- Morris, A. R., Stanton, D. L., Roman, D., & Liu, A. C. (2020). Systems Level Understanding of Circadian Integration with Cell Physiology. In *Journal of Molecular Biology* (Vol. 432, Issue 12). <https://doi.org/10.1016/j.jmb.2020.02.002>
- Moulager, M., Corellou, F., Vergé, V., Escande, M. L., & Bouget, F. Y. (2010). Integration of light signals by the retinoblastoma pathway in the control of S phase entry in the Pico-

phytoplanktonic cell *Ostreococcus*. *PLoS Genetics*, 6(5), 11. <https://doi.org/10.1371/journal.pgen.1000957>

Moulager, M., Monnier, A., Jesson, B., Bouvet, R., Mosser, J., Schwartz, C., Garnier, L., Corellou, F., & Bouget, F. Y. (2007). Light-dependent regulation of cell division in *Ostreococcus*: Evidence for a major transcriptional input. *Plant Physiology*, 144(3), 1360–1369. <https://doi.org/10.1104/pp.107.096149>

Ngan, C. Y., Wong, C. H., Choi, C., Yoshinaga, Y., Louie, K., Jia, J., Chen, C., Bowen, B., Cheng, H., Leonelli, L., Kuo, R., Baran, R., Garcíá-Cerdán, J. G., Pratap, A., Wang, M., Lim, J., Tice, H., Daum, C., Xu, J., ... Wei, C. L. (2015). Lineage-specific chromatin signatures reveal a regulator of lipid metabolism in microalgae. *Nature Plants*, 1, 15107. <https://doi.org/10.1038/nplants.2015.107>

Nishiwaki-Ohkawa, T., & Yoshimura, T. (2016). Molecular basis for regulating seasonal reproduction in vertebrates. In *Journal of Endocrinology* (Vol. 229, Issue 3). <https://doi.org/10.1530/JOE-16-0066>

Noordally, Z. B., & Millar, A. J. (2015). Clocks in algae. *Biochemistry*, 54(2), 171–183. <https://doi.org/10.1021/bi501089x>

Numata, H., Miyazaki, Y., & Ikeno, T. (2015). Common features in diverse insect clocks. *Zoological Letters*, 1(1). <https://doi.org/10.1186/s40851-014-0003-y>

O'Kelly, C. J., Sieracki, M. E., Thier, E. C., & Hobson, I. C. (2003). A transient bloom of *Ostreococcus* (Chlorophyta, Prasinophyceae) in West Neck Bay, Long Island, New York. *Journal of Phycology*, 39(5). <https://doi.org/10.1046/j.1529-8817.2003.02201.x>

Ogata, H., Goto, S., Sato, K., Fujibuchi, W., Bono, H., & Kanehisa, M. (1999). KEGG: Kyoto encyclopedia of genes and genomes. In *Nucleic Acids Research*. <https://doi.org/10.1093/nar/27.1.29>

Ohara, T., Fukuda, H., & Tokuda, I. T. (2015). An extended mathematical model for reproducing the phase response of *Arabidopsis thaliana* under various light conditions. *Journal of Theoretical Biology*, 382. <https://doi.org/10.1016/j.jtbi.2015.07.016>

Ottesen, E. A., Young, C. R., Eppley, J. M., Ryan, J. P., Chavez, F. P., Scholin, C. A., & DeLong, E. F. (2013). Pattern and synchrony of gene expression among sympatric marine microbial populations. *Proceedings of the National Academy of Sciences of the United States of America*, 110(6). <https://doi.org/10.1073/pnas.1222099110>

Paajanen, P., Lane de Barros Dantas, L., & Dodd, A. N. (2021). Layers of crosstalk between circadian regulation and environmental signalling in plants. In *Current Biology* (Vol. 31, Issue 8). <https://doi.org/10.1016/j.cub.2021.03.046>

Palenik, B., Brahamsha, B., Larimer, F. W., Land, M., Hauser, L., Chain, P., Lamerdin, J., Regala, W., Allen, E. E., McCarren, J., Paulsen, I., Dufresne, A., Partensky, F., Webb,

- E. A., & Waterbury, J. (2003). The genome of a motile marine Synechococcus. *Nature*, 424(6952). <https://doi.org/10.1038/nature01943>
- Palenik, B., Grimwood, J., Aerts, A., Rouzé, P., Salamov, A., Putnam, N., Dupont, C., Jorgensen, R., Derelle, E., Rombauts, S., Zhou, K., Ollilar, R., Merchant, S. S., Podell, S., Gaasterland, T., Napoli, C., Gandler, K., Manuell, A., Tai, V., ... Grigoriev, I. V. (2007). The tiny eukaryote Ostreococcus provides genomic insights into the paradox of plankton speciation. *Proceedings of the National Academy of Sciences of the United States of America*, 104(18). <https://doi.org/10.1073/pnas.0611046104>
- Pan, Y., Ballance, H., Meng, H., Gonzalez, N., Kim, S. M., Abdurehman, L., York, B., Chen, X., Schnytzer, Y., Levy, O., Dacso, C. C., McClung, C. A., O'Malley, B. W., Liu, S., & Zhu, B. (2020). 12-h clock regulation of genetic information flow by XBP1s. *PLoS Biology*, 18(1). <https://doi.org/10.1371/journal.pbio.3000580>
- Pan, Y., Michael, T. P., Hudson, M. E., Kay, S. A., Chory, J., & Schuler, M. A. (2009). Cytochrome P450 monooxygenases as reporters for circadian-regulated pathways. *Plant Physiology*, 150(2). <https://doi.org/10.1104/pp.108.130757>
- Panter, P. E., Muranaka, T., Cuitun-Coronado, D., Graham, C. A., Yochikawa, A., Kudoh, H., & Dodd, A. N. (2019). Circadian Regulation of the Plant Transcriptome Under Natural Conditions. In *Frontiers in Genetics* (Vol. 10). <https://doi.org/10.3389/fgene.2019.01239>
- Parsons, R., Parsons, R., Garner, N., Oster, H., & Rawashdeh, O. (2020). CircaCompare: A method to estimate and statistically support differences in mesor, amplitude and phase, between circadian rhythms. *Bioinformatics*, 36(4). <https://doi.org/10.1093/bioinformatics/btz730>
- Pereira, H., Sá, M., Maia, I., Rodrigues, A., Teles, I., Wijffels, R. H., Navalho, J., & Barbosa, M. (2021). Fucoxanthin production from *Tisochrysis lutea* and *Phaeodactylum tricornutum* at industrial scale. *Algal Research*, 56. <https://doi.org/10.1016/j.algal.2021.102322>
- Pertea, M., Kim, D., Pertea, G. M., Leek, J. T., & Salzberg, S. L. (2016). Transcript-level expression analysis of RNA-seq experiments with HISAT, StringTie and Ballgown. *Nature Protocols*, 11(9). <https://doi.org/10.1038/nprot.2016.095>
- Pertea, M., Pertea, G. M., Antonescu, C. M., Chang, T. C., Mendell, J. T., & Salzberg, S. L. (2015). StringTie enables improved reconstruction of a transcriptome from RNA-seq reads. *Nature Biotechnology*, 33, 290–295. <https://doi.org/10.1038/nbt.3122>
- Pfeuty, B., Thommen, Q., Corellou, F., Djouani-Tahri, E. B., Bouget, F. Y., & Lefranc, M. (2012). Circadian clocks in changing weather and seasons: Lessons from the picoalga ostreococcus tauri. *BioEssays*, 34(9), 781–790. <https://doi.org/10.1002/bies.201200012>

- Pilgrim, M. L., & McClung, C. R. (1993). Differential involvement of the circadian clock in the expression of genes required for ribulose-1,5-bisphosphate carboxylase/oxygenase synthesis, assembly, and activation in *Arabidopsis thaliana*. *Plant Physiology*, 103(2), 553–564. <https://doi.org/10.1104/pp.103.2.553>
- Pittendrigh, C. S. (1960). Circadian rhythms and the circadian organization of living systems. *Cold Spring Harbor Symposia on Quantitative Biology*, 25. <https://doi.org/10.1101/SQB.1960.025.01.015>
- Polle, J. E. W., Barry, K., Cushman, J., Schmutz, J., Tran, D., Hathwaik, L. T., Yim, W. C., Jenkins, J., McKie-Krisberg, Z., Prochnik, S., Lindquist, E., Dockter, R. B., Adam, C., Molina, H., Bunkenborg, J., Jin, E. S., Buchheim, M., & Magnuson, J. (2017). Draft nuclear genome sequence of the halophilic and beta-carotene-accumulating green alga *Dunaliella salina* strain CCAP19/18. In *Genome Announcements* (Vol. 5, Issue 43). <https://doi.org/10.1128/genomeA.01105-17>
- Potter, S. C., Luciani, A., Eddy, S. R., Park, Y., Lopez, R., & Finn, R. D. (2018). HMMER web server: 2018 update. *Nucleic Acids Research*, 46(W1). <https://doi.org/10.1093/nar/gky448>
- Prabhakaran, P. M., & Sheeba, V. (2012). Sympatric drosophilid species *melanogaster* and *ananassae* differ in temporal patterns of activity. *Journal of Biological Rhythms*, 27(5). <https://doi.org/10.1177/0748730412458661>
- Prendergast, S. C., Strobl, A. C., Cross, W., Pillay, N., Strauss, S. J., Ye, H., Lindsay, D., Tirabosco, R., Chalker, J., Mahamdallie, S. S., Sosinsky, A., Flanagan, A. M., & Amary, F. (2020). Sarcoma and the 100,000 Genomes Project: our experience and changes to practice. *Journal of Pathology: Clinical Research*, 6(4). <https://doi.org/10.1002/cjp2.174>
- Prochnik, S. E., Umen, J., Nedelcu, A. M., Hallmann, A., Miller, S. M., Nishii, I., Ferris, P., Kuo, A., Mitros, T., Fritz-Laylin, L. K., Hellsten, U., Chapman, J., Simakov, O., Rensing, S. A., Terry, A., Pangilinan, J., Kapitonov, V., Jurka, J., Salamov, A., ... Rokhsar, D. S. (2010). Genomic analysis of organismal complexity in the multicellular green alga *volvox carteri*. *Science*, 329(5988). <https://doi.org/10.1126/science.1188800>
- Radakovits, R., Jinkerson, R. E., Fuerstenberg, S. I., Tae, H., Settlage, R. E., Boore, J. L., & Posewitz, M. C. (2012). Draft genome sequence and genetic transformation of the oleaginous alga *Nannochloropsis gaditana*. *Nature Communications*, 3. <https://doi.org/10.1038/ncomms1688>
- Ral, J. P., Colleoni, C., Wattebled, F., Dauvillée, D., Nempon, C., Deschamps, P., Li, Z., Morell, M. K., Chibbar, R., Purton, S., D'Hulst, C., & Ball, S. G. (2006). Circadian clock regulation of starch metabolism establishes GBSSI as a major contributor to amy-

lopectin synthesis in *Chlamydomonas reinhardtii*. *Plant Physiology*, 142(1). <https://doi.org/10.1104/pp.106.081885>

Rayko, E., Maumus, F., Maheswari, U., Jabbari, K., & Bowler, C. (2010). Transcription factor families inferred from genome sequences of photosynthetic stramenopiles. *New Phytologist*, 188(1). <https://doi.org/10.1111/j.1469-8137.2010.03371.x>

Ripperger, J. A., & Merrow, M. (2011). Perfect timing: Epigenetic regulation of the circadian clock. In *FEBS Letters* (Vol. 585, Issue 10). <https://doi.org/10.1016/j.febslet.2011.04.047>

Ritchie, M. E., Phipson, B., Wu, D., Hu, Y., Law, C. W., Shi, W., & Smyth, G. K. (2015). limma powers differential expression analyses for RNA-sequencing and microarray studies. *Nucleic Acids Research*, 43(7), e47. <https://doi.org/10.1093/nar/gkv007>

Robbens, S., Khadaroo, B., Camasses, A., Derelle, E., Ferraz, C., Inzé, D., Van De Peer, Y., & Moreau, H. (2005). Genome-wide analysis of core cell cycle genes in the unicellular green alga *Ostreococcus tauri*. *Molecular Biology and Evolution*, 22(3). <https://doi.org/10.1093/molbev/msi044>

Rock, A., Wilcockson, D., & Last, K. S. (2022). Towards an Understanding of Circatidal Clocks. In *Frontiers in Physiology* (Vol. 13). <https://doi.org/10.3389/fphys.2022.830107>

Roenneberg, T., Foster, R. G., & Klerman, E. B. (2022). The circadian system, sleep, and the health/disease balance: a conceptual review. *Journal of Sleep Research*, April, 1–14. <https://doi.org/10.1111/jsr.13621>

Roenneberg, T., & Merrow, M. (2005). Circadian clocks - The fall and rise of physiology. In *Nature Reviews Molecular Cell Biology* (Vol. 6, Issue 12). <https://doi.org/10.1038/nrm1766>

Roenneberg, T., & Merrow, M. (2016). The circadian clock and human health. In *Current Biology* (Vol. 26, Issue 10). <https://doi.org/10.1016/j.cub.2016.04.011>

Roenneberg, T., Pilz, L. K., Zerbini, G., & Winnebeck, E. C. (2019). Chronotype and social jetlag: A (self-) critical review. In *Biology* (Vol. 8, Issue 3). <https://doi.org/10.3390/biology8030054>

Romero-Campero, F. J., Perez-Hurtado, I., Lucas-Reina, E., Romero, J. M., & Valverde, F. (2016). ChlamyNET: A *Chlamydomonas* gene co-expression network reveals global properties of the transcriptome and the early setup of key co-expression patterns in the green lineage. *BMC Genomics*, 17, 227. <https://doi.org/10.1186/s12864-016-2564-y>

Romero-Losada, A. B., Arvanitidou, C., de los Reyes, P., García-González, M., & Romero-Campero, F. J. (2022). ALGAEFUN with MARACAS, microALGAE FUNctional enrich-

ment tool for MicroAlgae RnA-seq and Chip-seq AnalysisS. *BMC Bioinformatics*, 23(1). <https://doi.org/10.1186/s12859-022-04639-5>

Roth, M. S., Cokus, S. J., Gallaher, S. D., Walter, A., Lopez, D., Erickson, E., Endelman, B., Westcott, D., Larabell, C. A., Merchant, S. S., Pellegrini, M., & Niyogi, K. K. (2017). Chromosome-level genome assembly and transcriptome of the green alga Chro-mochloris zofingiensis illuminates astaxanthin production. *Proceedings of the National Academy of Sciences of the United States of America*, 114(21), E4296–E4305. <https://doi.org/10.1073/pnas.1619928114>

Rufy, T. W., & Huber, S. C. (1983). Changes in Starch Formation and Activities of Sucrose Phosphate Synthase and Cytoplasmic Fructose-1,6-bisphosphatase in Response to Source-Sink Alterations. *Plant Physiology*, 72(2). <https://doi.org/10.1104/pp.72.2.474>

Sanz-Luque, E., Chamizo-Ampudia, A., Llamas, A., Galvan, A., & Fernandez, E. (2015). Understanding nitrate assimilation and its regulation in microalgae. In *Frontiers in Plant Science* (Vol. 6, Issue OCTOBER). <https://doi.org/10.3389/fpls.2015.00899>

Sekimoto, H. (2017). Sexual reproduction and sex determination in green algae. *Journal of Plant Research*, 130(3). <https://doi.org/10.1007/s10265-017-0908-6>

Serrano-Bueno, G., Romero-Campero, F. J., Lucas-Reina, E., Romero, J. M., & Valverde, F. (2017). Evolution of photoperiod sensing in plants and algae. *Current Opinion in Plant Biology*, 37, 10–17. <https://doi.org/10.1016/j.pbi.2017.03.007>

Serrano-Pérez, E., Romero-Losada, A. B., Morales-Pineda, M., García-Gómez, M. E., Couso, I., García-González, M., & Romero-Campero, F. J. (2022). Transcriptomic and Metabolomic Response to High Light in the Charophyte Alga Klebsormidium nitens. *Frontiers in Plant Science*, 13. <https://doi.org/10.3389/fpls.2022.855243>

Serrano, G., Herrera-Palau, R., Romero, J. M., Serrano, A., Coupland, G., & Valverde, F. (2009). Chlamydomonas CONSTANS and the Evolution of Plant Photoperiodic Signaling. *Current Biology*, 19(5). <https://doi.org/10.1016/j.cub.2009.01.044>

Sharma, A., Tripathi, V., & Kumar, V. (2022). Control and adaptability of seasonal changes in behavior and physiology of latitudinal avian migrants: Insights from laboratory studies in Palearctic-Indian migratory buntings. *Journal of Experimental Zoology Part A: Ecological and Integrative Physiology*, 35677956. <https://doi.org/10.1002/jez.2631>

Shen, M., Chang, Y. T., Wu, C. T., Parker, S. J., Saylor, G., Wang, Y., Yu, G., Van Eyk, J. E., Clarke, R., Herrington, D. M., & Wang, Y. (2022). Comparative assessment and novel strategy on methods for imputing proteomics data. *Scientific Reports*, 12(1). <https://doi.org/10.1038/s41598-022-04938-0>

- Sierra, E., Acién, F. G., Fernández, J. M., García, J. L., González, C., & Molina, E. (2008). Characterization of a flat plate photobioreactor for the production of microalgae. *Chemical Engineering Journal*, 138(1–3). <https://doi.org/10.1016/j.cej.2007.06.004>
- Six, C., Sherrard, R., Lionard, M., Roy, S., & Campbell, D. A. (2009). Photosystem II and Pigment Dynamics among ecotypes of the green alga *Ostreococcus*. *Plant Physiology*, 151(1). <https://doi.org/10.1104/pp.109.140566>
- Six, C., Worden, A. Z., Rodríguez, F., Moreau, H., & Partensky, F. (2005). New insights into the nature and phylogeny of prasinophyte antenna proteins: *Ostreococcus tauri*, a case study. *Molecular Biology and Evolution*, 22(11), 2217–2230. <https://doi.org/10.1093/molbev/msi220>
- Sorek, M., Yacobi, Y. Z., Roopin, M., Berman-Frank, I., & Levy, O. (2013). Photosynthetic circadian rhythmicity patterns of *Symbiodium*, the coral endosymbiotic algae. *Proceedings of the Royal Society B: Biological Sciences*, 280(1759). <https://doi.org/10.1098/rspb.2012.2942>
- Spudich, J. L., & Sager, R. (1980). Regulation of the chlamydomonas cell cycle by light and dark. *Journal of Cell Biology*, 85(1). <https://doi.org/10.1083/jcb.85.1.136>
- Sterck, L., Billiau, K., Abeel, T., Rouzé, P., & Van de Peer, Y. (2012). ORCAE: online resource for community annotation of eukaryotes. *Nature Methods*. <https://doi.org/10.1038/nmeth.2242>
- Sulpice, R., Flis, A., Ivakov, A. A., Apelt, F., Krohn, N., Encke, B., Abel, C., Feil, R., Lunn, J. E., & Stitt, M. (2014). Arabidopsis coordinates the diurnal regulation of carbon allocation and growth across a wide range of Photoperiods. *Molecular Plant*, 7(1). <https://doi.org/10.1093/mp/sst127>
- Sumová, A., Jáč, M., Sládek, M., Šauman, I., & Illnerová, H. (2003). Clock gene daily profiles and their phase relationship in the rat suprachiasmatic nucleus are affected by photoperiod. *Journal of Biological Rhythms*, 18(2). <https://doi.org/10.1177/0748730403251801>
- Sun, T. H., Liu, C. Q., Hui, Y. Y., Wu, W. K., Zhou, Z. G., & Lu, S. (2010). Coordinated Regulation of Gene Expression for Carotenoid Metabolism in *Chlamydomonas reinhardtii*. *Journal of Integrative Plant Biology*, 52(10). <https://doi.org/10.1111/j.1744-7909.2010.00993.x>
- Sun, T., Rao, S., Zhou, X., & Li, L. (2022). Plant carotenoids: recent advances and future perspectives. *Molecular Horticulture*, 2(1). <https://doi.org/10.1186/s43897-022-00023-2>

- Swanson, W. J., Aagaard, J. E., Vacquier, V. D., Monné, M., Sadat Al Hosseini, H., & Jovine, L. (2011). The molecular basis of sex: Linking yeast to human. *Molecular Biology and Evolution*, 28(7). <https://doi.org/10.1093/molbev/msr026>
- Swarbreck, D., Wilks, C., Lamesch, P., Berardini, T. Z., Garcia-Hernandez, M., Foerster, H., Li, D., Meyer, T., Muller, R., Ploetz, L., Radenbaugh, A., Singh, S., Swing, V., Tissier, C., Zhang, P., & Huala, E. (2008). The Arabidopsis Information Resource (TAIR): Gene structure and function annotation. *Nucleic Acids Research*, 36(SUPPL. 1). <https://doi.org/10.1093/nar/gkm965>
- Sweeney, B. M., & Haxo, F. T. (1961). Persistence of a photosynthetic rhythm in enucleated Acetabularia. *Science*, 134(3487). <https://doi.org/10.1126/science.134.3487.1361>
- Takahashi, J. S. (2021). The 50th anniversary of the konopka and benzer 1971 paper in PNAS: "Clock mutants of drosophila melanogaster." In *Proceedings of the National Academy of Sciences of the United States of America* (Vol. 118, Issue 39). <https://doi.org/10.1073/pnas.2110171118>
- Thaben, P. F., & Westermark, P. O. (2014). Detecting rhythms in time series with rain. *Journal of Biological Rhythms*, 29(6). <https://doi.org/10.1177/0748730414553029>
- Tian, T., Liu, Y., Yan, H., You, Q., Yi, X., Du, Z., Xu, W., & Su, Z. (2017). AgriGO v2.0: A GO analysis toolkit for the agricultural community, 2017 update. *Nucleic Acids Research*, 45(W1), W122–W129. <https://doi.org/10.1093/nar/gkx382>
- Tragin, M., & Vaulot, D. (2019). Novel diversity within marine Mamiellophyceae (Chlorophyta) unveiled by metabarcoding. *Scientific Reports*, 9(1). <https://doi.org/10.1038/s41598-019-41680-6>
- Tucker, D. E., Allen, D. J., & Ort, D. R. (2004). Control of nitrate reductase by circadian and diurnal rhythms in tomato. *Planta*, 219(2). <https://doi.org/10.1007/s00425-004-1213-x>
- Van Dongen, H. P. A., Kerkhof, G. A., & Klöppel, H. B. (1997). Seasonal covariation of the circadian phases of rectal temperature and slow wave sleep onset. *Journal of Sleep Research*, 6(1). <https://doi.org/10.1046/j.1365-2869.1997.00021.x>
- Van Gelderen, K. (2020). The rhythm of the light: How light and the clock drive cycling of transcript levels in barley. In *Plant Physiology* (Vol. 183, Issue 2). <https://doi.org/10.1104/pp.20.00360>
- Vatakis, A., Balci, F., Di Luca, M., & Correa, Á. (2018). Circadian Timing: From Genetics to Behavior. In *Timing and Time Perception: Procedures, Measures, & Applications*. https://doi.org/10.1163/9789004280205_002
- Veenstra, T. D. (2021). Omics in Systems Biology: Current Progress and Future Outlook. In *Proteomics* (Vol. 21, Issues 3–4). <https://doi.org/10.1002/pmic.202000235>

- Wang, Z., Gerstein, M., & Snyder, M. (2009). RNA-Seq: A revolutionary tool for transcriptomics. In *Nature Reviews Genetics* (Vol. 10, Issue 1). <https://doi.org/10.1038/nrg2484>
- Watanabe, T., Naito, E., Nakao, N., Tei, H., Yoshimura, T., & Ebihara, S. (2007). Bimodal clock gene expression in mouse suprachiasmatic nucleus and peripheral tissues under a 7-hour light and 5-hour dark schedule. *Journal of Biological Rhythms*, 22(1). <https://doi.org/10.1177/0748730406295435>
- Watson, J. V., Chambers, S. H., & Smith, P. J. (1987). A pragmatic approach to the analysis of DNA histograms with a definable G1 peak. *Cytometry*, 8(1), 1–8. <https://doi.org/10.1002/CYTO.990080101>
- Weckwerth, W. (2011). Green systems biology - From single genomes, proteomes and metabolomes to ecosystems research and biotechnology. In *Journal of Proteomics* (Vol. 75, Issue 1). <https://doi.org/10.1016/j.jprot.2011.07.010>
- Willforss, J., Chawade, A., & Levander, F. (2019). NormalizerDE: Online Tool for Improved Normalization of Omics Expression Data and High-Sensitivity Differential Expression Analysis. *Journal of Proteome Research*, 18(2). <https://doi.org/10.1021/acs.jproteome.8b00523>
- Worden, A. Z., Lee, J. H., Mock, T., Rouzé, P., Simmons, M. P., Aerts, A. L., Allen, A. E., Cuvelier, M. L., Derelle, E., Everett, M. V., Foulon, E., Grimwood, J., Gundlach, H., Henrissat, B., Napoli, C., McDonald, S. M., Parker, M. S., Rombauts, S., Salamov, A., ... Grigoriev, I. V. (2009). Green evolution and dynamic adaptations revealed by genomes of the marine picoeukaryotes micromonas. *Science*, 324(5924). <https://doi.org/10.1126/science.1167222>
- Worden, A. Z., Nolan, J. K., & Palenik, B. (2004). Assessing the dynamics and ecology of marine picophytoplankton: The importance of the eukaryotic component. *Limnology and Oceanography*, 49(1). <https://doi.org/10.4319/lo.2004.49.1.0168>
- Wu, T., Hu, E., Xu, S., Chen, M., Guo, P., Dai, Z., Feng, T., Zhou, L., Tang, W., Zhan, L., Fu, X., Liu, S., Bo, X., & Yu, G. (2021). clusterProfiler 4.0: A universal enrichment tool for interpreting omics data. *The Innovation*, 2(3). <https://doi.org/10.1016/j.xinn.2021.100141>
- Wucher, V., Sodaei, R., Amador, R., Irimia, M., & Guigó, R. (2022). Day-night and seasonal variation of human gene expression across tissues. *BioRxiv : The Preprint Server for Biology*. <https://doi.org/10.1101/2021.02.28.433266>
- Yang, M., Lin, X., Liu, X., Zhang, J., & Ge, F. (2018). Genome Annotation of a Model Diatom Phaeodactylum tricornutum Using an Integrated Proteogenomic Pipeline. *Molecular Plant*, 11(10). <https://doi.org/10.1016/j.molp.2018.08.005>

- Yang, Z., & Midmore, D. J. (2005). A model for the circadian oscillations in expression and activity of nitrate reductase in higher plants. *Annals of Botany*, 96(6). <https://doi.org/10.1093/aob/mci254>
- Youthed, G. J., & Moran, V. C. (1969). The lunar-day activity rhythm of myrmeleontid larvae. *Journal of Insect Physiology*, 15(7). [https://doi.org/10.1016/0022-1910\(69\)90235-2](https://doi.org/10.1016/0022-1910(69)90235-2)
- Yu, G., Wang, L. G., & He, Q. Y. (2015). ChIP seeker: An R/Bioconductor package for ChIP peak annotation, comparison and visualization. *Bioinformatics*, 31(14), 2382–2383. <https://doi.org/10.1093/bioinformatics/btv145>
- Zee, P. C., & Abbott, S. M. (2020). Circadian Rhythm Sleep-Wake Disorders. In *CONTINUUM Lifelong Learning in Neurology* (Vol. 26, Issue 4). <https://doi.org/10.1212/CON.0000000000000884>
- Zhang, Z., Han, T., Sui, J., & Wang, H. (2022). Cryptochrome-mediated blue-light signal contributes to carotenoids biosynthesis in microalgae. *Frontiers in Microbiology*, 13, 1083387. <https://doi.org/10.3389/fmicb.2022.1083387>
- Zhao, L., Chang, W., Xiao, Y., Liu, H., & Liu, P. (2013). Methylerythritol phosphate pathway of isoprenoid biosynthesis. *Annual Review of Biochemistry*, 82, 497–530. <https://doi.org/10.1146/annurev-biochem-052010-100934>
- Zhao, X., Rastogi, A., Deton Cabanillas, A. F., Ait Mohamed, O., Cantrel, C., Lombard, B., Murik, O., Genovesio, A., Bowler, C., Bouyer, D., Loew, D., Lin, X., Veluchamy, A., Vieira, F. R. J., & Tirichine, L. (2021). Genome wide natural variation of H3K27me3 selectively marks genes predicted to be important for cell differentiation in Phaeodactylum tricornutum. *New Phytologist*, 229(6). <https://doi.org/10.1111/nph.17129>
- Zheng, Y., Jiao, C., Sun, H., Rosli, H. G., Pombo, M. A., Zhang, P., Banf, M., Dai, X., Martin, G. B., Giovannoni, J. J., Zhao, P. X., Rhee, S. Y., & Fei, Z. (2016). iTAK: A Program for Genome-wide Prediction and Classification of Plant Transcription Factors, Transcriptional Regulators, and Protein Kinases. In *Molecular Plant* (Vol. 9, Issue 12). <https://doi.org/10.1016/j.molp.2016.09.014>
- Zhu, B., Zhang, Q., Pan, Y., Mace, E. M., York, B., Antoulas, A. C., Dacso, C. C., & O'Malley, B. W. (2017). A Cell-Autonomous Mammalian 12 hr Clock Coordinates Metabolic and Stress Rhythms. *Cell Metabolism*, 25(6). <https://doi.org/10.1016/j.cmet.2017.05.004>
- Zhu, L. J. (2013). Integrative analysis of ChIP-chip and ChIP-seq dataset. *Methods in Molecular Biology*, 1067. https://doi.org/10.1007/978-1-62703-607-8_8
- Zones, J. M., Blaby, I. K., Merchant, S. S., & Umen, J. G. (2015). High-resolution profiling of a synchronized diurnal transcriptome from *Chlamydomonas reinhardtii* reveals con-

tinuous cell and metabolic differentiation. *Plant Cell*, 27(10). <https://doi.org/10.1105/tpc.15.00498>

Zurbriggen, M. D., Moor, A., & Weber, W. (2012). Plant and bacterial systems biology as platform for plant synthetic bio(techno)logy. *Journal of Biotechnology*, 160(1–2). <https://doi.org/10.1016/j.biotec.2012.01.014>